

**Standard Title Page - Report on Federally Funded Project**

1. Report No. FHWA/VTRC 06-CR3	2. Government Accession No.	3. Recipient's Catalog No.	
4. Title and Subtitle Development of an Optimized Continuity Diaphragm for New PCBT Girders		5. Report Date September 2005	
		6. Performing Organization Code	
7. Author(s) C.D. Newhouse, C.I. Roberts-Wollmann, and T.E. Cousins		8. Performing Organization Report No. VTRC 06-CR3	
9. Performing Organization and Address  Virginia Transportation Research Council 530 Edgemont Road Charlottesville, VA 22903		10. Work Unit No. (TRAIS)	
		11. Contract or Grant No. 64028	
12. Sponsoring Agencies' Name and Address Virginia Department of Transportation      FHWA 1401 E. Broad Street                              P.O. Box 10249 Richmond, VA 23219                                Richmond, VA 23240		13. Type of Report and Period Covered Final	
		14. Sponsoring Agency Code	
15. Supplementary Notes			
<p>16. Abstract</p> <p>Over the past 50 years, many states have recognized the benefits of making precast, prestressed multi-girder bridges continuous by connecting the girders with a continuity diaphragm. Although there is widespread agreement on the benefits of continuous construction, there has not been as much agreement on either the methods used for design of these systems or the details used for the continuity connections.</p> <p>To aid designers in choosing the most appropriate method, an analytical and experimental study was undertaken at Virginia Tech. Analyses were done to compare the differences in the predicted continuity moments for different design methods and assumptions over a range of commonly used systems of precast concrete bulb tee (PCBT) girders and cast-in-place slabs. The results of the analyses were used to develop three continuity connection details for testing during the experimental study. Three different continuity connections were tested using full-depth PCBT 45 in deep girders made continuous with a 6 ft wide slab.</p> <p>The bottom of the ends of the girders were made continuous with the continuity connection by extending prestressing strands for the first test and extending 180 degree bent bars for the second test. Both connections adequately resisted service, cyclic, and ultimate loads. But, the test with the extended bars remained stiffer during cyclic loading and is recommended for use. The third test was performed on a system using only a slab cast across the top of the girders without the full-depth diaphragm. Two primary cracks formed above the ends of the girders at the joint during service testing, after which no significant increase in damage took place.</p> <p>Results from the analytical study indicate that the predicted positive thermal restraint moments may be significant, similar in magnitude to the positive cracking moment. Results from the experimental study indicate that restraint moments develop early due to thermal expansion of the deck during curing and subsequent differential shrinkage; however, the magnitudes of the early age restraint moments are much less than conventional analyses predict. Due to the great number of uncertainties involved in the attempt to predict restraint moments, it is recommended that the diaphragms be designed for the thermal restraint moments, but not to exceed 1.2 times the cracking moment of the diaphragm-beam interface.</p>			
17 Key Words Prestressed concrete, precast concrete bulb-tee girders, bridge girders, concrete bridges, continuous bridges, continuity diaphragms		18. Distribution Statement No restrictions. This document is available to the public through NTIS, Springfield, VA 22161.	
19. Security Classif. (of this report) Unclassified	20. Security Classif. (of this page) Unclassified	21. No. of Pages 77	22. Price

**FINAL CONTRACT REPORT**  
**DEVELOPMENT OF AN OPTIMIZED CONTINUITY DIAPHRAGM**  
**FOR NEW PCBT GIRDERS**

**Charles D. Newhouse, Ph.D., P.E.**  
**Graduate Research Assistant**

**Carin L. Roberts-Wollmann, Ph.D., P.E.**  
**Associate Professor**

**Thomas E. Cousins, Ph.D., P.E.**  
**Associate Professor**

**Via Department of Civil and Environmental Engineering**  
**Virginia Polytechnic and State University**

*Project Manager*  
Rodney Davis, Ph.D., P.E., Virginia Transportation Research Council

Contract Research Sponsored by  
Virginia Transportation Research Council

Virginia Transportation Research Council  
(A Cooperative Organization Sponsored Jointly by the  
Virginia Department of Transportation and  
the University of Virginia)

Charlottesville, Virginia

September 2005  
VTRC 06-CR3

## NOTICE

The project that is the subject of this report was done under contract for the Virginia Department of Transportation, Virginia Transportation Research Council. The contents of this report reflect the views of the authors, who are responsible for the facts and the accuracy of the data presented herein. The contents do not necessarily reflect the official views or policies of the Virginia Department of Transportation, the Commonwealth Transportation Board, or the Federal Highway Administration. This report does not constitute a standard, specification, or regulation.

Each contract report is peer reviewed and accepted for publication by Research Council staff with expertise in related technical areas. Final editing and proofreading of the report are performed by the contractor.

Copyright 2005 by the Commonwealth of Virginia.

## ABSTRACT

Over the past 50 years, many states have recognized the benefits of making precast, prestressed multi-girder bridges continuous by connecting the girders with a continuity diaphragm. Although there is widespread agreement on the benefits of continuous construction, there has not been as much agreement on either the methods used for design of these systems or the details used for the continuity connections.

To aid designers in choosing the most appropriate method, an analytical and experimental study was undertaken at Virginia Tech. Analyses were done to compare the differences in the predicted continuity moments for different design methods and assumptions over a range of commonly used systems of precast concrete bulb tee (PCBT) girders and cast-in-place slabs. The results of the analyses were used to develop three continuity connection details for testing during the experimental study. Three different continuity connections were tested using full-depth PCBT 45 in deep girders made continuous with a 6 ft wide slab.

The bottom of the ends of the girders were made continuous with the continuity connection by extending prestressing strands for the first test and extending 180 degree bent bars for the second test. Both connections adequately resisted service, cyclic, and ultimate loads. But, the test with the extended bars remained stiffer during cyclic loading and is recommended for use. The third test was performed on a system using only a slab cast across the top of the girders without the full-depth diaphragm. Two primary cracks formed above the ends of the girders at the joint during service testing, after which no significant increase in damage took place.

Results from the analytical study indicate that the predicted positive thermal restraint moments may be significant, similar in magnitude to the positive cracking moment. Results from the experimental study indicate that restraint moments develop early due to thermal expansion of the deck during curing and subsequent differential shrinkage; however, the magnitudes of the early age restraint moments are much less than conventional analyses predict. Due to the great number of uncertainties involved in the attempt to predict restraint moments, it is recommended that the diaphragms be designed for the thermal restraint moments, but not to exceed 1.2 times the cracking moment of the diaphragm-beam interface.

**FINAL CONTRACT REPORT**

**DEVELOPMENT OF AN OPTIMIZED CONTINUITY DIAPHRAGM  
FOR NEW PCBT GIRDERS**

**C.D. Newhouse, Ph.D., P.E.**  
**Graduate Research Assistant**

**C.L. Roberts-Wollmann, Ph.D., P.E.**  
**Associate Professor**

**T.E. Cousins, Ph.D., P.E.**  
**Associate Professor**

**Via Department of Civil and Environmental Engineering  
Virginia Polytechnic and State University**

**INTRODUCTION**

Beginning in the late 1950s in the United States, the advantages of making a multi-span, simply supported prestressed I-girder bridge continuous by connecting the ends of the girders over the supports with a continuity diaphragm connection began to be investigated. Early in this process, the Portland Cement Association recognized that continuity could be beneficial in three distinct ways (Kaar et al. 1960). First, continuity over a support could reduce both the deflections and maximum moments at the mid-span of a girder. This could allow for fewer strands to be used (approximately 5 to 15 percent fewer strands) or for longer span lengths to be achieved (Freyermuth 1969). Second, the elimination of the joints over the supports could improve the long term durability of a girder by reducing the amount of water and salt that potentially would cause deterioration of the concrete. Also, the elimination of the joints could provide for an improved riding surface. Third, the continuity could help to provide reserve load capacity in the event of an overload condition.

Over the past 50 years, many states have recognized these benefits and are designing their precast, prestressed girder bridges as continuous. Although there is good agreement on the benefits of continuous construction, there is not as much agreement on either the methods used for design of these systems or the details used for the continuity connections. The purpose of this study is to obtain a better understanding of both the design and behavior of precast, prestressed girders, with cast-in-place slabs, made continuous. To achieve this purpose, an initial analytical study was undertaken to compare the prediction of restraint moments with the most commonly used current design methods. Restraint moments due to time dependent effects such as creep and shrinkage as well as restraint moments due to thermal gradients were considered. Results from the analytical study were then used to propose three continuity connections for testing. Full-depth girder sections were fabricated and shipped to Virginia Tech where the girders were connected with a continuity connection and tested for service, cyclic, and ultimate load capacities.

## **Overview of the Problem**

In comparison to a composite girder-slab system comprising simple spans, it is more difficult to predict the behavior of a similar system when it is made continuous with a continuity connection because the structure undergoes time dependent changes. When a simple span precast, prestressed girder is initially placed on its supports, the prestressing force and the self-weight cause the concrete to creep. For typical simple span structures, this causes an upward deflection to occur. When the cast-in-place slab is placed, an initial downward deflection occurs. Over time, creep effects will generally cause additional deflections to occur. Since the girders and the deck are usually made of concretes having different strengths and are cast at different times, differential shrinkage may occur within the composite system. This differential shrinkage may also cause deflections to occur. The net deflection of the system due to these factors (and others) must then be predicted. After the continuity connection is made, any deflections in the system will cause rotations over the supports which cause the development of restraint moments and shears in the ends of the girders at the connection because the system is now indeterminate. Accounting for all of the possible factors is difficult, and has resulted in several different design methods to predict the behavior of these systems.

In Virginia, precast, prestressed girders made composite with a cast-in-place deck have been commonly used for highway construction since the 1960s. In the earlier days of their use, many bridges were designed as simple spans. The issue of predicting restraint moments did not exist, since a joint was provided instead of a continuity connection. Throughout the years, it was found that simply eliminating the joints in a bridge could help to reduce the maintenance costs throughout the life of the structure. Today, many bridges in Virginia are made continuous, requiring the prediction of the restraint moments.

Recently, the Virginia Department of Transportation (VDOT) began to use a different standard shape girder for typical highway bridges, the precast concrete bulb-tee (PCBT) shape. To gain the full advantages of the new shape, this research was initiated to investigate the continuity detail for this newer shape.

## **Overview of Factors Influencing Behavior**

The main reason that there is not better uniformity in the design of girders made continuous is the fact that there are so many variables which influence the behavior of the system. Unlike some structural systems which have properties that remain relatively static over time, a system of girders made continuous is influenced by many factors that cause the properties of the system to change over time. The primary material for the girders and the diaphragm, concrete, has properties that change dramatically in the early stages of hydration and continue to change years after the final set has occurred. The addition of the prestressing steel to the system introduces additional material and time dependent influences on the behavior of the system, making the behavior of the system more difficult to predict.

Most precast, prestressed girders used for bridge construction are non-composite for self-weight and the dead load of the deck, but are later made composite by the addition of a cast-in-place concrete deck. Therefore, both composite and non-composite properties must be

considered in the design process. Also, unique to this type of construction, the construction sequencing can have a large influence on the behavior of the system.

Once a multi-span system is made continuous, thermal restraint moments will develop and induce additional stresses in the system. Some design methods do not consider these influences; however, the stresses caused by the thermal restraint moments may be significant and have been considered in this study.

Considering just some of these influences, it can be seen that the behavior of a system made of precast, prestressed concrete made continuous can be difficult to predict. As response begins to include cracking, crushing, yielding and other non-linear material behavior, the validity of using the law of superposition begins to be questioned, making the prediction of the behavior of these systems even more difficult.

### **Overview of the Current Design Process**

In the United States, there have been two main design procedures used in the past for predicting the required design moments at the continuity connections, the PCA Method (Freyermuth, 1969) and the National Cooperative Highway Research Program (NCHRP) 322 Method (Oesterle et al. 1989). Currently, a third document has been developed under the NCHRP 12-53 research. This research has been published as NCHRP Report 519 (Miller et al. 2004). A recent survey performed for the NCHRP 519 Project revealed that about 35 percent of those responding use the PCA Method while about 9 percent use the NCHRP 322 method (Hastak et al. 2003). In addition, the survey revealed that about 48 percent of those responding use some type of standard detail for the positive moment connection while about 25 percent do not use any positive moment connection. Clearly, differences in the design process exist throughout the country. Regardless of the differences, the single goal of the design process is to predict the moments at the continuity support so that the appropriate amount of steel can be provided for both the positive and negative moments for both service and ultimate loads. When both of the current methods are used to predict the restraint moments of the same system, the predicted moments often differ significantly for girder and slab systems commonly used in highway construction. It is commonly believed that the PCA Method predicts a higher positive moment than does the NCHRP 322 method.

A designer is then faced with a difficult decision: which method should be used for the design? One procedure that practicing engineers use is to design using both methods and use the method that is most conservative. However, always using the most conservative method can at times produce designs with so much positive moment steel that the section can not be easily constructed. On the other hand, recommending a less conservative design is sometimes difficult if not impossible for a practicing engineer to do without assurances that the method producing the design is backed by sound engineering. Therefore, it is desirable to understand what influences the different design methods and why they can at times predict significantly different moments.

## **Overview of Previous Research**

Prior to the testing phase of this project, a literature review was performed to determine the current state of practice. This review, and additional information not contained in this document, can be found in Newhouse (2005). This document is available online at <http://scholar.lib.vt.edu>.

### **PURPOSE AND SCOPE**

#### **Purpose**

The purpose of this research was to obtain a better understanding of the behavior of precast, prestressed girders made continuous with a continuity diaphragm. Through a better understanding of the behavior of this type of structural system, recommendations can be made to improve the current design practices. To achieve this overall purpose, five specific objectives were considered.

The first objective of the research was to develop and test several continuity diaphragm details for PCBT girder bridges, and propose an optimum continuity detail to VDOT. Six full-depth PCBT girders were fabricated and transferred to the Structures and Materials Laboratory at Virginia Tech in order to test three different continuity connections. The research included tests designed to determine the cracking moment of the different continuity connections. Also, the ability of the connection to remain serviceable when exposed to cyclic loads was investigated.

The second objective was to monitor the fabrication of the girders during the steam curing process so that the influence of the curing process on the behavior of the girders could be determined.

A third objective of the research was to investigate the influences of the creep, shrinkage, and temperature on the behavior of the continuous structural system. Shrinkage specimens for the deck concrete were made and monitored for each test. Thermocouples were placed within the girders and the deck to monitor changes in temperature during the curing process. The end reactions were closely monitored during the deck curing phase so that the influences of the heat of hydration and shrinkage could be better understood. In the most recent work performed for the NCHRP 519 project, it was found that the curing process has a significant influence on the development of restraint moments which has generally not been considered (Miller et al. 2004).

A fourth objective was to investigate the effective continuity that can be achieved with the continuity connection. End reactions and member deflections were recorded for every test to determine the ability of the connection to transfer moments. The ability of the connections to transfer loads over an expected 10,000 thermal cycles was also investigated.

A fifth objective was to determine the structural model that best predicts the behavior of the composite structural system, and the most appropriate method for establishing the design moments for the continuous system, including thermal restraint moments.

## Scope

The scope of the research addressed the entire life of precast, prestressed PCBT girders made continuous. The presentation of the research is organized into four phases: the design phase, the fabrication phase, the static phase, and the service/cyclic phase.

From the analytical study, three continuity connections were developed for testing. The first two continuity sections tested had a full continuity diaphragm with a cast-in-place deck. To connect the bottom of the girders to the diaphragm in tension, Test 1 used extended prestressing strands extending from the bottom of the girders and bent at a 90 degree angle while Test 2 used extended 180 degree No. 6 U bars extending from the bottom of the girders. The third continuity connection tested, Test 3 consisted of a slab only, cast continuous over the girders.

At the fabricator, six full-depth PCBT-45 girders, each 15 ft, 4 in long, were instrumented and monitored during steam curing and detensioning. Concrete cylinders and beam specimens were made to determine material properties of the concrete. The girders were then shipped to Virginia Tech where the girders for each test were connected with the different continuity diaphragms. The continuous systems were monitored throughout all stages to obtain a better understanding of the early age development of restraint moments. After the concrete decks had reached 28 day strength, service moments were applied to the continuity diaphragm connections to determine the initial cracking moment. Cyclic loads were then applied to determine how much the stiffness of the connections degraded over time. Finally, the sections were loaded to near ultimate conditions to determine the ultimate moment capacities.

### Design Phase

This phase included an analytical study that was performed to determine the influence that design methods and assumptions have on the final design loads. This study is summarized in the paper *Influences of Design Methods and Assumptions on Continuity Moments in Multi-Girder Bridges*, which is included in the work by Newhouse (2005).

### Fabrication Phase

This phase began when six full-depth, PCBT specimens were fabricated with different positive moment end connections in order to test the strength and serviceability of three different continuity connections. At the fabricator, vibrating wire gauges (VWG) and thermocouples were installed and monitored with a Campbell CR23X data collection system. The gauges were monitored throughout both the steam curing process and detensioning of the strands.

### Static Phase

The six specimens were then transported to the Structures and Materials Laboratory at Virginia Tech. For each of the three tests, two beams were placed end to end. Once positioned, formwork and reinforcing steel were placed to connect the specimens with a diaphragm and a continuous 6 ft wide and 7 ½ in deep deck was cast, beginning the static phase. Electrical resistance gauges in the deck, vibrating wire gauges in the girders, and end reactions were

monitored in order to document the effects of the heat of hydration and shrinkage of the deck on the composite system. After a week of curing, the formwork was removed and the system was monitored until the deck concrete reached at least its design strength of 4 ksi.

### **Service/Cyclic Phase**

This phase began when transfer beams were placed across the top of the specimens at the passive end and the center and bolted down to the reaction floor. The support for the active end was removed and a frame with an MTS actuator was moved in place over the support. The actuator was attached to the end of the specimen with collar beams and a series of service and cyclic tests were performed to determine the cracking moment of the composite system at the diaphragm and the ability of the system to maintain integrity over 10,000 load cycles. Finally, the system was taken to near failure.

## **METHODS AND MATERIALS**

### **Analytical Review**

An analytic review was performed to predict the restraint moments that may occur in typical girder and slab systems using the PCBT sections. This was required to determine which girder and slab systems should be tested and to investigate the restraint moments which are predicted using several different analysis methods. Five different methods were used to predict these moments. Details of the prediction models and a design example are in the work by Newhouse (2005). The predicted moments were used to establish the design moments used for the experimental study.

PCBT-45 sections were investigated in this study. It was found that the smallest beam spacing of 6 ft-0 in would create the largest positive moments. This makes sense since it is expected that larger beam spacings, and hence larger area of deck per girder, will result in greater differential shrinkage forces and creep due to dead loads. Since both of these loads reduce the positive moment at the continuity connection, the smallest beam spacing will cause the largest positive moment.

It was decided to select a span length which would require less than the absolute maximum number of strands that could be placed in the section. A PCBT-45 section with 28 strands was found to work well at a span length of 80 ft. VDOT provided preliminary design tables which indicated that for a 28 strand pattern, a span length of 85 ft could be achieved. However, it was decided to model a slightly shorter span arrangement because shorter spans will provide for the potential for more positive moment (for a given number of strands). Therefore, the analytic review resulted in a model of a two span continuous system, each span being 80 ft in length, with a PCBT-45 precast, prestressed girder and a 7 ½ in slab that is 6 ft-0 in wide. A 1 ½ in bolster was assumed to be present over the top of the top flange.

Based on current recommendations (Hastak et al. 2003), the positive and negative cracking moments were calculated using gross properties of the composite section. The composite section used for the calculations was based on the full width of the deck (6 ft-0 in)

with a modular ratio of 1.0. The full area of the girder with a 1 ½ in bolster was also used. The cracking stress of the concrete for determining both the positive and the negative cracking moments was taken as 7.5 times the square root of the 28 day compressive strength of the diaphragm concrete, 4,000 psi.

Moments due to creep, shrinkage, and temperature were calculated and averaged for the different methods. The live loads were determined using SAP2000 assuming a two span continuous structure with 80 ft-0 in spans. A summary of the design loads that were used for testing is presented in Table 1. Live loads are shown for the negative case only, but were checked for different span arrangements for the positive case and found not to control. Both HS-20 and lane loading were investigated to produce the maximum loading. The composite dead loads provided by VDOT were reduced by a factor of 2 so that they would not reduce the predicted positive moments.

**Table 1. Design Moments for Specimens**  
**Design Moments at Interior Support, k-ft**

Type		Calculated Value	Factor				
			1.2	1	0.75	0.5	0.25
Positive	Cracking	524	629	524	393	262	131
	Ult. Cap. – Test 1	711					
	Ult. Cap. – Test 2	773					
	Restraint	205					
	Thermal	442					
Negative	Cracking	-919	-1103	-919	-689	-460	-230
	Ult. Cap. – Test 1	-2654					
	Ult. Cap. – Test 2	-2654					
	Restraint	-1127					
	Thermal	-105					
	Live Load	-531/0					

### Overview of Testing

Figure 1 shows a timeline that summarizes the testing that was performed for each of the three tests. The age of the girder is shown along the top of the timeline and the age of the deck placed on the girder for each test is shown along the bottom of the timeline.

### Fabrication Phase

The six girder specimens, named VT1 through VT6, were fabricated by Bayshore Concrete Products, Inc., at their Chesapeake, Virginia, plant. The shop drawing showing the complete bed layout and girder details is presented in Newhouse (2005). Important details of the diaphragms are presented in Figures 36 through 38. A typical sequence of construction usually begins with jacking the strands and placing the reinforcing steel within the bed on the first day. Within 24 to 48 hours from jacking the strands, the concrete for all members within the bed is placed. Steam curing begins and occurs for 12 to 18 hours, the forms are stripped and the strands

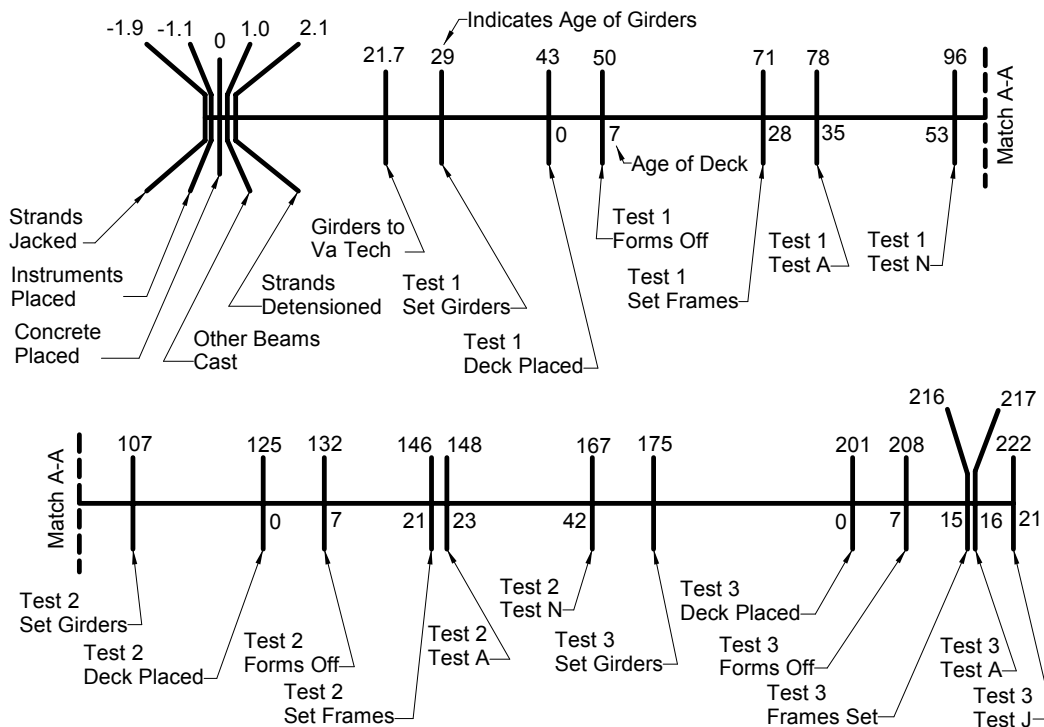


**Figure 1. Timeline of Events (in days)**

are released the following day. Often, the entire process can occur within a time period of two days. For this project, several things occurred during the fabrication phase that were not typical for the construction of prestressed girders (see the timeline in Figure 1.) A complete log of the events in the casting yard is presented in Newhouse (2002). First, the six specimens were only part of the pour; three larger beams were included in the same bed. The concrete for the beam specimens was cast one day and the concrete for the other beams was cast the following day. The strands were approximately four days old at the time of detensioning (the concrete was 2.1 days old), instead of the typical two days old. Type II cement was used because of the scarcity of the Type III cement which is typically used. Table 2 shows the mix design for a 5.0 cubic yard mix used for construction of the girders. Newcem is a slag cement, Daravair is an air entraining agent, Sika 6100 is a superplasticizer, Plastiment is a water reducing admixture, and DCI-S is a corrosion inhibitor.

During the casting operations, vibrating wire gauges and thermocouples were installed in the girders. The locations of the vibrating wire gauges are presented in Figure 2. The embedded instrumentation was connected to a data acquisition system and monitored during curing and detensioning.

**Table 2. Mix Design for Girder Concrete**

5.00 Cubic Yard Batch					
Material	Quantity		Admixture	Quantity	
Sand	6187	lb	Daravair	30	oz
No 57 Stone	9040	lb	Sika 6100	233	oz
Type II Cement	2325	lb	Plastiment	117	oz
Newcem	1550	lb	DCI-S	1280	oz
Water	94	gal			

### **Static Phase**

The purpose of the static phase testing was to monitor and record early age changes in the reactions of the two girders made continuous in order to estimate the magnitude of the early age restraint moments that develop. The electrical resistance gauges in the deck and the vibrating wire gauges in the girder were recorded to determine the changes in strain. Thermocouples placed within the girders and the decks were monitored so that the magnitude of the thermal gradients could be determined. Two shrinkage specimens were cast with the deck concrete in order to monitor shrinkage of the deck. To confirm movements, dial gauges were placed under the girders and monitored.

Figure 2 shows the test setups used for the static phase. Under the passive end, two 50-kip load cells were placed and under the active end, two 10-kip load cells were placed. With this arrangement, the overall stability seemed adequate and the end reactions could be measured accurately. To reduce the weight to facilitate easy specimen removal, the slabs were cast approximately 9 ft-6 in from the interior ends of the girders, instead of over the full length of the girder.

Once the beams were set in place, formwork was installed as can be seen in Figure 3. To follow the same procedures used by most contractors, the deck forms were supported from the girders and the continuity diaphragm forms were supported from the reaction floor. Once the formwork was in place, the reinforcing steel for the deck was placed. The steel was supported on high chairs and tied together with wire ties.

End forms were constructed of Plyform with holes drilled at the location of the longitudinal steel to so that the steel could extend beyond the ends of the slab. The top two center bars were gauged with electrical resistance gauges. A maximum number of gauges that could be read by the two switch and balance units were installed. Near the center, two gauges were placed side by side in order to obtain a backup reading in case one of the gauges failed. Three thermocouples were placed in the center of the active span above the center of the girders and three were placed in the center of the active span 3 in from the outside edge. The thermocouples were placed in the center of the deck vertically and ½ in from the top and bottom of the deck.

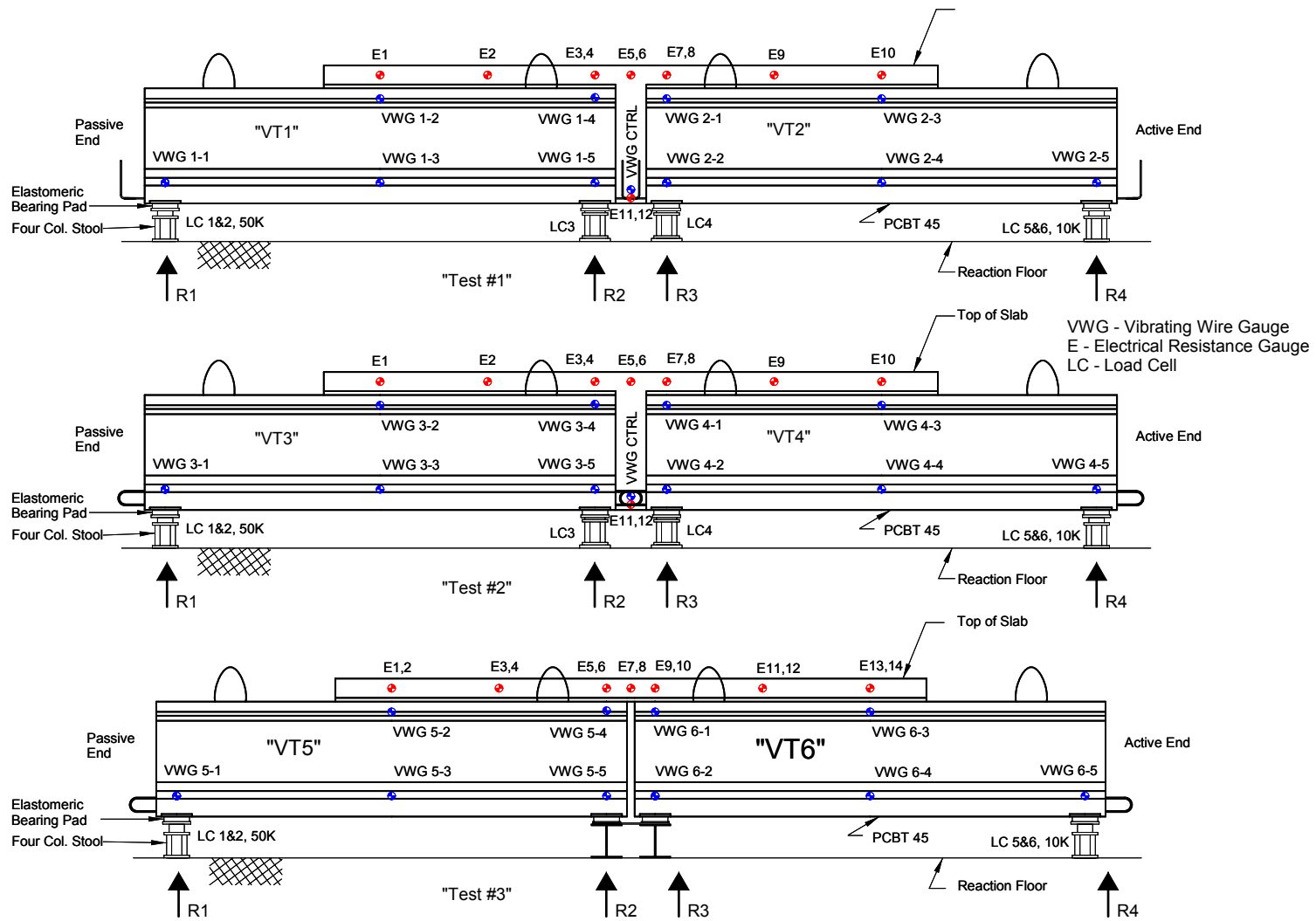


Figure 2. Static Phase Test Setup

In preparation for casting the deck, the vibrating wire gauges were attached to the homemade vibrating wire gauge switch box and the electrical resistance gauges were attached to the two switch and balance units. The load cells were also attached to the switch and balance units.

Table 3 shows the mix design for the deck concrete. The deck concrete for all three tests was the same mix, a Class A-4 General Use mix with a target slump of 2-4 in and a target air content of 6 +/- 1 percent. Sika AE is an air entraining admixture. To ensure workability, the actual slump used for all tests was 5 +/- 0.5 in.

**Table 3. Mix Design for Deck Concrete**

1.00 Cubic Yard Batch					
Material	Quantity		Material	Quantity	
Sand	1317	lb	Pozzolans	317	lbs
#57 Stone	1741	lb	Water	34.3	gals
Type I/II Cement	318	lb	Sika AE	2-4	oz

Figure 3 shows an overall test setup with the formwork in place for Test 2. The setups for Test 1 and Test 2 were similar, with the only difference being the details of the continuity connection. For Test 1, the bottom level of 12 prestressing strands was extended 9 in out and bent up at a 90 degree angle an additional 15 in. The beams were placed 12 in apart and the continuity diaphragm was cast flush with the ends of the girders. In other words, there was no embedment of the girders into the diaphragms. For Test 2, 4 No. 6 mild reinforcing bars each bent 180 degrees extended 11 in from the end of the girders. The beams were placed 13 in apart and the continuity diaphragm was cast flush with the ends of the girders. For Test 3, no continuity diaphragm was provided at the interior supports. The girders were placed approximately 3 in apart and the deck was cast continuous over the opening.



**Figure 3. Overall Test Setup**

Figure 4 shows a close up of the continuity diaphragm with part of the formwork in place and the different connections used for Test 1 and Test 2. Figure 5 shows details of the reinforcing which was used for both the deck and the continuity diaphragm.

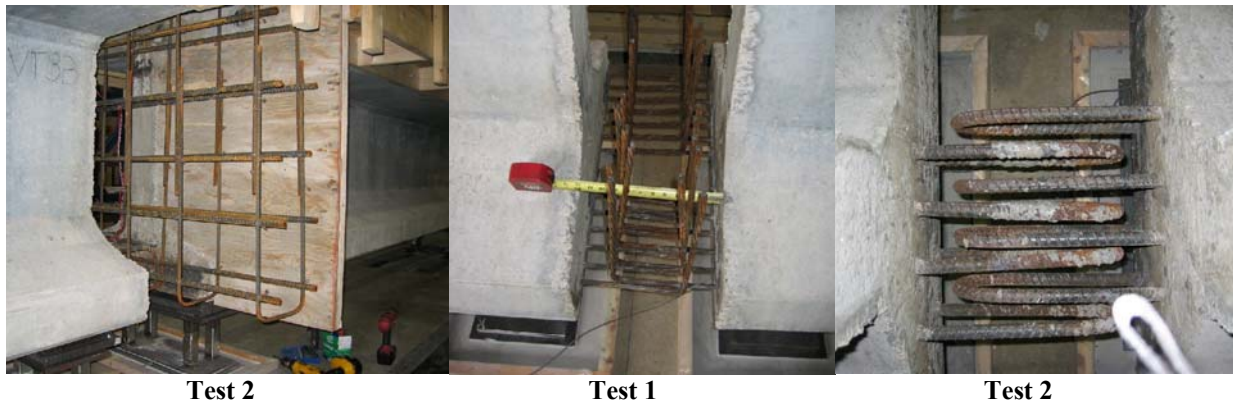


Figure 4. Details of Continuity Diaphragm

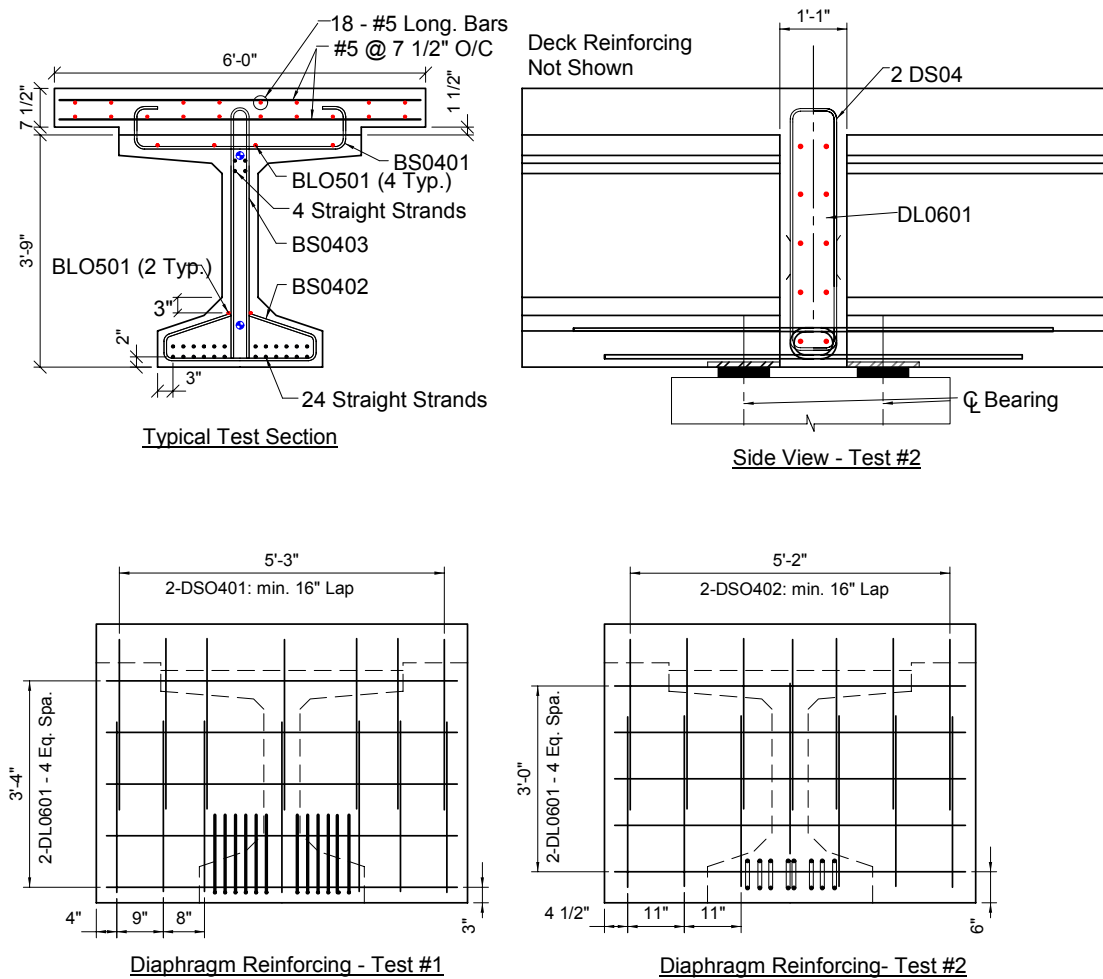


Figure 5. Reinforcing Details for Tests

## Service/Cyclic Loading Phase

The purpose of the service loading phase for Test 1 and Test 2 was to determine the positive moment at the girder and diaphragm interface that would cause initial cracking,  $M_{cr}$ . Since positive moment connections are more difficult to construct than negative moment connections, the first cracking at the interface due to positive moment was investigated. Also, the ability of the diaphragm connection to resist service moments of at least 1.2 times the anticipated cracking moment of the section was investigated. For Test 3, the negative moment that caused first cracking was determined. The purpose of the cyclic loading phase was to subject the connections to 10,000 cyclic loads caused by positive and negative thermal gradients and to measure the degradation of the connections over the cycles. It was anticipated that most transportation structures would not encounter more than 10,000 maximum thermal cycles throughout a 75 year service life.

Figure 6 shows the typical setup for each of the three tests. After the deck and diaphragm concrete had reached at least 4,000 psi, the end blocks were placed on both the active and passive ends and 9x14x2 in elastomeric bearing pads were placed above the supports at the interior of the setup. At the passive end, a W18x76 transfer beam was placed across the top of the end block and bolted down to the reaction floor beam with four 1 in diameter all-thread rods at each end. In the center of the setup, spacer plates were placed on top of the elastomeric pads and a W10x33 short transfer member was placed longitudinally on top of the spacer plates. A second W18x76 transfer beam was then placed perpendicularly across the top of the W10 transfer member and bolted down to the reaction floor beam also with a total of eight 1 in diameter all threaded rods. At the active end, two hydraulic jacks were placed under the girder and the end was lifted just enough to remove the active end bearing assembly. The frame supporting the MTS ram was then moved into position so that the ram was directly over the bearing at the active end. Two W10x88 collar beams were then clamped to the end of the beam with two 1 in diameter all-thread rods on each side. The top collar beam was bolted to the bottom of the MTS ram, thereby attaching the active end of the beam to the ram. The active end was temporarily supported with the jacks until testing began.

Prior to each test, the wires for the electrical resistance gauges were removed from the switch and balance units and attached to the System 5000 data recorder. Also, to measure vertical displacements, wirepots were installed at the ends of the beams and at the center of the diaphragm and were attached to the System 5000. To measure the opening of the crack at the girder-diaphragm interface, LVDTs were installed at approximately 1 in from the bottom of the end of the beam for Test 1 and Test 2. For Test 3, the LVDTs were installed at the bottom of the interior ends of the beams and near the top of the web for the beams. The LVDTs and the cable attached to the MTS system were also attached to the System 5000. Figure 8 shows the LVDTs in place at the bottom of the girder/diaphragm interface for Test 3.

The following steps outline the typical procedure that was used for each of the service and cyclic tests:



6. For the service phase tests, the load on the MTS system was increased to the first recording point and all sensors were recorded with the software. Also, the dial gauges, load cells, and vibrating wire gauges were recorded.
7. For the cyclic phase tests, the MTS system was set to run the first 1000 or 2000 cycles. The DC set point was set to the average of the predetermined load range and the frequency was adjusted to 0.25 Hertz. The program was then set to Run.
8. After the cycles were complete, the set point was taken back to 0.0 kips and all the sensors were recorded. The active end of the specimen was then loaded to produce certain percentages of the cracking moment, such as 0.25, 0.5, 0.75, 1.0, 0.5, 0.0 and the sensors were recorded at the different load values.
9. After the final reading, again with a DC set point load of 0.0 kips, the hydraulic jacks were pumped up to support the active end and the MTS system was turned off.

Since there was no continuity connection for Test 3, the active end could not be allowed to cantilever. The jacks were left in place until the MTS system was turned on and allowed to support the active end. For the first two tests, load control was used and the end was loaded up to a given load. For the remainder of the tests, displacement control was used, allowing the active end to be moved up and down a predetermined displacement.

## **Material Testing**

### **Concrete Testing**

The concrete material tests were performed to determine the actual compressive strength,  $f'_c$ , the split tensile strength,  $f_t$ , the flexural beam strength,  $f_r$ , and the modulus of elasticity,  $E_c$ , at different ages for the girder and the deck concretes so that the actual values of these properties could be used in calculations.

All of the specimens made at the fabricator were placed alongside the girders so that they would receive the same steam curing that the girders received. The specimens made for the decks were covered with plastic and kept covered for 7 days, the same amount of time that a conventional deck is covered. At the time that the prestressing strands were released, the cylinders made for the girders were transported from the fabricator to Virginia Tech where they were stored outdoors.

### **Shrinkage Testing**

Shrinkage specimens were made for each of the three decks. To better match the volume to surface ratio of an actual deck, the specimens were made 6 in by 6 in by 11 in. After removal from the forms, the sides and ends of the specimens were sprayed with a sealant to prevent evaporation. Whittemore points or Demec points were installed at an 8 in gauge length to monitor the shrinkage of the specimens during the static phase.

For Test 1, Whittemore points were installed in the shrinkage specimens while the concrete was still plastic. The concrete was then allowed to cure the full 7 days prior to taking the first readings. It was decided that readings prior to 7 days would be useful, therefore, for

Test 2, the Whittemore points were installed while the concrete was still plastic, but readings commenced as soon as the concrete had gained sufficient strength to ensure that the points were secure in the concrete. Since difficulty was encountered taking the readings for both of the first two tests, Demec points were attached to the surface of the specimens for Test 3 with epoxy. These points have a much smaller hole in the center which was found to enable a more consistent reading with the Whittemore gauge. Readings commenced for Test 3 as soon as the concrete and the epoxy had set.

### **Mild Steel Testing**

The purpose of the mild steel testing was to determine the actual properties for a sample of the reinforcing bars used in the deck. Testing was done in accordance to the requirements of ASTM A 370 (1997). The yield strength,  $F_y$ , the tensile strength,  $F_u$ , and the modulus of elasticity,  $E_s$ , were determined from the tests.

### **Prestressing Steel Testing**

The purpose of the prestressing steel testing was to determine the actual properties for a sample of the prestressing steel used for the fabrication of the six girders. Similar to the mild steel, the testing was done in accordance with the requirements of ASTM A 370 (1997). The maximum tensile strength,  $f_{pu}$ , and the modulus of elasticity,  $E_p$ , are determined in the same manner as is used for the mild steel. Since the yield strength of prestressing steel is not as distinct as the yield strength of mild reinforcing steel, the procedure in Appendix A7 of ASTM A 370 (1997) was used for determining the yield strength.

Three specimens of the  $\frac{1}{2}$  in diameter steel used in the fabrication of the beams were tested. Since a 24 in extensometer was not available for testing, the exact procedures of the ASTM could not be followed and elongation values were not obtained. The three specimens were cut to 40 in, which allowed for a 20 in length between the V-grips. The ends of the strands were wrapped with aluminum foil to aid in gripping. The strands were then placed in the testing machine and a 2 in gauge length extensometer was installed at the beginning of each test. The specimens were loaded in tension at a rate of 40,000 psi/minute until the approximate yielding occurred, then the test machine was switched to a position controlled loading that raised the tension head at a rate of 0.5 in/minute. To avoid damage, the extensometer was removed after yielding occurred.

### **Measurement Techniques**

#### *Load Cells*

In order to measure the changes in reactions during the static phase, load cells were used under the elastomeric bearings and steel bearing plates. Since the readings were taken over a period of up to 1 month, it was decided to measure the reactions with a P-3500 strain indicator hooked up to two switch and balance units. Each balance unit allows for reading 10 channels; therefore, a total of 20 channels could be read with the system.

## *Vibrating Wire Gauges*

Geokon Model 4200 vibrating wire gauges (VWG) were chosen for installation in the girder specimens and at the center of the diaphragm connection for Tests 1 and 2. Figure 7 shows the model 4200 gauge attached to a No. 3 bar with wood spacer blocks and ties ready for installation in the girder. These gauges were chosen because of their ability to provide reliable readings of strain when embedded in concrete.

During the fabrication phase, the VWGs were read using the CR23X Micrologger. Since the wire used inside of the gauges is made out of metal, the coefficient of thermal expansion of the wire and the surrounding concrete are different. The manufacture recommends correcting for this by adding a term to correct the actual (apparent) reading. Each gauge has a thermistor which records the gauge temperature in °C.

The vibrating wire gauges measure changes in compression as a negative number and changes in tension as positive number. The manufacturer recommends using a value for the coefficient of thermal expansion for the wire,  $C_1$ , of 12.2 microstrain/°C (6.78 microstrain/°F), and for the concrete,  $C_2$ , of 10.4 microstrain/°C (5.78 microstrain/°F). If the temperature changes from an initial reading ( $T_0$ ) to a final reading ( $T_1$ ), the correction for temperature is given as:

$$(T_1 - T_0)(C_1 - C_2) \quad (1)$$



**Figure 7. Vibrating Wire Gauge**

One 6 in by 12 in control cylinder was cast during the fabrication phase with a vibrating wire gauge located in the center of the specimen along the vertical axis of the cylinder. When the recommended correction for temperature is made, the change in strain for a specimen that undergoes only thermal movements should be zero. To confirm that this is actually the case, two experiments were conducted to test the ability of the vibrating wire gauges to correctly compensate for changes in temperature.

The purpose of the first experiment was to determine the actual coefficient of thermal expansion for the concrete being used. Four cylinders, one from deck 1, one from deck 2, and two from the girders, were instrumented with Demec points at a 6 in gauge length. The cylinders were then placed in an oven at 110 °C for 20 hours. The cylinders were then allowed to cool to room temperature overnight, and a series of readings at different temperatures were made using the Whittemore gauge.

The purpose of the second experiment was to confirm the temperature correction formula of the vibrating wire gauges. The strain reading of the control cylinder with the vibrating wire gauge was recorded at room temperature. The cylinder was then subjected to different temperatures by heating in an oven and cooling in a refrigerator and/or a freezer. Once the cylinder reached the equilibrium temperature, the strain reading and the thermistors were recorded. To confirm the operation of the gauge, the control cylinder was also loaded in the Satec UTM and strain readings were recorded at different load levels.

### *Electrical Resistance Gauges*

Conventional electrical resistance gauges were used on the longitudinal reinforcing in the deck for all tests and on a stirrup located near the bottom of the continuity connection for Test 1 and Test 2. For the static phase, the gauges were recorded with the P-3500 strain indicator and the switch and balance units. For the service and cyclic phase, the gauges were recorded with the StrainSmart software. For all gauges used on the reinforcing steel, 350 ohm gauges were used.

### *Displacements*

During the static and cyclic phase, four methods were used to monitor deflections of the test specimen. Three of the methods used the StrainSmart software and the System 5000 to monitor the gauges. For the first method, end deflections were monitored with Celesco position transducer wirepots. The wirepots have a 10 in measurement range and were attached to the underside of the ends of the girder with magnets.

The second method used Trans-Tek series 350 gaging transducers, commonly called LVDTs or barrels, to measure the crack openings at the bottom of the girder and diaphragm interface for Test 1 and Test 2, and to measure relative girder end movements at the bottom of the girders and near the top of the web for Test 3. Figure 8 shows one of these LVDTs.

The third method used the output from the MTS 458.10 MicroConsole to give the actual active end displacement as determined by the MTS loading ram.

To confirm the electronic measuring devices, the fourth method used conventional dial gauges capable of reading 0.001 in. Under the girder, a dial gauge with a 2 in stroke was used at the active end and gauges with a 1 in stroke were used at the other locations. Dial gauges were also placed at the end of girder and diaphragm interface for Test 2 and at the ends of the girders at the center for Test 3.



**Figure 8. LVDT Used in Static and Cyclic Tests**

### *Thermocouples*

Type TT-T-20-SLE thermocouple wire, with a positive blue wire (copper) and a negative red wire (constantan), was used. The ends of the wire were twisted together and soldered with a silver solder to produce the thermocouple. In order to attach to the HH21 microprocessor, type NMP mini connectors were attached to the wire allowing the ends to be plugged into the thermocouple reader.

## **RESULTS**

### **Laboratory Results**

#### **Concrete Testing Overview**

Figure 9 shows the averaged measured compressive strength and the modulus of elasticity/1000 in ksi for the concrete in the girders. The concrete for the girders gained strength rapidly, reaching the specified 28 day strength of 8 ksi at an age of approximately 3 days. Also, the modulus of elasticity reached the predicted value of 57 times the square root of the actual compressive strength by the time of the release of strands at 2.1 days. Multiple tests were made at a given time and all data points presented are averaged values. For compressive strength and modulus of elasticity tests, each data point is the average of 2 to 4 tests. For the split cylinder and the flexural beam tests, each data point is usually the average of 2 tests.

Figure 10 shows the results of the split cylinder and the flexural beam testing for the girder concrete. Typically, the flexural beam tests produce results as much as 20-50 percent higher than the split cylinder tests (MacGregor, 1997). However, none of the tests were this much higher. For tests performed at 5, 28, and 222 days, the flexural beam tests were 1.14, 0.95, and 1.04 times the split cylinder tests. The values for both of the tests remained fairly constant over the course of testing. Split cylinder testing has become more common because it is easier.

Figure 11 shows the development of the compressive strength, the modulus of elasticity, and the split tensile strength for each of the separate deck concretes. The same mix was ordered for all three tests and the slumps at the time of placing the decks were all within 5 in +/- 0.5 in. The concrete for Tests 1 and 2 developed similar compressive and split cylinder strengths throughout the testing. The modulus of elasticity of the concrete in Test 2 developed more slowly than it did in Test 1, but at approximately 28 days, reached the same value. Generally, all properties for the concrete in Test 3 developed more slowly and were lower at a given concrete age than the same properties for Tests 1 and 2. It is likely that although the same mix was ordered, a slightly different mix was provided. The average of two tests was used for each data point, and the data points are connected to show the trend.

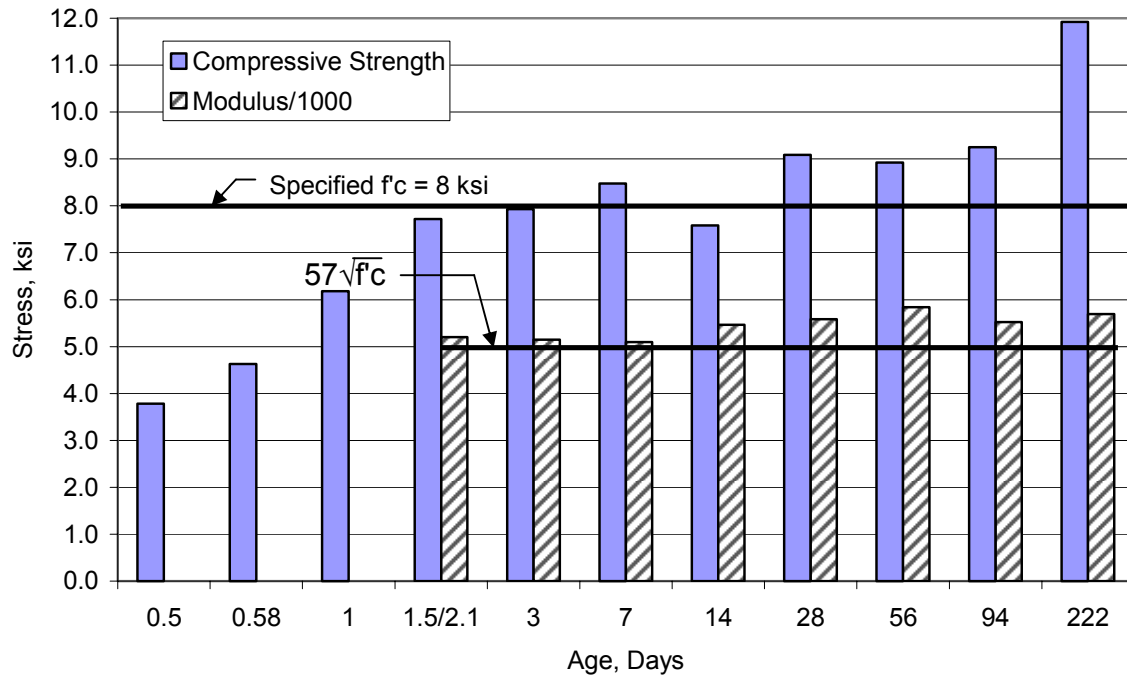
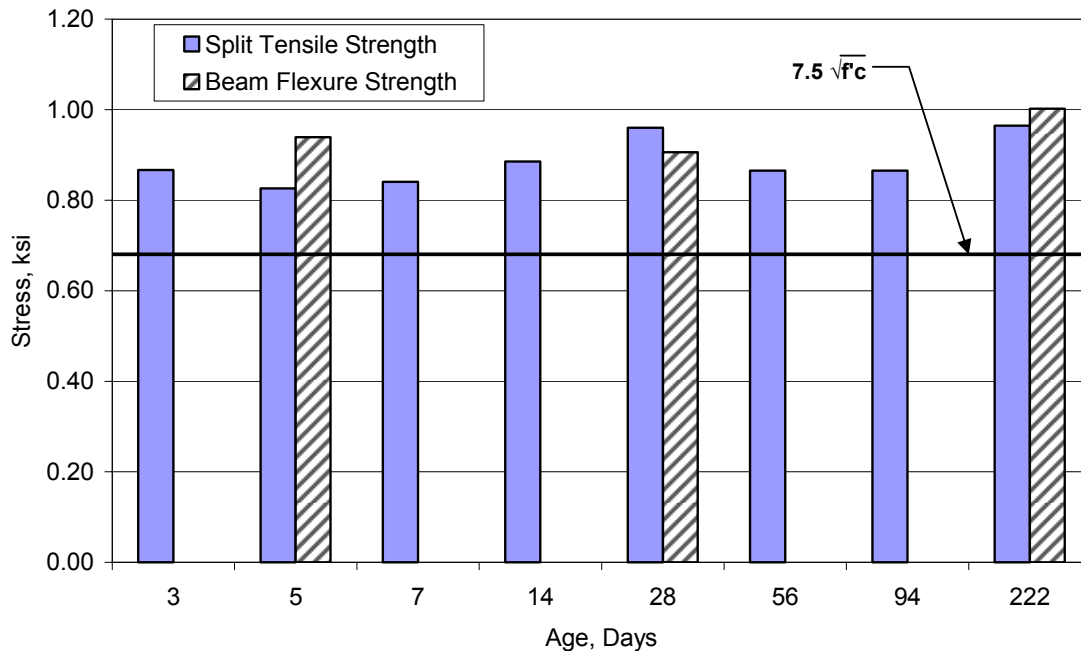


Figure 9. Girder Concrete Compressive Strength and Modulus Results

### Shrinkage Testing

Figure 12 and Figure 13 show the results of the shrinkage tests for all three tests as well as the predicted shrinkage from ACI 209 and MC-90 (CEB 1990). Figure 12 shows the cumulative shrinkage strain from the time of the first reading while Figure 13 shows the cumulative shrinkage strain from the end of the moist curing which was at 7 days.

The results indicate that the MC-90 predicted shrinkage is much less at the early ages of the deck than actually observed. Both the ACI-209 and MC-90 predict similar ultimate shrinkage values at 10,000 days, 521 and 505 microstrain respectively, but it is clear that at the early ages, the MC-90 predicts much lower shrinkage. The ACI-209 prediction is similar to the results of Test 1, both approximately 200 microstrains of shrinkage at 28 days.



**Figure 10. Girder Concrete Split Cylinder and Flexural Beam Results**

Considering the shrinkage that occurred from the 7 day cure period, Test 2 displayed shrinkage of approximately 275 microstrain at 28 days while ACI 209 predicts 200 microstrain and MC-90 predicts only approximately 80 microstrain of shrinkage.

Test 3, unlike Test 2, showed positive shrinkage values for approximately the first 8 days. This indicates that expansion of the specimen occurred during this period. This is certainly possible since the results of the static phase tests showed that the end reactions first increase, indicating an expansion at the top of the composite section. There is not enough data to make any definitive conclusions about the shrinkage testing, but it is evident that the actual shrinkage that occurs during the early ages of curing may vary a great deal from batch to batch.

## **Mild Steel and Prestressing Steel Testing**

### *Mild Steel Testing*

Three samples of the No. 5 reinforcing bars used for the deck reinforcing were tested. The results of these tests are shown in Table 4. All of the specimens displayed a distinct linear region after the V-grips had settled into place and firmly gripped the specimens. The modulus of elasticity was calculated over the linear range of the stress versus the strain plot for a stress from 15 ksi to 55 ksi by determining the best fit line over this region. The slope of this line is the modulus of elasticity.

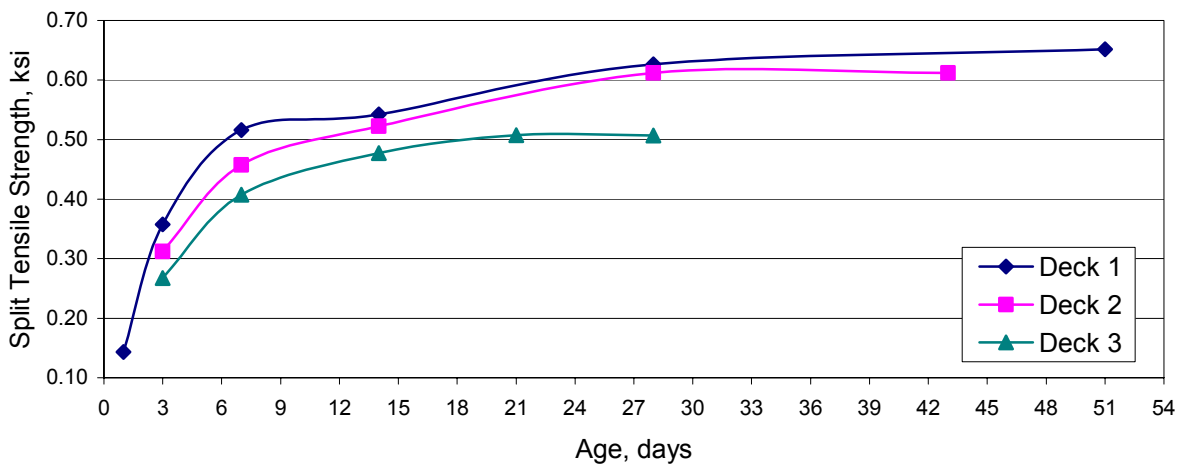
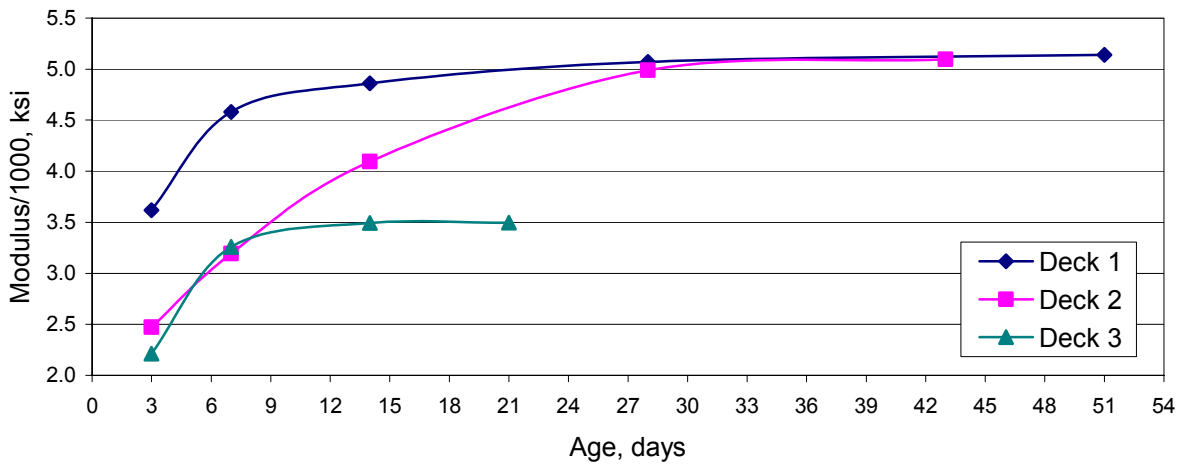
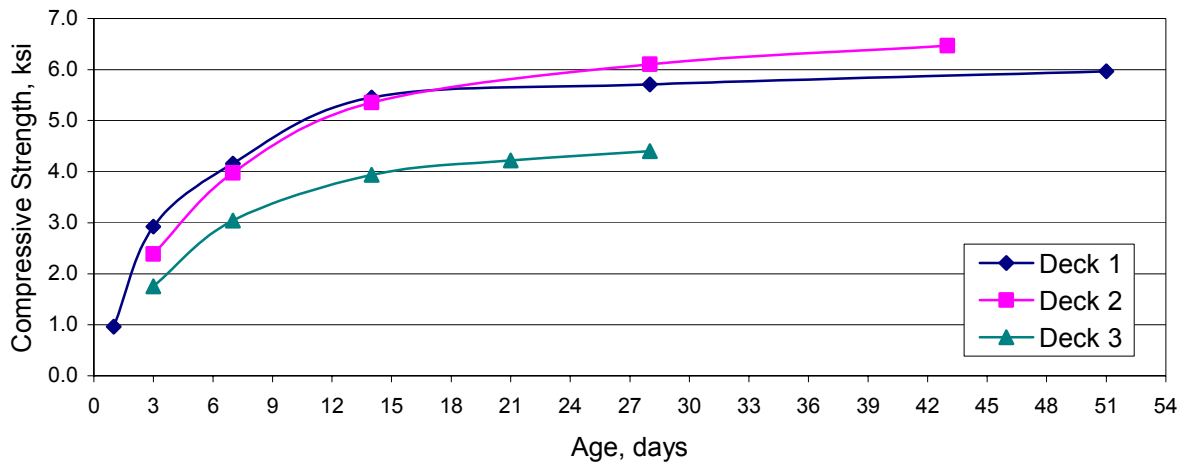


Figure 11. Deck Concrete Test Results

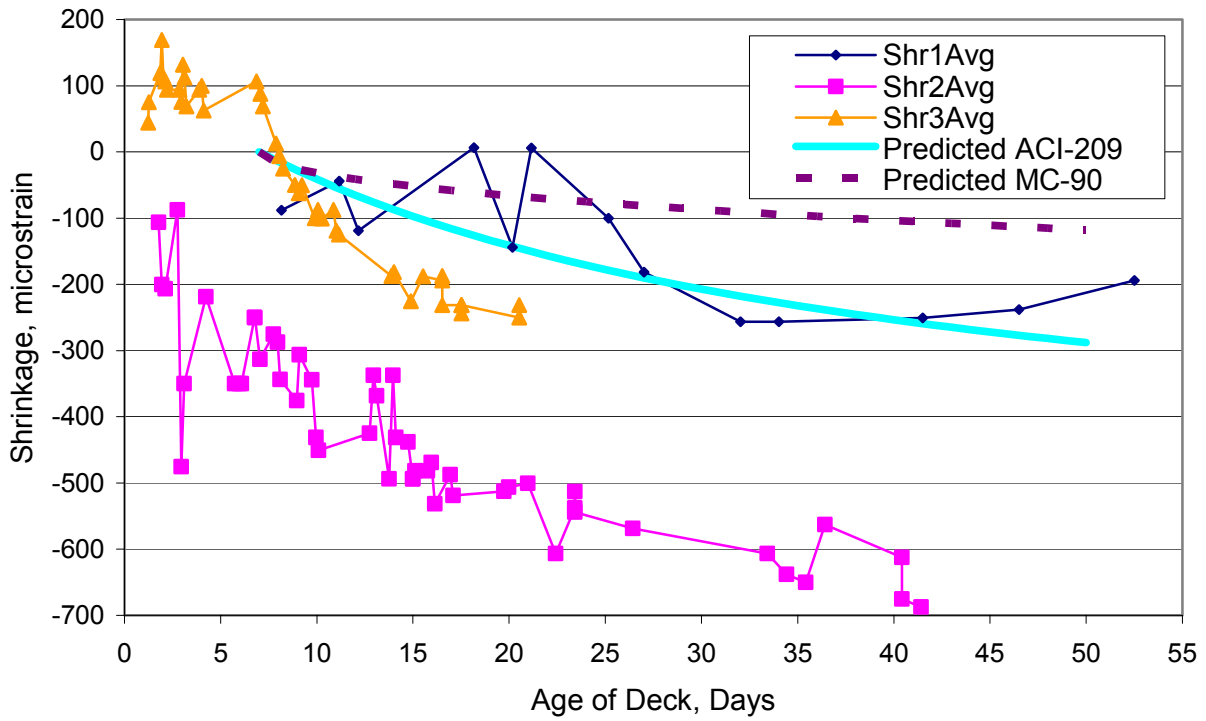


Figure 12. Shrinkage From Earliest Readings

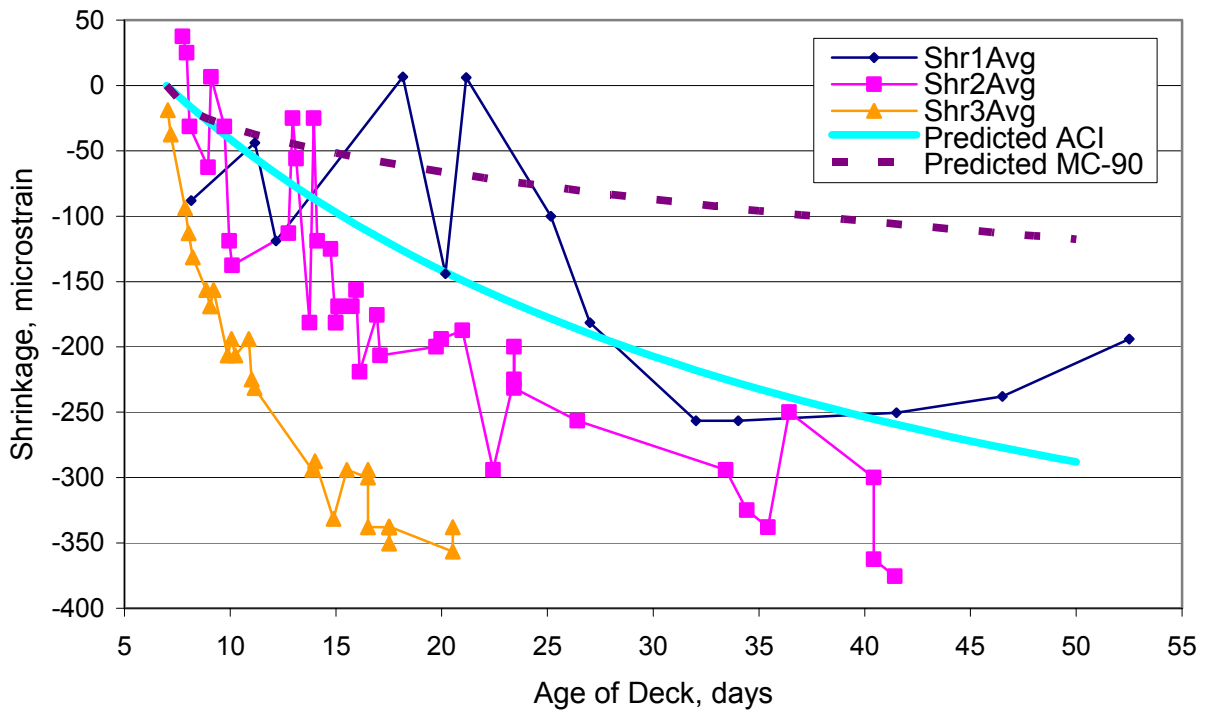


Figure 13. Shrinkage From 7 Day Cure

The tensile strength, yield strength, and elongation values all met the requirements of steel usually used in decks, ASTM A 615 (1996). The average modulus of elasticity was determined to be 27,700 ksi, which is slightly lower than the commonly used value of 29,000 ksi.

**Table 4. Summary of Mild Steel Reinforcing Properties**

<b>Bar Mark</b>	<b>Yield Strength ksi</b>	<b>Tensile Strength ksi</b>	<b>Mod. of Elasticity ksi</b>	<b>Percent Elongation %</b>
A	61.5	99.5	27,500	14
B	64.5	102.5	28,500	14
C	62.0	100.0	27,000	14
Average	<b>62.7</b>	<b>100.7</b>	<b>27,667</b>	<b>14</b>
Min. Required	60.0	90.0	N/A	9

### *Prestressing Steel Testing*

Three samples of the ½ in diameter grade 270 prestressing strands used for fabrication of the girders were tested. The results of these tests are shown in Table 5. All of the specimens displayed a distinct linear region after the V-grips had settled into place and firmly gripped the specimens. The modulus of elasticity was calculated over the linear range of the stress versus strain plot for a stress from 50 ksi to 200 ksi by determining the best fit line over this region.

**Table 5. Summary of Prestressing Steel Properties**

<b>Strand Mark</b>	<b>Yield Strength ksi</b>	<b>Tensile Strength ksi</b>	<b>Modulus of Elasticity ksi</b>
A	255	275	29,000
B	257	282	29,500
C	257	275	29,000
Average	<b>256</b>	<b>277</b>	<b>29,167</b>
Min. Required	243	270	N/A

The tensile strength, yield strength, and elongation values all met the requirements of strands usually used in girders, ASTM A 416 (1999). The average modulus of elasticity was determined to be 29,200 ksi, which is slightly higher than the commonly used range of 27,000 ksi to 28,500 ksi.

### **Fabrication Phase Results**

#### **Overview of Steam Curing**

Five thermocouples were installed in each girder as shown in Figure 14. Figure 2 shows the location of the vibrating wire gauges. Seven of the thermocouples in the girders and two additional ones within the prestressing bed were monitored and recorded at ten minute intervals with the Campbell CR23X during the fabrication of the girders. The remaining thermocouples were recorded periodically with the hand held HH21 reader. In addition to the thermocouples, the 31 thermistors within the vibrating wire gauges were monitored and recorded.

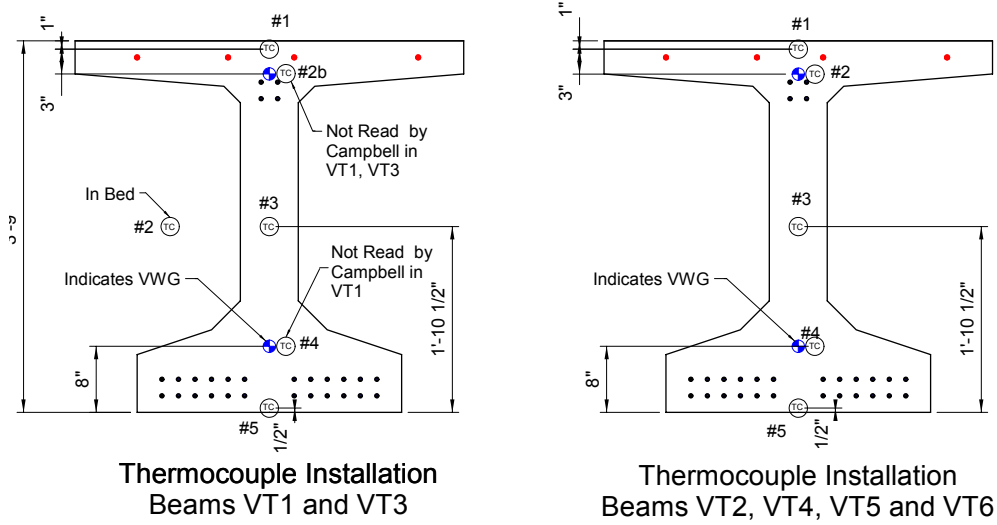


**Figure 14. Thermocouple and Vibrating Wire Gauge Locations**

According to both the Standard and LRFD AASHTO Specifications, application of the heat from the steam curing shall “increase at an average rate not exceeding 40°F per hour until curing temperature is reached.” Also, the “maximum curing temperature within the enclosure shall not exceed 160°F.” The steam shall be turned off in such a way so that bed temperature shall “not decrease at a rate to exceed 40°F per hour until a temperature 20°F above the temperature of the air to which the concrete will be exposed has been reached (AASHTO 2001, 2002).” The *PCI Bridge Design Manual* indicates that some codes allow a maximum concrete temperature of 190°F and that some producers allow temperatures to rise to 200°F (PCI 1997). The Bayshore Steam Schedule Sheet shows a maximum allowable rise of 40°F per hour and that the temperature in the bed is to be held between 145°F and 150°F.

### *Temperature Readings*

Figure 15 shows the minimum and maximum recorded thermocouple and thermistor readings recorded during the fabrication of the girders. Prior to placing the concrete, the average thermocouple reading had increased to 98°F, approximately 20°F higher than the ambient temperature when the strands were jacked the previous day. This increase in temperature prior to placing the concrete causes a loss in the prestress force prior to casting the concrete. Assuming a 365 ft bed length ( $L_0$ ) with approximately 28 ft of strand not exposed to the increased temperature ( $L_1 = 365 - 28 = 337$ ), and using the coefficient of thermal expansion of the prestressing steel,  $\alpha$ , of  $6.78 \mu\epsilon / ^\circ\text{F}$  ( $12.2 \mu\epsilon / ^\circ\text{C}$ ) and an increase in temperature ( $\Delta T$ ) of 20°F, the change in stress in the prestressing steel is given by:

$$\Delta f = \frac{E\alpha\Delta TL_1}{L_0} \quad (2)$$

which indicates a prestressing loss  $\Delta f = 3.6$  ksi may have occurred prior to casting the concrete. This loss is often not considered in design, primarily because the designer has no control over when a girder will be fabricated. If the temperature at the time of casting was lower than at the time the strands were jacked, then a gain in prestressing force would have occurred instead of a loss. This loss is approximately the same magnitude as the loss due to relaxation, which is considered in design. When combined with the relaxation loss, this loss may be significant. This is a type of loss that should be considered and adjusted for in the field at the time of fabrication.

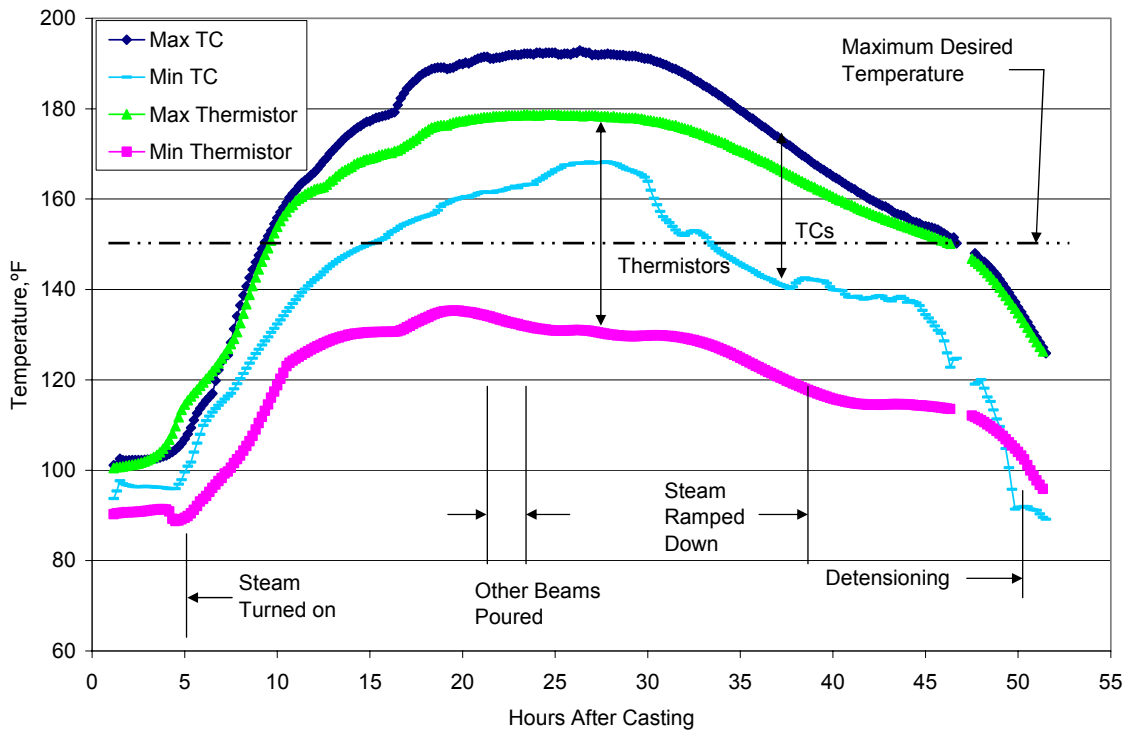


**Figure 15. Temperature Readings During Casting**

As shown in Figure 15, although the target curing temperature range established by the fabricator was between 145°F and 150°F, the actual temperatures in the bed and in the girders were higher. Two temperature gauges were placed through the tarps about mid-height of the specimens and monitored by the fabricator's quality control person. The maximum temperature recorded by these gauges was only 155°F. However, the hottest bed temperature recorded by the thermocouples and the thermistors was 190°F and the hottest concrete temperature recorded was 192°F. Actual temperatures were more than 40°F higher than the fabricator had anticipated. The highest recorded temperatures were in beam VT3, which was near the exit of a steam feed pipe. As expected, since the steam rises under the tarps, higher temperatures were recorded near the top of the specimens.

## *Vibrating Wire Gauge Readings*

The temperature correction for the vibrating wire gauges was considered using several approaches. Figure 16 shows the vibrating wire gauge readings in one location using three of the approaches. A positive reading indicates expansion while a negative reading indicates contraction. Also included is the average thermocouple reading within the girders recorded. Since the gauges were unstable during the casting and immediately after due to the external vibration, the first reading was taken approximately one hour after casting was complete, at 2:22 p.m.

The first series shows the cumulative strain reading corrected for the temperature using a constant value of  $4.7 \mu\epsilon / ^\circ\text{F}$  ( $8.46 \mu\epsilon / ^\circ\text{C}$ ) for the coefficient of thermal expansion. This is the value determined experimentally using the cylinders cast during fabrication. The second series shows the cumulative strain reading corrected for the temperature using a constant value of  $5.78 \mu\epsilon / ^\circ\text{F}$  ( $10.4 \mu\epsilon / ^\circ\text{C}$ ) for the coefficient of thermal expansion. This value is recommended by the manufacturer of the vibrating wire gauges. Based on the work of Kada, the third series shows the cumulative strain reading corrected for the temperature using a value for the coefficient of thermal expansion of the concrete that varies for the first 12 hours (Kada et al. 2002). It was assumed that the coefficient of thermal expansion would reach an average value of  $5.1 \mu\epsilon / ^\circ\text{F}$  ( $9.18 \mu\epsilon / ^\circ\text{C}$ ) at an age of 12 hours. Prior to this time, the value would start off as three times this value at an age of zero and decrease linearly for 12 hours. Theoretically, since there is more free water in the concrete at very early ages, and since water has a much higher coefficient of thermal expansion than concrete, the concrete at early ages will also have a higher coefficient of thermal expansion. The coefficient of thermal expansion for the steel in the vibrating wire gauge of  $6.78 \mu\epsilon / ^\circ\text{F}$  ( $12.2 \mu\epsilon / ^\circ\text{C}$ ) is used for all three cases.

Since the correction for thermal expansion is made for all gauges in the data presented, any changes in strain observed during the curing process should not be due to thermal expansion or contraction. Therefore, the strains observed should most likely be due to shrinkage effects or expansion of the concrete due to hydration.

All three series indicate that the concrete began to gradually expand after being placed, up to about the time the steam was turned on, 4.5 hours. At this time, the two series using the constant values for the coefficient of thermal expansion indicate that the concrete began to expand more rapidly until approximately 9 hours after casting. However, the series with the variable coefficient of thermal expansion indicates that the concrete rapidly contracted for about  $1 \frac{1}{2}$  hours, and then began to expand. From 9 to 15 hours, the first two series show that the concrete contracted. For the next two hours, the concrete expanded and then began to gradually contract until detensioning.

### **Detensioning of Strands**

One of the objectives of recording the vibrating wire gauges during casting was to be able to estimate the effective prestressing force after detensioning of the strands. By knowing the effective prestressing force, the total prestress loss up to that point can be estimated. The change in the strain measured by the vibrating wire gauges immediately before and after detensioning

can be used to estimate the change in stress at detensioning. Since the modulus of elasticity is needed for this calculation, a cylinder was tested immediately after the detensioning took place to determine the modulus of elasticity of the girder concrete at that time. The average modulus of elasticity measured at detensioning was 5,200 ksi.

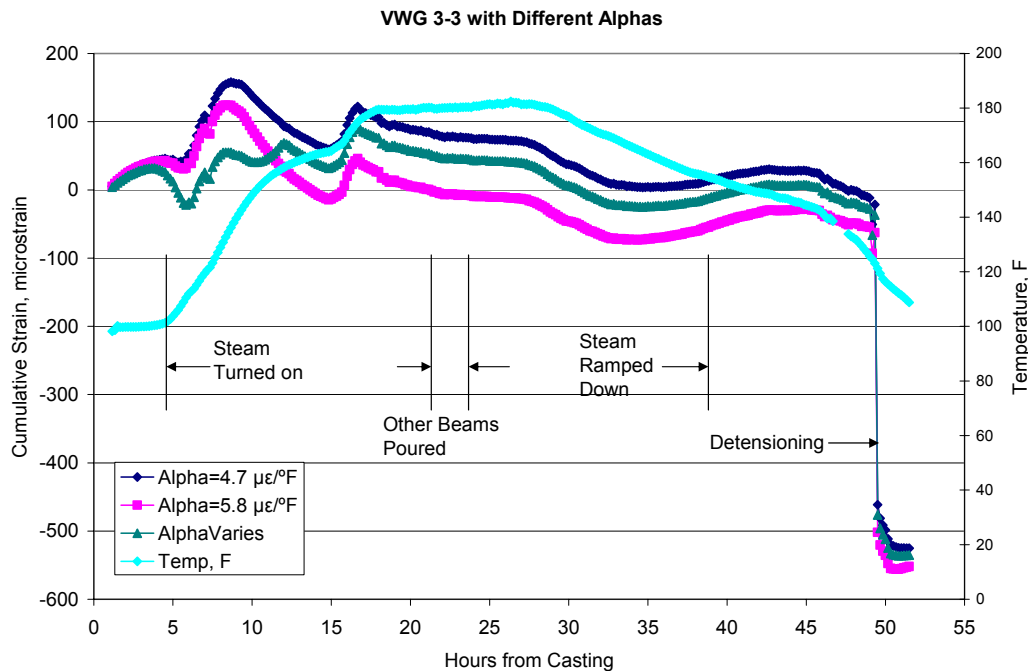
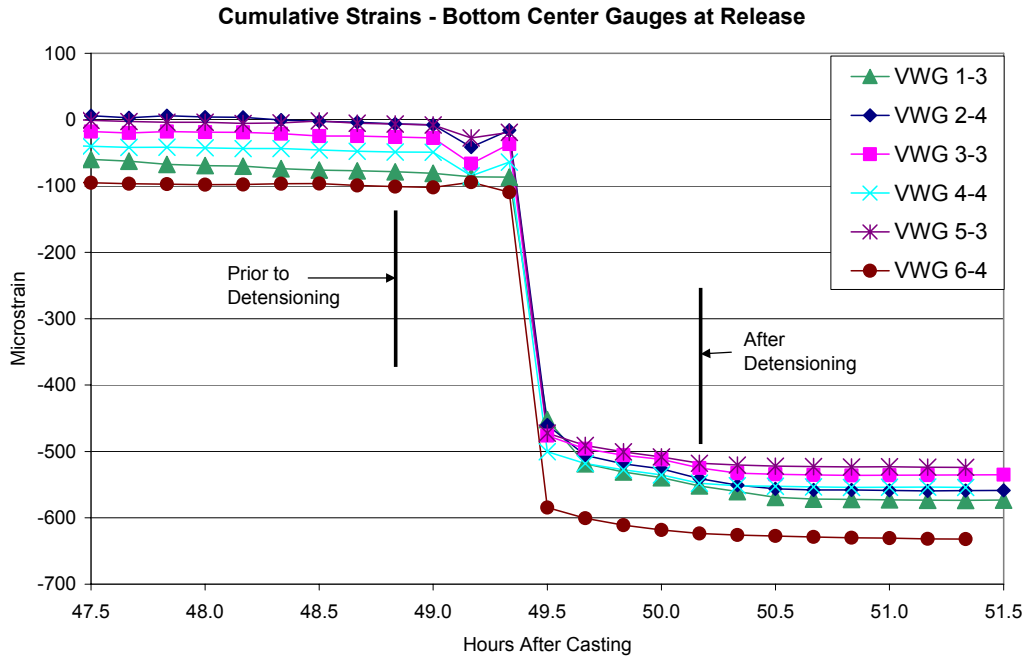


Figure 16. Vibrating Wire Gauge 3-3

### Curvature Measurements

Figure 17 shows the bottom center vibrating wire gauges immediately before and after detensioning of the strands. Because of the thunderstorm that occurred, the process of detensioning took longer than usual. The points labeled show where the data for the curvature calculations is obtained. The point after detensioning is 80 minutes after the point prior to detensioning. These points were chosen at points where the data had stabilized. As can be seen in the figure, the strain readings were stable prior to and after these points.

Table 6 shows the predicted effective prestressing stress immediately after detensioning for three methods: the Zia, Scott, Preston, and Workman Method (Z,S,P,W), the PCI Stepwise Method (PCI), and the NCHRP 496 method (Tadros method). The top portion of the table, “As Designed,” shows the values that a designer most likely would predict without modifying the prediction based on the actual field data. The bottom portion of the table, “As Observed,” shows the predicted values based on the field measured modulus of elasticity and the actual amount of time the strands had been stressed prior to detensioning (approximately 4 days instead of the normal 2 days). The as designed jacking stress is based on 0.75 times  $f_{pu}=270$  ksi and the as observed jacking stress is based on the actual jacking force of 32 kips per strand. AASHTO equations for relaxation loss are used in the Z,S,P,W method (Zia et al. 1979).



**Figure 17. Bottom Vibrating Wire Gauges at Detensioning**

The average as observed effective stress of 195.4 ksi after detensioning was used to calculate the predicted curvature immediately after detensioning. Table 7 shows the actual curvature measured at the center of all six girders as well as the predicted curvature.

All of the measured curvature values are higher than the predicted curvature value of negative  $10.7(10^{-6}) \mu\epsilon/\text{in}$ . The average measured curvature value is 17.1 percent higher than the predicted value, with a range of 9.7 percent to 24.8 percent higher. A higher negative curvature indicates that there is more compression in the bottom of the girder or more tension in the top of the girder than predicted. More prestressing force below the neutral axis would cause both of these effects. The average measured change in strain at detensioning in the top gauge is  $-93 \mu\epsilon$  compression while the predicted change in strain is  $-15 \mu\epsilon$ . The average measured change in strain in the bottom gauge is  $-507 \mu\epsilon$  compression while the predicted change in strain is  $-368 \mu\epsilon$ .

## Static Phase Results

### Overview of Static Phase

The purpose of the static phase was to monitor the early age development of restraint moments due to curing of the deck, thermal changes, shrinkage, and creep. The outside reactions, Reactions R1 and R4, were monitored along with the electrical resistance gauges in the deck and the vibrating wire gauges from the time the decks were cast until the service testing began. The restraint moment at the center of the two-span system was estimated by multiplying the change in reaction by the span length from centerline of bearing to centerline of bearing (14 ft). See Figure 2 for the locations of the instrumentation.

**Table 6. Predicted Effective Prestressing Stress at Detensioning**

<b>As Designed</b>				
<b>Method</b>	<b>f<sub>Jacking</sub> ksi</b>	<b>Relaxation ksi</b>	<b>Elast. Short. ksi</b>	<b>f<sub>Release</sub> ksi</b>
Z,S,P,W	203	-2.4	-10.8	189
PCI	203	-2.1	-11.3	189
NCHRP 496	203	-1.8	-11.4	189
			Average	<b>189</b>
<b>As Observed</b>				
<b>Method</b>	<b>f<sub>Jacking</sub> ksi</b>	<b>Relaxation ksi</b>	<b>Elast. Short. ksi</b>	<b>f<sub>Release</sub> ksi</b>
Z,S,P,W	209	-3.2	-10.1	196
PCI	209	-2.9	-12.0	194
NCHRP 496	209	-2.4	-10.8	196
			Average	<b>195</b>

**Table 7. Curvature at Detensioning**

<b>Girder Mark</b>	<b>Top Gauge <math>\Delta\epsilon, \mu\epsilon</math></b>	<b>Bottom Gauge <math>\Delta\epsilon, \mu\epsilon</math></b>	<b>Measured Curv., <math>\Phi</math> (<math>10^6</math>) <math>\mu\epsilon/in</math></b>	<b>Predicted Curv., <math>\Phi</math> (<math>10^6</math>) <math>\mu\epsilon/in</math></b>	<b>Percent Difference</b>
VT1	-86	-473	-11.7	-10.7	9.7
VT2	-103	-534	-13.1	-10.7	22.2
VT3	-106	-499	-11.9	-10.7	11.2
VT4	-90	-499	-12.4	-10.7	15.8
VT5	-91	-511	-12.7	-10.7	18.9
VT6	-82	-522	-13.3	-10.7	24.8
Average	-93	-507	-12.5	-10.7	17.1

Significant restraint moments were observed within the first week of monitoring for the two tests which had a continuity diaphragm. Test 1, which had the extended strands produced higher restraint moments than Test 2, which had the extended 180 degree bent bars. Even though Test 3 did not have a continuity diaphragm, some changes in reactions occurred after casting the continuous deck.

### **Development of Early Age Restraint Moments**

#### *Test 1 and Test 2*

Figure 18 shows the changes in reactions and strains for Test 1. Lines are used to connect the data points. Compression is negative for both the reactions and the strains. The reaction values are absolute reactions in kips. The strain gauge values are the change in strain

from the first reading taken immediately after the deck was cast. At day zero, the deck is cast and the average outside reactions increase from approximately 5.69 kips to 8.96 kips due to the weight of the deck. Almost immediately, the outside reactions begin to increase until a maximum outside reaction of 12.7 kips is recorded at 0.9 days after casting. The reactions then quickly decrease to a value of 7.13 kips at an age of 3.8 days. Over the next 24 days, the reactions slowly decrease to a final value of 5.17 kips at 28 days, when setup for the service testing began. Thermal effects caused by daily fluctuations in temperature cause the reactions to cycle up and down daily.

The strain gauges indicate that the strain increases for the first day, indicating that the gauges are being pulled in tension, and then decrease for the remaining time, indicating that the gauges are being compressed. The gauges in the top center of the two span unit, gauges E5 and E6, decrease the most, approaching 340  $\mu\epsilon$  compression at 28 days. The gauges in the bottom of the continuity diaphragm, gauges E11 and E12, also show significant compression, approaching 290  $\mu\epsilon$  compression at 28 days. Gauge E1 was most likely damaged during casting the deck and did not function. Also, a wire became loose during the early readings, causing some noise in the electrical resistance gauge readings for the early readings of gauges E2 through E10.

Figure 19 shows the changes in reactions and strains for Test 2. The reactions follow a trend similar to Test 1. Immediately after casting the deck at age zero, the average outside reactions increase from 6.67 kips to 8.55 kips due to the weight of the deck. The reactions begin to increase rapidly until a maximum reaction of 10.35 kips occurs at 0.7 days after casting. The reactions then begin to decrease rapidly until an average reaction of 6.88 kips is reached at 4.2 days. Unlike Test 1, the reactions in Test 2 do not change much from 4.2 days until set up for the service testing began at day 20.

The strains in the electrical resistance gauges did not change as much in Test 2 as they did in Test 1. This was unexpected, since the girders for Test 2 were older than the girders for Test 1 at the time the decks were cast. More differential shrinkage should have taken place in Test 2 than in Test 1. Gauges E5 and E6, the top center gauges, approach a compression of 220  $\mu\epsilon$  while the bottom gauges in the diaphragm, gauges E11 and E12, only approach a compression of approximately 70  $\mu\epsilon$ .

The restraint moment, derived by multiplying the change in reaction by the distance of 14 ft, for Test 1 is twice as much as the restraint moment for Test 2, 52.4 kip-ft versus 25.2 kip-ft, at the early age of 0.9 and 0.7 days, respectively. The restraint moments at the intermediate ages of 3.8 and 4.2 days are similar in magnitude, -25.7 kip-ft and -23.4 kip-ft. At the final age of 28 and 20 days, respectively, Test 1 has nearly twice the restraint moment of Test 2, -53.1 kip-ft and -22.5 kip-ft.

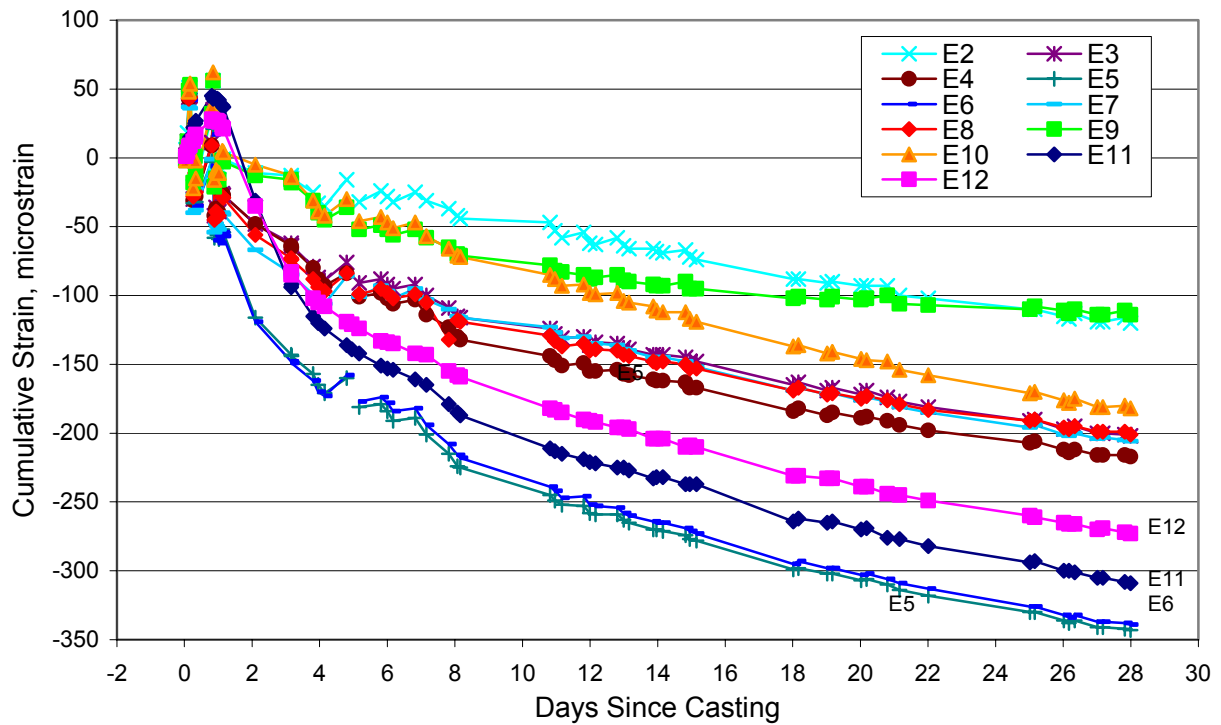
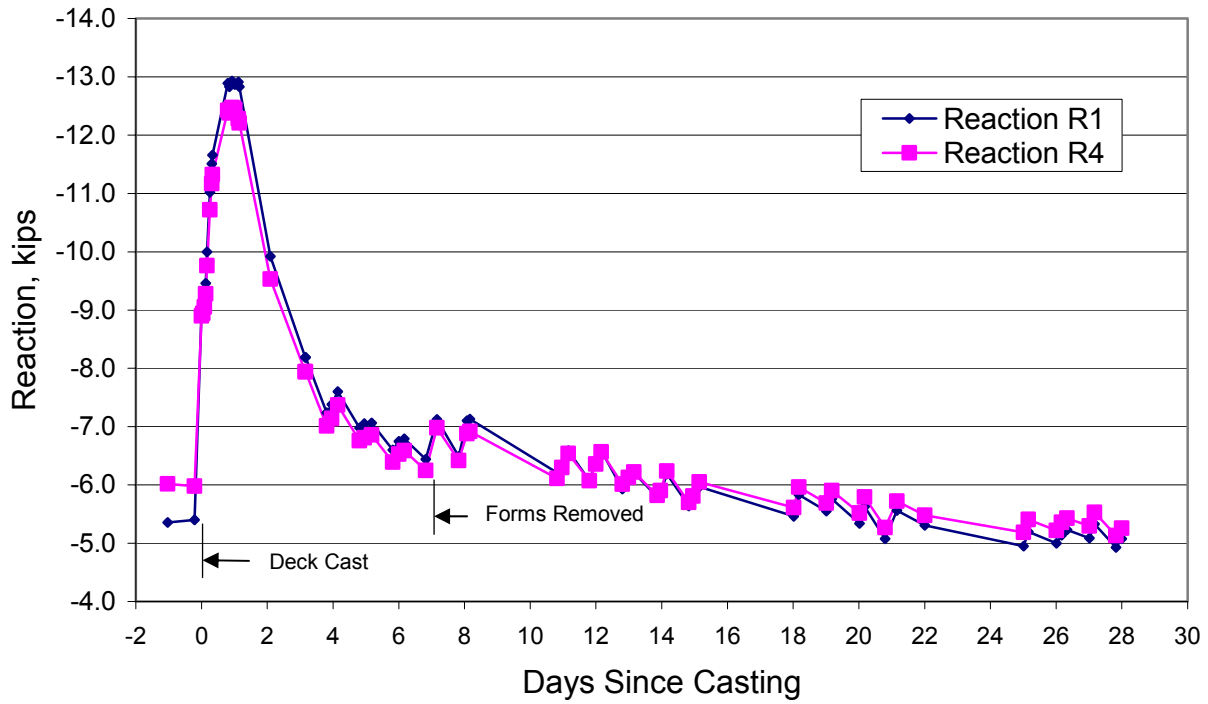


Figure 18. Changes in Reactions and Strains for Test 1

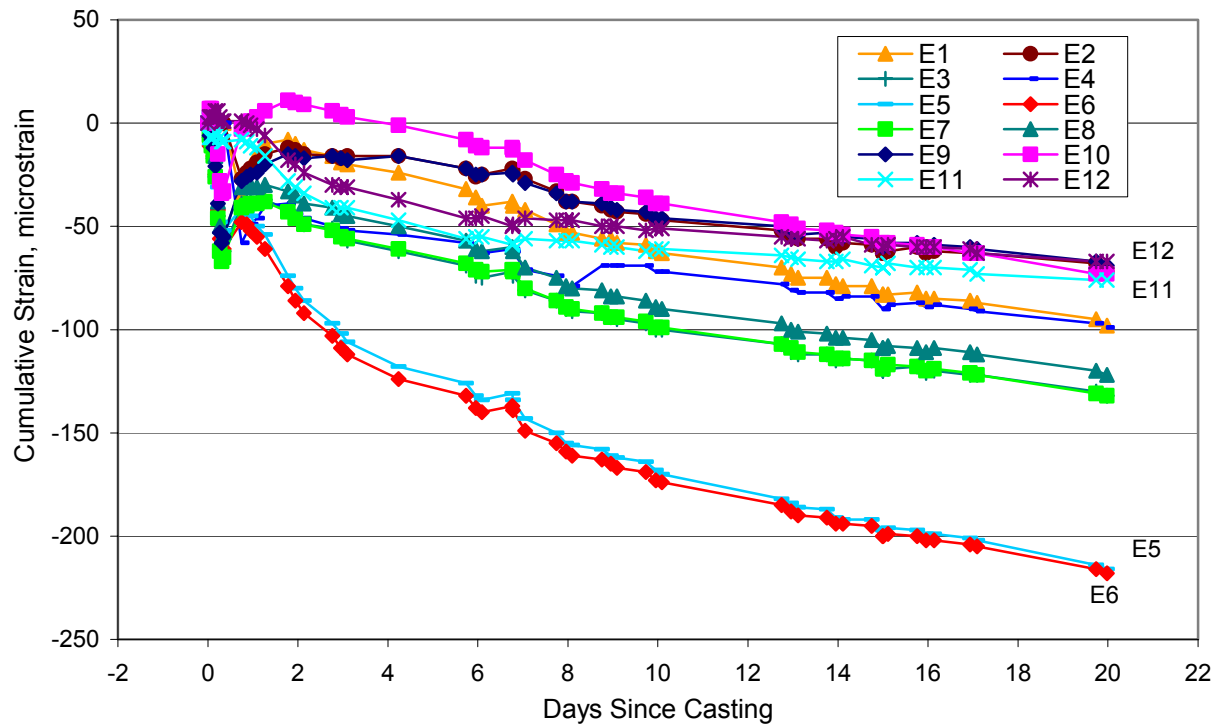
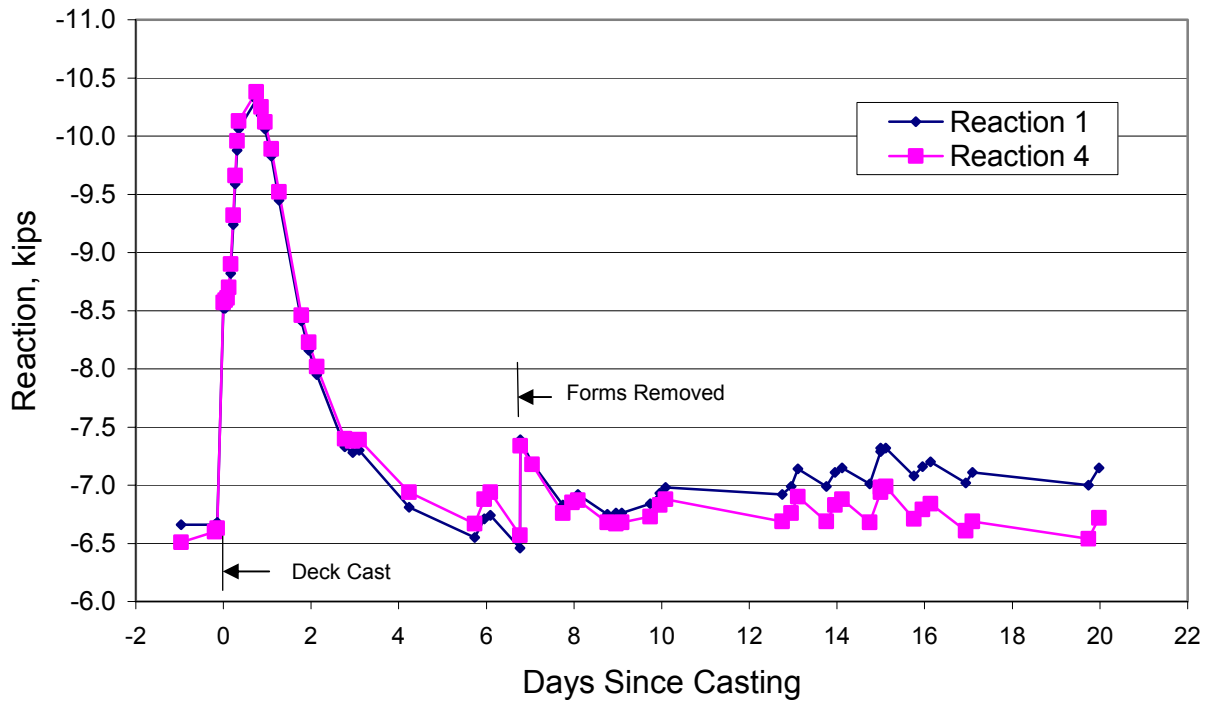


Figure 19. Changes in Reactions and Strains for Test 2

### *Test 3*

Figure 20 shows the changes in reactions and strains for Test 3. As expected, since there is no continuity diaphragm, the changes in reaction are much smaller than Tests 1 and 2. After casting the deck, the reactions remain approximately 8.46 kips from the time of casting to 0.9 days after casting. A slight decrease in the reactions then occurs to 7.77 kips at 4.0 days. The average reactions then remain fairly constant; decreasing only to approximately 7.24 kips at 14 days. Also, the strains do not change as much as Test 1 and 2. The center two gauges, gauges E7 and E8, approach a value of approximately 90  $\mu\epsilon$  compression at 14 days.

### *Summary of Restraint Moments*

Table 8 shows a summary of the changes in reactions and resulting moments for each of the three tests. The Net Reaction is the actual reaction recorded. The Delta Reaction is the change in the reaction from one time to the next. The Net Moment is the actual calculated restraint moment using a moment arm of 14 ft. The Delta Moment is the change in the moment from one time to the next.

## **Service/Cyclic Phase Results**

### **Overview of the Tests Performed**

Table 9 shows a summary of the tests performed for Test 1 and Test 2 and Table 10 shows a summary of the tests performed for Test 3. Load Control was used for all tests in Test 1 and 2. The Range column shows the range of the applied moment as a fraction of the predicted cracking moment,  $M_{cr}$ , calculated with the gross section properties at the interface and the typically used modulus of rupture of 7.5 times the square root of the compressive strength. A value of 0, 0.75, 0 indicates that the active end load is adjusted to apply zero moment at the continuity connection, then gradually increased to  $0.75M_{cr}$ , and then gradually decreased to zero moment again. The Number of Cycles column shows the number of cycles of thermal restraint moments applied prior to performing a static test of 0,  $1.0M_{cr}$ , 0. The magnitude of the thermal restraint moments is increased as described in the Notes column. The Interface Crack Width column shows the range of the manually measured crack widths using a crack comparator card near the bottom of the girder and diaphragm interface. This value is similar in magnitude to the value measured with the LVDTs at the same location. For Test 3, Load Control was used for Tests A and B and Deflection Control was used for the remaining tests. The Range column shows both the applied moment and the active end deflection measured by the MTS System. The Number of Cycles Column shows the number of deflection controlled cycles ranging from an active end deflection of 0.7 in to -0.2 in for negative moment and ranging from 0.7 in to 1.6 in for positive moment. The Maximum Top of Deck Crack Width Column shows the visually measured crack widths along the top of the deck.

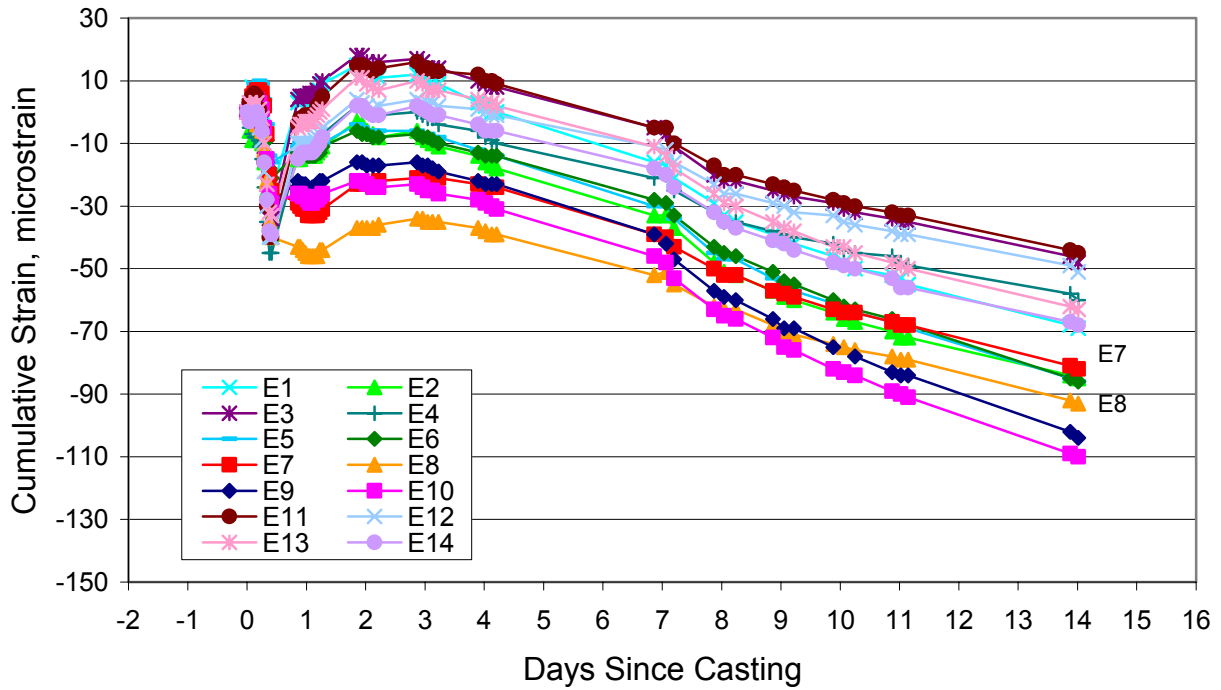
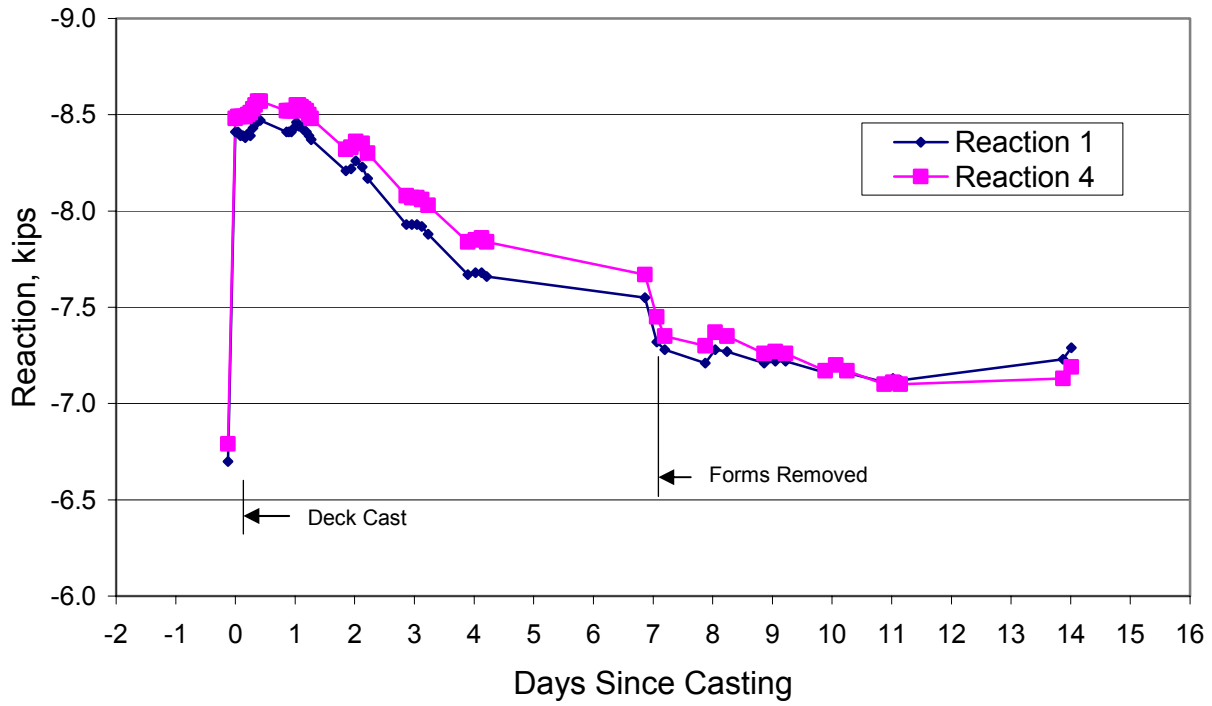


Figure 20. Changes in Reactions and Strains for Test 3

**Table 8. Summary of Restraint Moments**

<b>Test Number 1 Average Outside Reactions and Restraint Moments</b>				
<b>Time</b>	<b>Net Reaction kips</b>	<b>Delta Reaction kips</b>	<b>Net Moment kip-ft</b>	<b>Delta Moment kip-ft</b>
After Casting Deck	-8.96		0.00	
		-3.74		52.4
At 0.9 Days	-12.7		52.4	
		5.58		-78.1
At 3.8 Days	-7.13		-25.7	
		1.96		-27.4
At 28 Days	-5.17		-53.1	
<b>Test Number 2 Average Outside Reactions and Restraint Moments</b>				
<b>Time</b>	<b>Net Reaction kips</b>	<b>Delta Reaction kips</b>	<b>Net Moment kip-ft</b>	<b>Delta Moment kip-ft</b>
After Casting Deck	-8.55		0.00	
		-1.80		25.2
At 0.7 Days	-10.4		25.2	
		3.47		-48.6
At 4.2 Days	-6.88		-23.4	
		-0.06		0.84
At 20 Days	-6.94		-22.5	
<b>Test Number 3 Average Outside Reactions and Restraint Moments</b>				
<b>Time</b>	<b>Net Reaction kips</b>	<b>Delta Reaction kips</b>	<b>Net Moment kip-ft</b>	<b>Delta Moment kip-ft</b>
After Casting Deck	-8.45		0.00	
		-0.02		0.28
At 0.9 Days	-8.47		0.28	
		0.70		-9.80
At 4.0 Days	-7.77		-9.52	
		0.52		-7.35
At 14 Days	-7.24		-16.9	

### **Service Load Testing**

For Test 1 and Test 2, test series A through C were performed to investigate the response of the structure to initial service loads prior to the application of any cyclic loads. For Test 3, test series A and B were performed to investigate the same response. As the loads were slowly applied, the structure was visually monitored to determine when first cracking of the interface of the diaphragm and the girder occurred due to positive moment. The electronic data was manually recorded with the System 5000 at predetermined magnitudes of applied moment. All loads were applied as a fraction of the predicted cracking moment,  $M_{cr}$ , and are presented as such.

### *Initial Cracking Moment*

Current design methods recommend using the initial cracking moment of the positive moment connection,  $M_{cr}$ , to be based on the gross section properties of the girder, bolster, and deck at the interface and the tensile capacity of the concrete equal to the modulus of rupture of the diaphragm concrete, which is 7.5 times the square root of the compressive strength of the diaphragm concrete. Since the diaphragm concrete is placed against the end of the already cured girder, it was suspected that the modulus of rupture would overestimate the actual tensile capacity of the concrete at the interface. The results of the initial cracking moment tests for all three tests confirm that the initial cracking does occur at a calculated tensile stress of the concrete lower than the modulus of rupture.

Table 11 shows the First Cracking moments observed (when first cracking was noticed at the bottom of the girder/diaphragm interface) and predicted for all three tests. The predicted tensile capacity of the concrete is presented two ways for five different methods. The first set of predicted values is based on the As Designed value of the tensile capacity of the concrete based on the 28 day compressive strength of 4,000 psi. The second set of predicted values is based on the As Observed values of compressive strength and modulus of rupture determined from the cylinder testing. Method 1 uses the currently recommended value of the modulus of rupture,  $7.5(f'_c)^{1/2}$ . Method 2 uses the ACI code recommended low range for direct tensile strength equal to  $0.1f'_c$  (ACI Building 2002). Method 3 uses a recommended formula for direct tensile strength as a function of the unit weight of the concrete (assumed to be 145 pcf) and the compressive strength of the concrete as proposed by Branson,  $(1/3)(w f'_c)^{(1/2)}$  (Branson 1977). Method 4 uses a relationship proposed by Mehta for direct tension as a function of the modulus of rupture,  $0.59f_r$  (Mehta 1986). Method 5 is a proposed method based on the Branson method with the fraction (1/3) reduced to (1/4).

### *Initial Loading Behavior*

Figure 21 shows the initial loading behavior for tests A through C for Test 1 and Test 2. The applied moment is presented as a percent of the calculated cracking moment,  $M_{cr}$ , and is plotted versus the average LVDT reading at the bottom of the girder and diaphragm interface. The average LVDT reading gives approximately the same value as the average measured crack width using a crack comparator card. The response of both tests to the applied positive moments is similar. Test 2, with the 180 degree U-bars, displays a slightly stiffer response to the application of the positive moment. For an applied moment of  $1.2M_{cr}$ , the average opening as measured by the LVDTs is 0.022 in versus an average opening of 0.029 in for Test 1. Based on the ultimate predicted capacities, this behavior is expected. Test 1, with the strands, has a predicted ultimate positive moment capacity of 711 k-ft and Test 2, with the bars, has a predicted ultimate positive moment capacity of 773 k-ft, giving a ratio of 0.92.

**Table 9. Summary of Static and Cyclic Tests for Test 1 and Test 2**

<b>Test Name</b>	<b>Range %Mcr</b>	<b>No. of Cycles</b>	<b>Interface Crack Width, in</b>	<b>Notes</b>
1A	0 , 0.75 , 0	0	0.007	Initial cracking at interface prior to 0.5Mcr, 0.002 in max
1B	0 , 1.0 , 0	0	0.010 - 0.013	Interface cracking returns to 0.002 in
1C	0 , 1.20 , 0	0	0.016 - 0.025	Initial cracking in edge of deck
1D	0 , 1.0 , 0	1,000	0.020 - 0.025	Cycles at 0.25 Mthermal
1E	0 , 1.0 , 0	2,000	0.020 - 0.025	Cycles at 0.50 Mthermal
1F	0 , 1.0 , 0	2,000	0.020 - 0.025	Cycles at 0.75 Mthermal, minor spalling noticed
1G	0 , 1.0 , 0	2,000	0.030 - 0.040	Cycles at 1.00 Mthermal, one reading up to 0.050 in
1H	0 , 1.0 , 0	2,000	0.030 - 0.040	Cycles at 1.00 Mthermal, concrete dusting and spalling
1J	0 , 1.0 , 0	1,000	0.040 - 0.050	Cycles at 1.00 Mthermal, cracks remain 0.007 to 0.010 in
1K	0,1,0,-1,0	0	0.040 - 0.050	Additional cracking in deck up to 0.010 in
1L	0,1,0,-1,0,1,0,-1,0	0	0.040 - 0.050	Cracks in deck and at interface not completely closed
1M	0,1,0,-1,0,1,7,0	0	0.105	Initial cracking in bottom of diaphragm at 1.56 Mcr
1N	0 , 1.83 , 0	0	0.150	Continuous record to near failure
<b>Test Name</b>	<b>Range %Mcr</b>	<b>Number of Cycles</b>	<b>Interface Crack Width, in</b>	<b>Notes</b>
2A	0 , 0.75 , 0	0	0.005 - 0.010	Initial cracking at interface prior to 0.5Mcr, 0.005 in max
2B	0 , 1.0 , 0	0	0.009 - 0.016	Interface cracking returns to 0.002 to 0.003 in
2C	0 , 1.20 , 0	0	0.016 - 0.025	Cracking extends half way up web, none in deck
2D	0 , 1.0 , 0	1,000	0.010 - 0.020	Cycles at 0.25 Mthermal
2E	0 , 1.0 , 0	2,000	0.016 - 0.020	Cycles at 0.50 Mthermal, cracking to top of girder
2F	0 , 1.0 , 0	2,000	0.016 - 0.020	Cycles at 0.75 Mthermal, minor spalling noticed
2G	0 , 1.0 , 0	2,000	0.016 - 0.025	Cycles at 1.00 Mthermal, minor cracking on side of deck
2H	0 , 1.0 , 0	2,000	0.016 - 0.025	Cycles at 1.00 Mthermal, minor cracking on web fillet
2J	0 , 1.0 , 0	1,000	0.016 - 0.025	Cycles at 1.00 Mthermal, cracks remain 0.007 to 0.009 in
2K	0,1,0,-1,0	0	0.016 - 0.025	Cracking on edge of deck 0.013 in
2L	0,1,0,-1,0,1,0,-1,0	0	0.016 - 0.025	Maximum crack on deck 0.016 in
2M	0 , 2.07 , 0	0	0.130	Continuous record to near failure

**Table 10. Summary of Static and Cyclic Tests for Test 3**

Test Name	Range, Moment (k-ft) and Deflection (in)						No. of Cycles	Max. Crack Width, in	
								Top	Bottom
3A	Moment	-0.1	-73.1	-0.6	68.1	-0.1	0	0.016 - 0.020	0.009
	Deflection	0.702	-0.186	0.402	1.540	0.562			
3B	Moment	-0.3	-71.4	-0.5	68.6	-0.2	0	0.020 - 0.040	0.025
	Deflection	0.505	-0.212	0.429	1.600	0.516			
3C	Moment	23.6	-50.4	20.4	62.6	16.4	2,000	0.016 - 0.030	0.025
	Deflection	0.700	-0.202	0.703	1.601	0.701			
3D	Moment	17.2	-51.6	19.5	60.7	15.2	2,000	0.016 - 0.040	0.03
	Deflection	0.699	-0.202	0.699	1.599	0.699			
3E	Moment	18.2	-51.0	18.2	60.4	15.2	2,000	0.020 - 0.040	0.025
	Deflection	0.700	-0.200	0.698	1.601	0.702			
3F	Moment	15.5	-50.8	18.8	59.8	15.1	2,000	0.016 - 0.040	0.03
	Deflection	0.701	-0.201	0.698	1.600	0.700			
3G	Moment	17.0	-49.8	19.5	60.7	15.3	2,000	0.016 - 0.040	0.03
	Deflection	0.700	-0.200	0.701	1.602	0.700			
3H	Moment	18.7	-47.2	21.3	60.9	17.6	0	0.016 - 0.040	0.03
	Deflection	0.701	-0.202	0.700	1.602	0.700			
3J	Moment	19.1	-48.1	23.3	64.3	17.6	0	0.100 (+)	0.100 (+)
	Deflection	0.702	-0.209	0.712	1.605	0.690			
	Moment	-47.1	-134.2	118.0	14.2				
	Deflection	-0.195	-1.502	3.004	0.698				

The ratio of the average LVDT readings for Test 2 to Test 1 is also less than one, but even lower at 0.76. Therefore, Test 2 is slightly stiffer than Test 1 for the initial loading phase. The ultimate calculated capacity of Test 1 is based on a reduced allowable stress in the prestressing strands at ultimate loading. Based on the embedment of the 90 degree bent strands in the diaphragm, the predicted stress at ultimate is 98.2 ksi. This is much lower than the ultimate breaking strength of a strand, which is generally taken as 270 ksi. In the design procedure it is assumed that the strands are not able to reach the full tensile capacity of a fully developed tensioned strand (Salmons 1974). The allowable tensile stress,  $f_{pu}$ , as a function of the total embedded length of the strand,  $L_e$ , is:

$$f_{pu} = \frac{L_e - 8.25}{0.163}, \text{ ksi} \quad (3)$$

where,  $L_e$  is the total length of the embedded strand in inches.

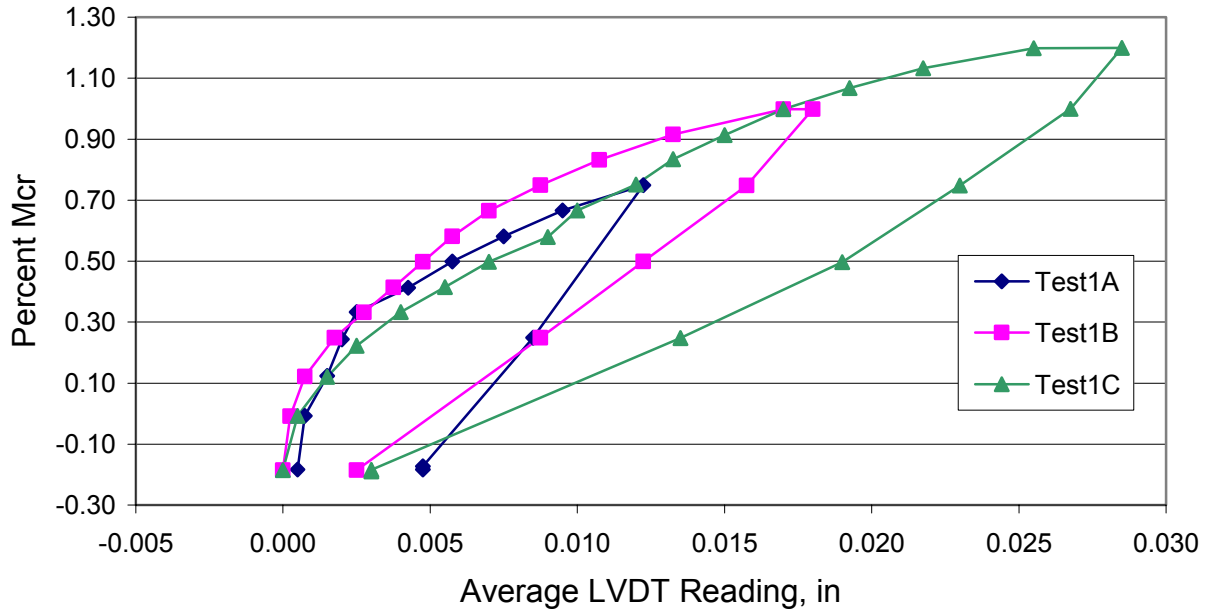
Figure 22 shows the behavior of Test 3 for tests A and B. The applied moment is plotted versus the active end deflection and the LVDT readings near the bottom of the section and the top of the web at the joint location. The section was slowly loaded and the formation of cracks documented.

**Table 11. Summary of Initial Cracking**

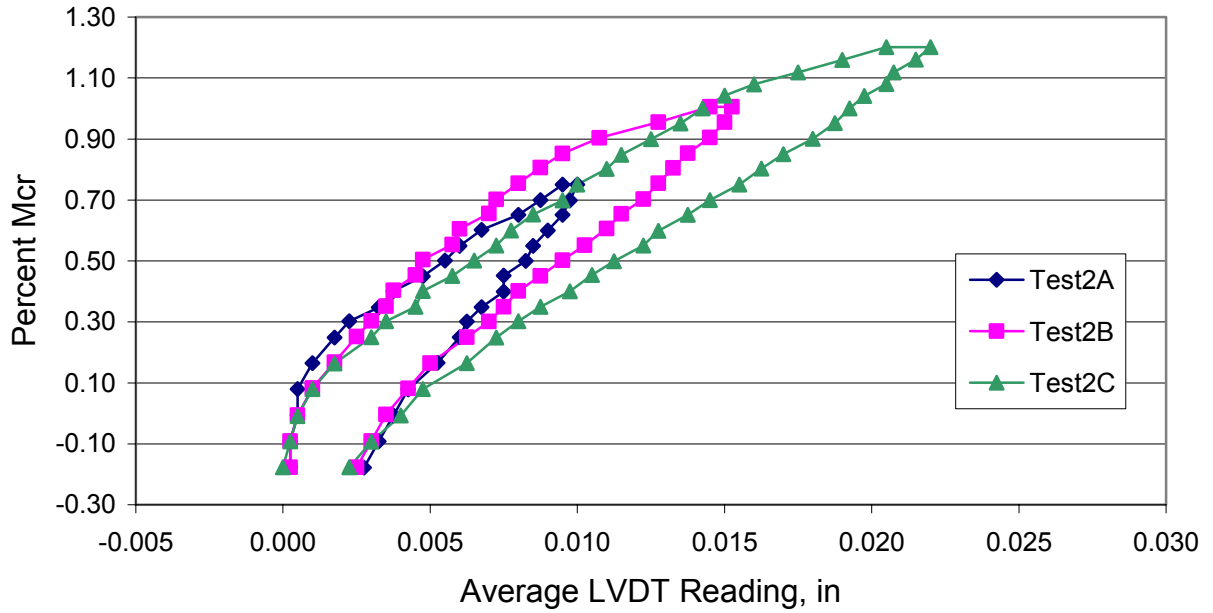
<b>Test Number 1 - First Cracking</b>					
	<b>1</b>	<b>2</b>	<b>3</b>	<b>4</b>	<b>5</b>
	<b><math>7.5(f'_c)^{0.5}</math></b>	<b><math>0.1f'_c</math></b>	<b><math>(1/3)(wf'_c)^{0.5}</math></b>	<b><math>0.59f_r</math></b>	<b><math>(1/4)(wf'_c)^{0.5}</math></b>
$f_t$ as Designed, psi	474	400	253	280	190
$M_{cr}$ as Designed, k-ft	531	448	283	314	213
$M_{cr}$ Observed, k-ft	215	215	215	215	215
Designed/Observed	2.47	2.09	1.32	1.46	<b>0.99</b>
$f_t$ as observed, psi	630	579	304	372	228
$M_{cr}$ as Designed, k-ft	706	649	341	416	256
$M_{cr}$ Observed, k-ft	215	215	215	215	215
Designed/Observed	3.29	3.02	1.59	1.94	<b>1.19</b>
<b>Test Number 2 - First Cracking</b>					
	<b>1</b>	<b>2</b>	<b>3</b>	<b>4</b>	<b>5</b>
	<b><math>7.5(f'_c)^{0.5}</math></b>	<b><math>0.1f'_c</math></b>	<b><math>(1/3)(wf'_c)^{0.5}</math></b>	<b><math>0.59f_r</math></b>	<b><math>(1/4)(wf'_c)^{0.5}</math></b>
$f_t$ as Designed, psi	474	400	253	280	190
$M_{cr}$ as Designed, k-ft	531	448	283	314	213
$M_{cr}$ Observed, k-ft	236	236	236	236	236
Designed/Observed	2.25	1.90	1.20	1.33	<b>0.90</b>
$f_t$ as observed, psi	580	584	306	342	229
$M_{cr}$ as Designed, k-ft	650	654	342	383	2567
$M_{cr}$ Observed, k-ft	236	236	236	236	236
Designed/Observed	2.76	2.78	1.45	1.63	<b>1.09</b>
<b>Test Number 3 - First Cracking</b>					
	<b>1</b>	<b>2</b>	<b>3</b>	<b>4</b>	<b>5</b>
	<b><math>7.5(f'_c)^{0.5}</math></b>	<b><math>0.1f'_c</math></b>	<b><math>(1/3)(wf'_c)^{0.5}</math></b>	<b><math>0.59f_r</math></b>	<b><math>(1/4)(wf'_c)^{0.5}</math></b>
$f_t$ as Designed, psi	474	400	253	280	190
$M_{cr}$ as Designed, k-ft	-26.7	-22.5	-14.2	-15.7	-10.7
$M_{cr}$ Observed, k-ft	-17.5	-17.5	-17.5	-17.5	-17.5
Designed/Observed	1.52	1.29	0.81	<b>0.90</b>	0.61
$f_t$ as observed, psi	490	402	254	289	190
$M_{cr}$ as Designed, k-ft	-27.6	-22.6	-14.3	-16.3	-10.7
$M_{cr}$ Observed, k-ft	-17.5	-17.5	-17.5	-17.5	-17.5
Designed/Observed	1.57	1.29	0.82	<b>0.93</b>	0.61

Figure 23 shows that under the initial service loads, two primary cracks formed through the deck on each side of the 3 in gap between the ends of the beams. The cracks are shown marked in black to the right of the sign. The cracks were approximately 9 in apart on the outside edge of the deck and slightly closer together at the interior of the deck. It was expected that one crack would form instead of two. However, based on the initial service testing and the location of the formation of these cracks, it can be concluded that two relief joints instead of one should

**Test # 1 - Percent Mcr vs Average LVDT Reading**



**Test # 2 - Percent Mcr vs Average LVDT Reading**



**Figure 21. Initial Service Tests for Test 1 and Test 2**

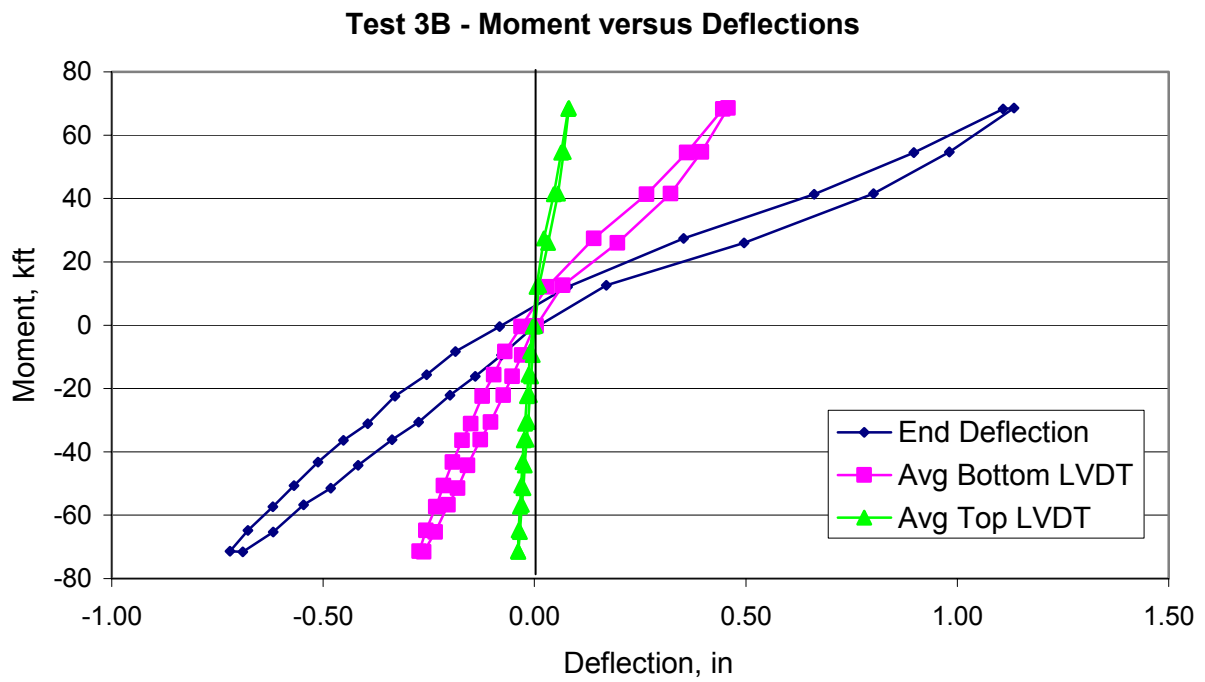
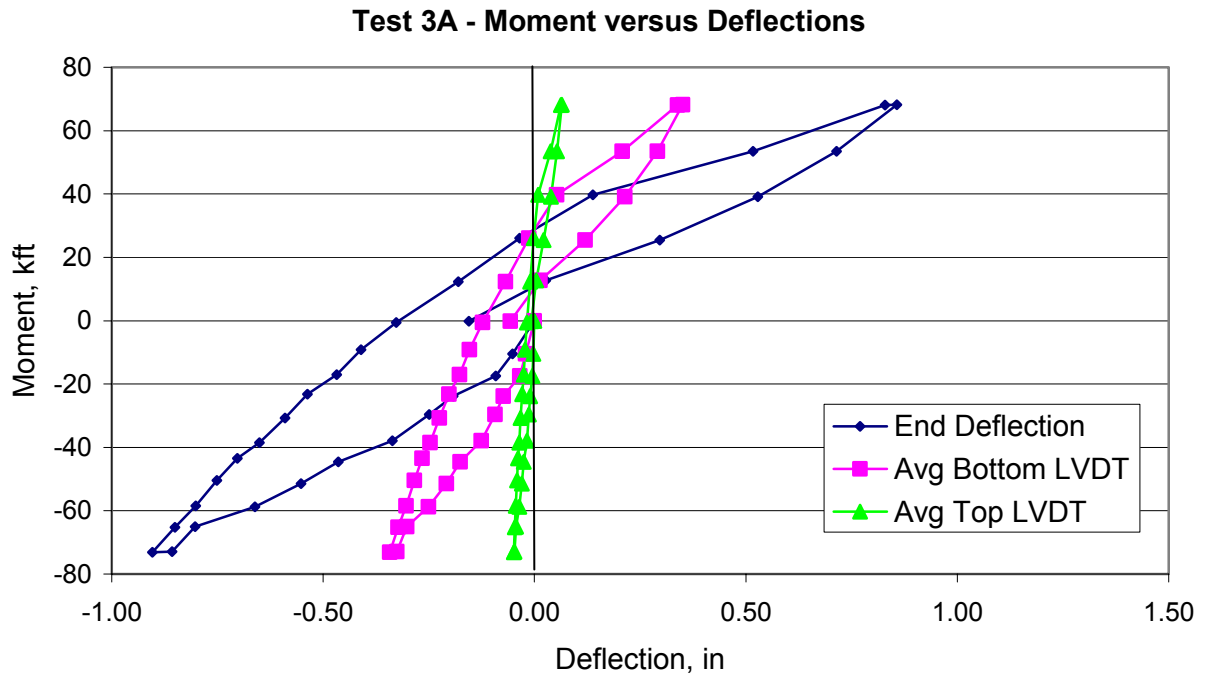


Figure 22. Initial Service Tests for Test 3

be used in the slab above the gap between the ends of the beams. The two relief joints should be centered above the space between the beams and spaced at the maximum of (A) the slab thickness or (B) the joint opening plus two times the bolster thickness. For this test, the relief joints would be placed at 7.5 in, the maximum of (A) 7.5 in or (B)  $3 + 2(1.5) = 6$  in.



Figure 23. Initial Cracking in Deck, Test 3

## Cyclic Load Testing

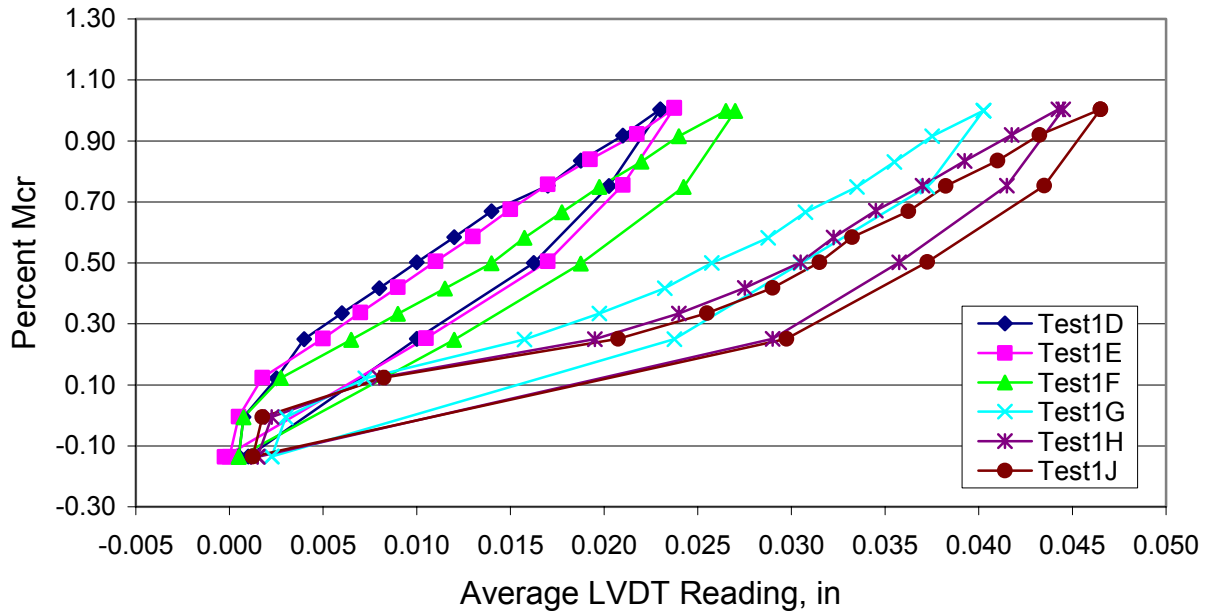
The purpose of the cyclic Load Testing phase was to determine the ability of the three continuity details to withstand moments due to expected thermal cycles.

### *Behavior During Cyclic Loads*

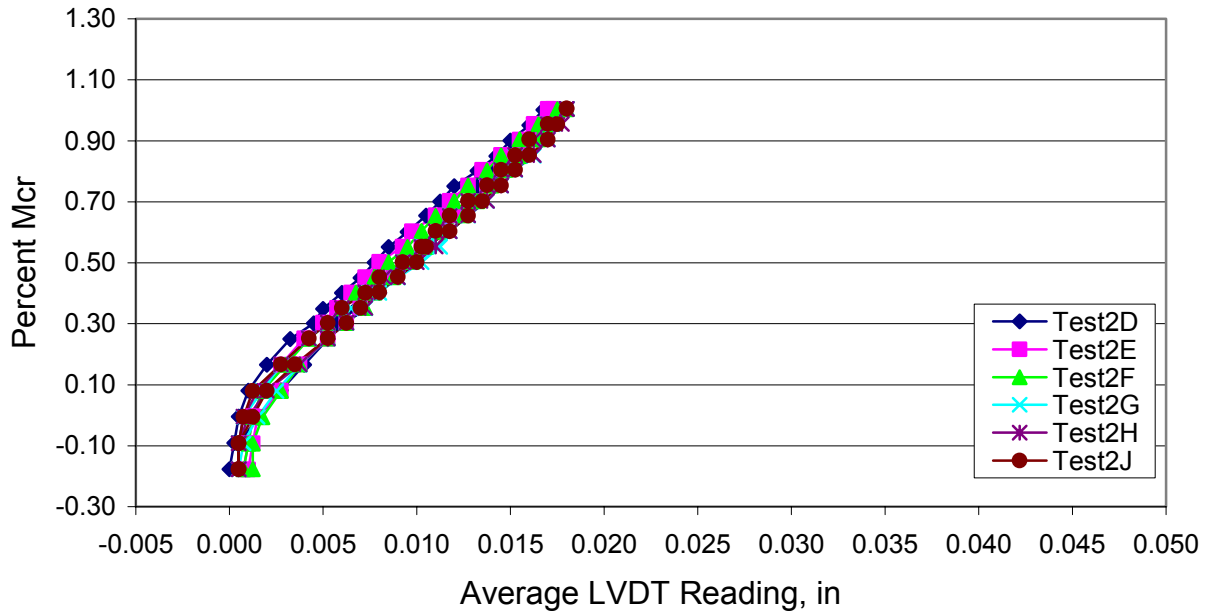
Figure 24 shows the cyclic tests D through J for Test 1 and Test 2. The percent of the cracking moment is plotted versus the average LVDT opening at the bottom of the interface. The results are presented at the same scale so that a visual comparison can be easily made between the two. Both tests maintained integrity throughout the cyclic loading phase. Although both specimens were able to withstand the 10,000 thermal cycles and continue to carry loads, it is apparent that Test 2 with the embedded bars performed better than Test 1 with the strands. After the final 10,000 cycles had been applied, Test 1 displayed an average LVDT opening of 0.047 in while Test 2 displayed an average LVDT opening of only 0.018 in, 2.6 times less opening. This indicates that Test 2 was stiffer under the cyclic loads.

Figure 25 shows the cyclic test behavior for test C and test G for Test 3. After the initial cracking which occurred during the service load phase, the behavior of Test 3 during the cyclic loads did not change appreciably. Therefore, only the initial and final cyclic test results are provided. Most of the cracking in the deck occurred during the initial loads with only a minor increase in damage due to the thermal cycles.

**Test # 1 - Percent Mcr vs Average LVDT Reading**



**Test # 2 - Percent Mcr vs Average LVDT Reading**



**Figure 24. Cyclic Tests for Test 1 and Test 2**

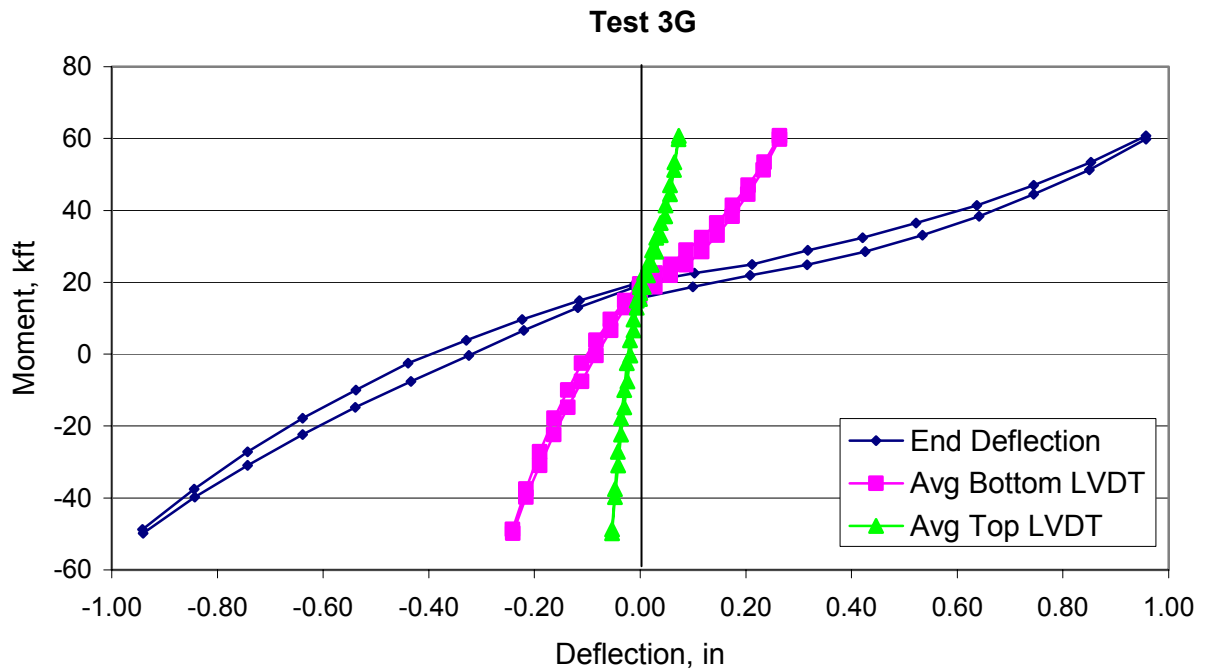
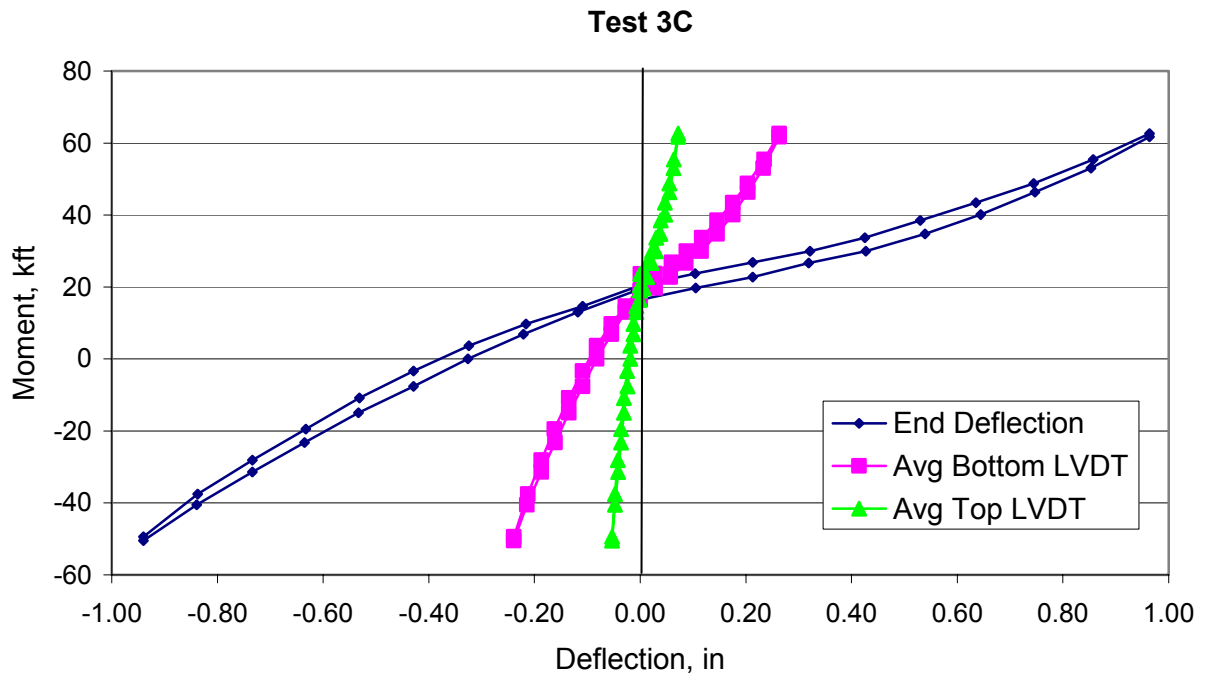


Figure 25. Cyclic Test C and G for Test 3

### *Increase in Deck Damage due to Cyclic Loads*

Table 12 shows a summary of the increase in deck damage due to the cyclic loads and Figure 26 shows the deck damage plans. The top of the table shows the maximum observed crack width following the testing phase indicated. For Test 1 and Test 2, no significant deck cracking was noticed after the service tests since the tests were performed with positive moment only. But for Test 3, which used both positive and negative moment for the service testing, significant deck cracking was observed. Test 1 and Test 2 showed an increase in the deck crack widths due to the thermal cycles while Test 3 did not exhibit a significant change. The bottom of the table shows the increase in deck damage as measured by the increase in the linear feet of cracking for Test 3. Most of the damage occurred in the first test. The final damage shows the total linear feet of cracks noted for all three tests after all testing, including the ultimate strength testing, was performed. The cracking for Test 1 and Test 2 occurred as much as 5.5 ft and 6.9 ft respectively out from the center of the test specimen indicating that the continuity connection is able to transfer significant negative moments away from the center. For Test 3, most of the cracking occurred near the center joint within 1 ft to 2 ft, indicating that once cracking occurred, the section does not transfer significant moments through the joint. The numbers at the top of the deck damage plans are the maximum crack size and the linear feet of cracking observed.

**Table 12. Deck Damage Summary**

	<b>Max Deck Crack Width, in</b>		
	<b>Test 1</b>	<b>Test 2</b>	<b>Test 3</b>
Service Tests	< 0.002	< 0.002	0.040
Cyclic Tests	0.007	0.013	0.040
Negative Tests	0.010	0.013	0.040
	<b>Increase In Damage, LF</b>		
	<b>Test 1</b>	<b>Test 2</b>	<b>Test 3</b>
Static Phase	N/A	N/A	5.0
3A	N/A	N/A	13.4
3B	N/A	N/A	1.0
3C	N/A	N/A	4.1
3D	N/A	N/A	0.4
3E	N/A	N/A	1.7
3F	N/A	N/A	0.0
3G	N/A	N/A	0.0
Final Damage	73.7	45.3	25.6

Note: LF is Linear Feet of Cracking

In Test 1 and Test 2, the maximum measured crack widths in the deck were generally less than approximately 0.013 in. The current ACI Code does not specifically address crack widths, but the previous versions of the ACI Code recommended keeping crack widths less than 0.016 in for interior exposure and 0.013 in for exterior exposure (MacGregor, 1988). Since the crack widths observed are at the limit for exterior exposure, precautions should be taken to prevent corrosion of the steel in the deck due to deicer salts.

note: numbers indicate maximum crack width, in/ lineal ft of cracking

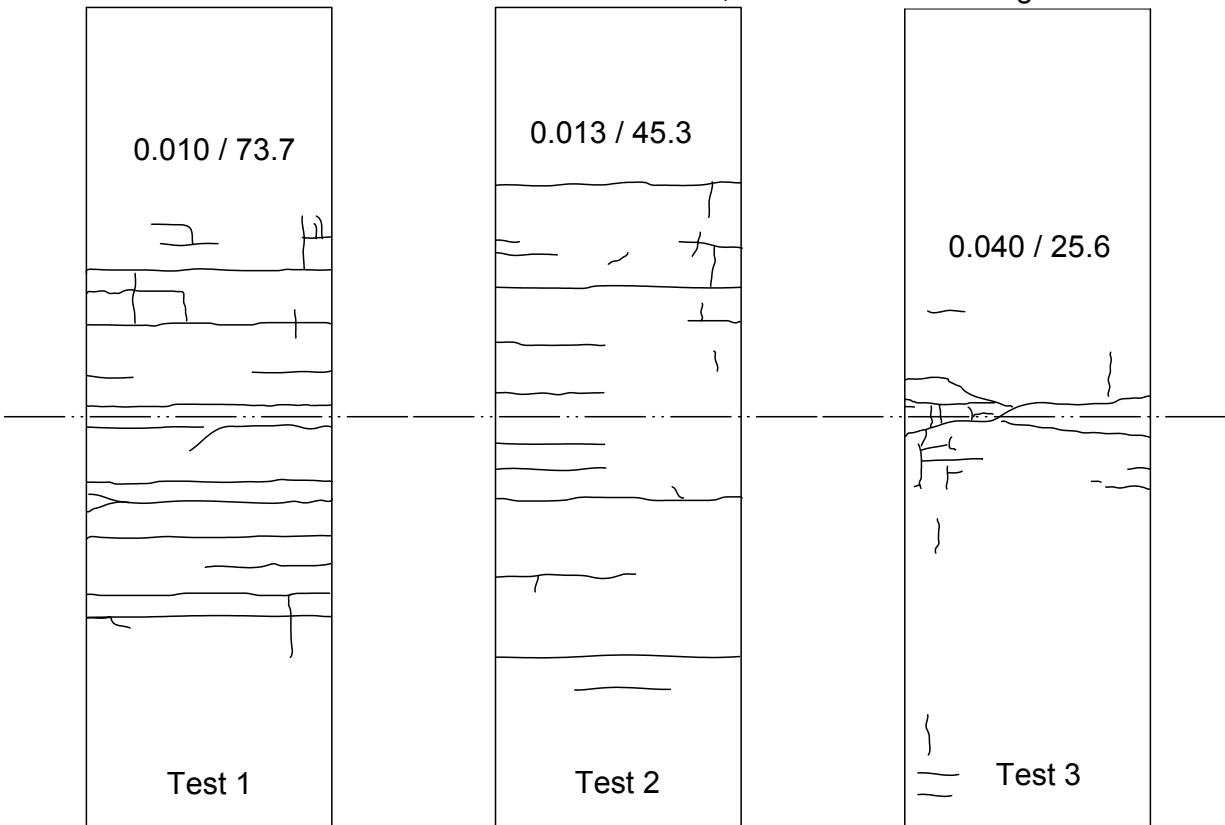


**Figure 26. Deck Damage Plans**

Based on the cracking patterns in Test 3, it is expected that if this detail is used in an actual structure two control joints placed above the 3 in gap between the ends of the girders will help to reduce and control the magnitude and number of cracks in the area of the joint. Since the crack widths observed were as large as 0.040 in, extra precautions, such as sealing the joints, should also be taken to prevent corrosion of the steel in the deck due to deicer salts.

### **Negative Moment Testing**

The purpose of the negative moment testing was to confirm the repeatability of the response of the structure after being subjected to full negative cracking moments. Figure 27 shows test L for Test 1 and Test 2. Both tests were performed by first applying a positive cracking moment and then applying a negative cracking moment. Two complete load cycles were performed for each test, the first cycle is designated “A,” and the second cycle is designated “B.” Both tests display good repeatability from the first cycle to the second. Test 1 continues to display a range of loading with a low slope indicating that the strands are twisting through the diaphragm until the 90 degree bend is engaged. Test 2 displays a nearly linear response in both the positive and negative moment directions. In Tests 1K and 2K, the specimens exhibited similar responses.

## Ultimate Strength Testing

The purpose of the Ultimate Strength Testing was to confirm the predicted ultimate positive moment capacities. Test 1 and Test 2 were taken to a near failure positive moment. This point was determined by monitoring the end deflection and applied moment. When the deflection began to increase substantially without a substantial increase in moment, the tests were considered near failure. A complete failure was avoided because it was deemed too dangerous. Test 3 was taken to the maximum end deflection possible. The negative moment was determined when the collar beam nearly touched the floor and the positive moment was determined when the MTS ram began to bind because of the excessive end rotation.

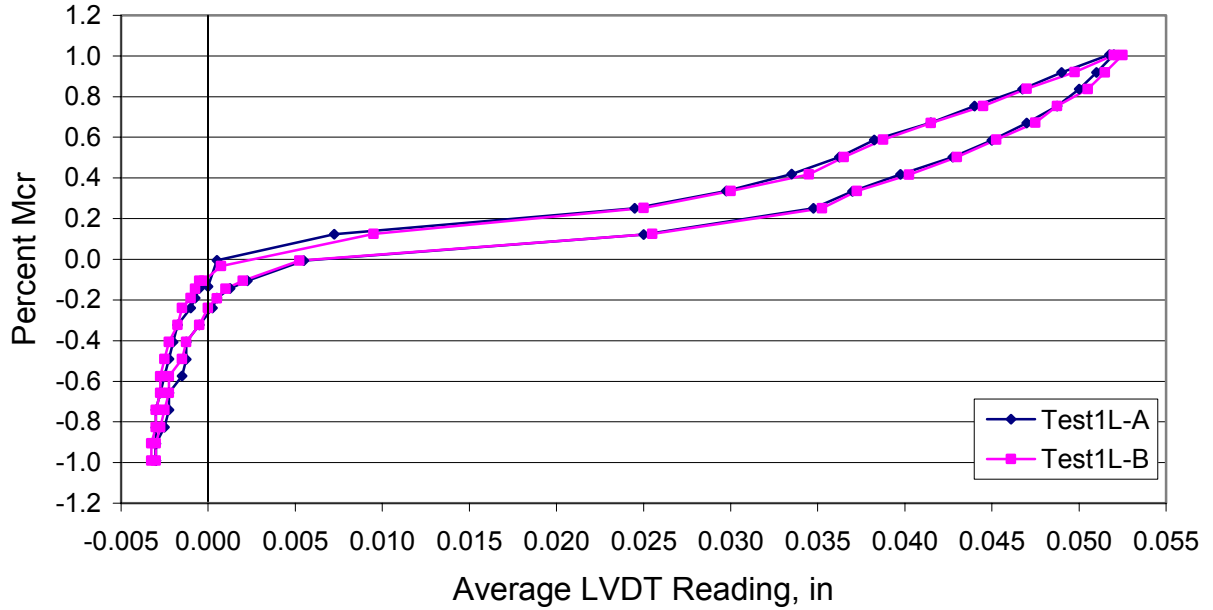
Figure 28 shows the results for the ultimate strength testing for Test 1 and Test 2. Both Test 1 and Test 2 reached and exceeded the predicted ultimate positive moment capacities. For consistency, the capacities are presented as a fraction of the cracking moment, 524 k-ft. For Test 1, the ultimate capacity approached slightly over  $1.8M_{cr}$  while the predicted ultimate capacity  $\phi M_n$  is  $1.36M_{cr}$ . The ratio of the observed to predicted capacity is 1.32 for Test 1. For Test 2, the ultimate capacity approached slightly over  $2.0M_{cr}$  while the predicted ultimate capacity  $\phi M_n$  is  $1.48M_{cr}$ . The ratio of the observed to predicted capacity is 1.35 for Test 2. Both design methods for predicting ultimate positive moment capacity provide conservative estimates for the ultimate moments, over-predicting the capacity by factors of 1.32 and 1.35.

Figure 29 shows the results for the ultimate strength testing of the deck in Test 3J. It is believed that significant binding of the MTS ram began to occur as the loads were increased. The binding occurred because the end rotation at the active end was restrained by the collar beams. Because of the binding effect, the actual loads applied at the center of the deck are most likely much lower than the moments indicated in the figure. Therefore, the figure should be used only for its shape, and not the magnitude of the loads.

Figure 30 shows the bottom of the diaphragm connection following the ultimate strength testing. The significant cracking which occurred during the ultimate strength testing indicates that substantial stresses were introduced in the bottom of the continuity diaphragm connection. The cracking is located primarily within the limits of the bottom flange of the girders. Similar crack patterns were noticed for the two, with slightly less cracking in Test 2 than in Test 1.

There was no noticeable cracking in the girders for Test 1 with the strands. For Test 2, there was some minor cracking in the girders near the bottom of the web and along the top of the bottom flange. The cracking was first noticed at the end of 9000 thermal cycles, and was less than 0.002 in in width. After the ultimate strength test, the number of cracks increased, with cracks forming at all four corners of the end of the girders at the diaphragm. The cracks never opened much more than 0.002 in, and extended a maximum of only 19 in into the girder. Figure 31 shows the final cracking at two locations. Any cracking is undesirable, but the cracking at the ends of the girders is minor both in crack widths and lengths, and should not pose a significant problem.

**Test # 1L - Percent Mcr vs Average LVDT Reading**



**Test # 2L - Percent Mcr vs Average LVDT Reading**

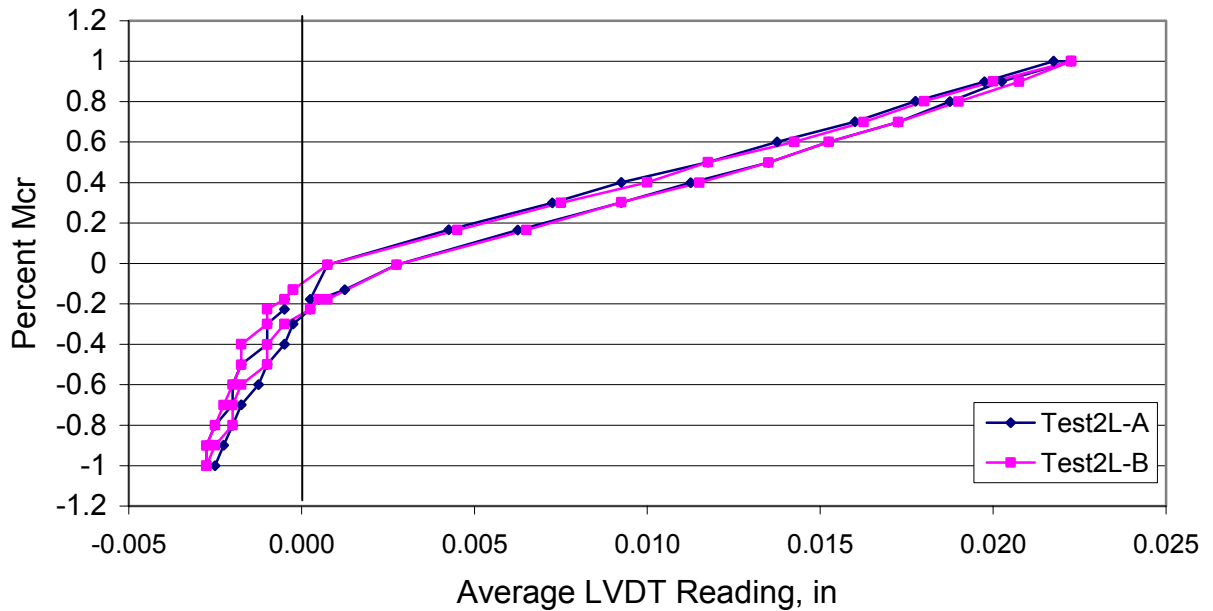


**Figure 27. Negative Moment Testing for Test 1 and Test 2**

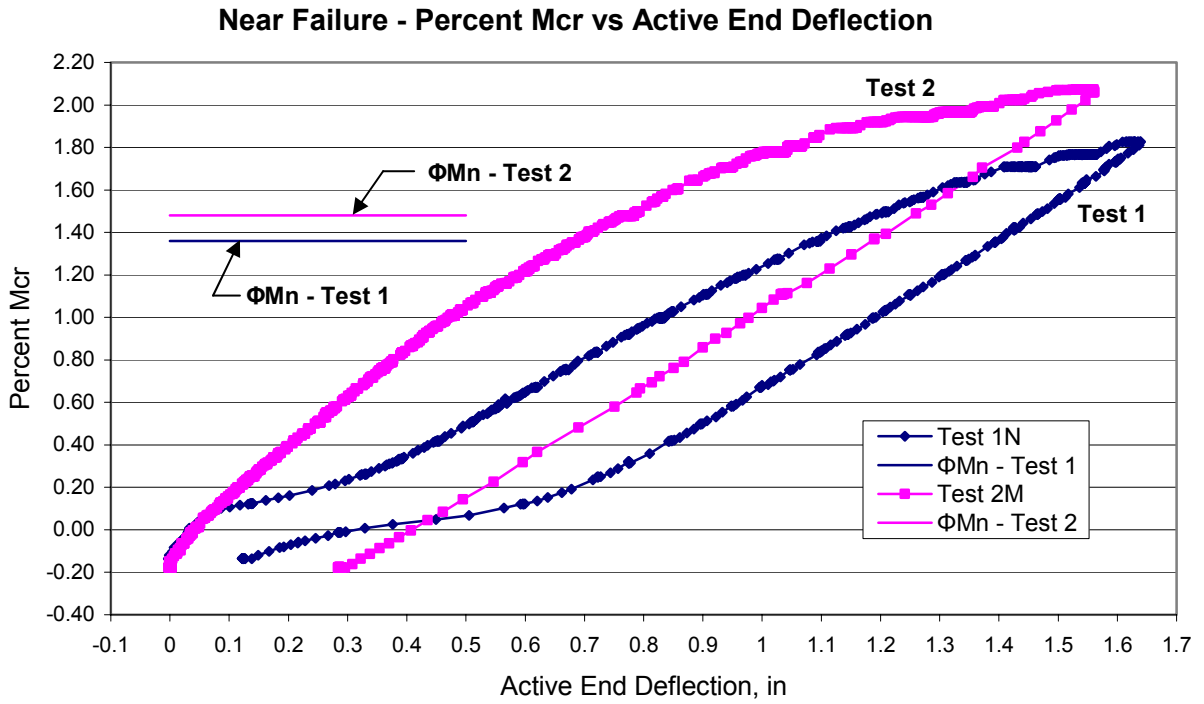


Figure 28. Ultimate Strength Tests for Test 1 and Test 2

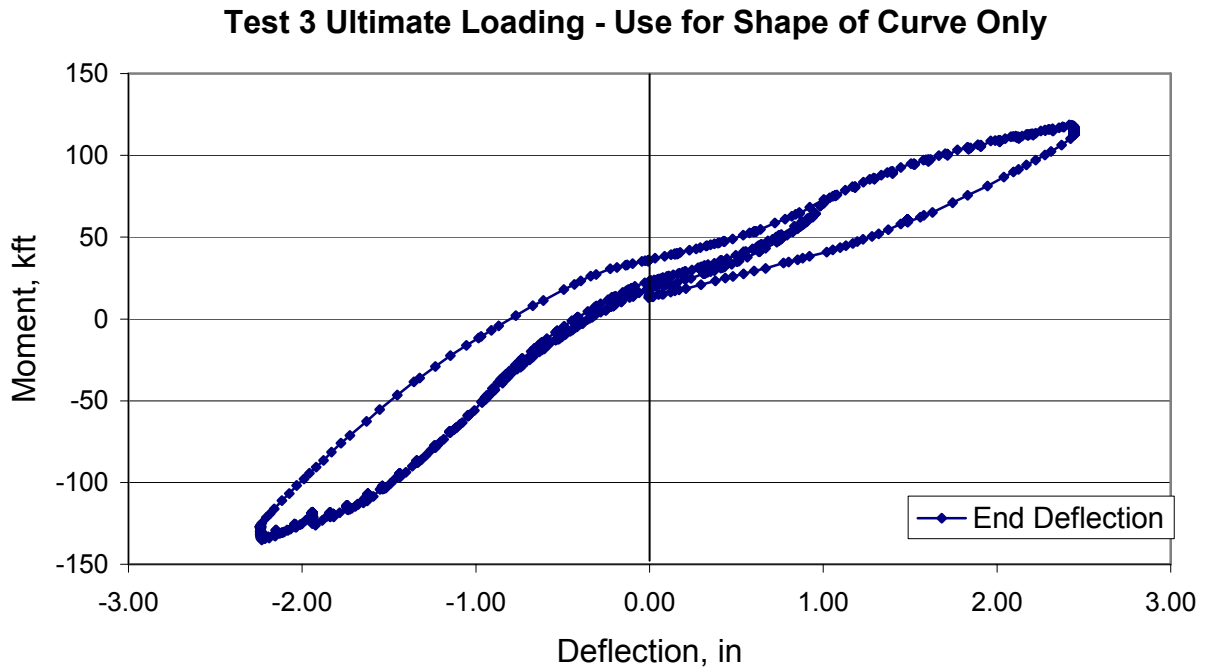


Figure 29. Ultimate Strength Test for Test 3



Figure 30. Underside of Continuity Diaphragm for Test 1 and Test 2



Figure 31. Cracking in End of Girders for Test 2

## DISCUSSION

### Discussion of Fabrication Phase

#### Steam Curing

It is clear that the assumptions used for the coefficient of thermal expansion of the concrete have a significant influence on the cumulative strain readings. As seen in Figure 16, at 21 hours after casting, the plot with an assumed CTE of  $5.8 \mu\epsilon/^\circ\text{F}$  indicates approximately zero strain while the plot with CTE of  $4.7 \mu\epsilon/^\circ\text{F}$  indicates approximately 90 microstrains. The behavior of the plot based on a variable coefficient of thermal expansion magnifies the slight decrease seen from 4 to 6 hours in series one and two. After 12 hours, the three plots follow a similar trend with only the magnitudes of the strains differing. At detensioning, the change in strain from all three series is approximately the same, since the change in temperature over this short time period was small.

From the data, it is impossible to determine the exact time when the concrete reached final set. Most likely, the concrete had set by the time the steam was turned on at 4.5 hours after casting. At this point, heating the system with the steam caused the overall expansion of the

girders and the metal formwork which occurred until approximately 8.5 hours after casting. The average temperature in the girders continued to rise after this time, but a contraction occurred despite the rise in temperature. This contraction is most likely due to autogenous shrinkage. At approximately 16 hours after casting, the steam was most likely increased, and a subsequent expansion took place due to the thermal expansion of the system. A gradual contraction took place after this point which is most likely due to a combination of autogenous and drying shrinkage.

### **Detensioning of Strands**

It is unusual to record changes in strain at detensioning that are larger in magnitude in compression than predicted. Many of the studies which have been performed to monitor the stress in the strands during detensioning conclude that the stress in the strand is less than the current methods predict. Less stress in the strands would cause less compression at detensioning. A recent report for the Louisiana Department of Transportation monitored AASHTO Type III girders (very similar to the shape of the PCBT girders used in this study) during fabrication with load cells placed on select strands between the bulkhead and the chucking devices (Roller et al. 2003). The load cells indicated that the stress in the strands decreases more than predicted during the steam curing process. At detensioning, the average force in the strands decreased from an initial jacking force of 30.1 kips to 28.7 kips, a 7 percent loss in force. The authors concluded that the thermal expansion of the girders during curing caused the loss in the prestressing force.

It is certainly possible that the thermal expansion of the girders could cause stress in the strand outside of the girders to decrease if the detensioning occurs while the girders are in an expanded state. As shown in Figure 16 if detensioning had occurred before 28 to 30 hours after casting the concrete, it would have been likely that the expansion of the concrete would have caused a reduced stress in the strands outside of the girders. However, a reduction in stress in the strands outside of the girder does not necessarily indicate a reduction in the stress in the strands within the girder. If the concrete sets early and acts composite with the strands, then the force at detensioning will have already been locked into the girder, and the change in force in the strand outside the girder will not necessarily effect the final force applied to the concrete at detensioning by the prestressing strands.

There are several possibilities that exist to explain why more compression was measured at detensioning than predicted. It is possible that the modulus of elasticity of the actual girder concrete was lower than the measured modulus of the control cylinder. This is unlikely because the control cylinder was measured at the time of detensioning and the modulus of the actual girder concrete is usually higher instead of lower than the modulus of test cylinders.

A second possible explanation is the presence of thermal gradients at the time the concrete set or at the time of detensioning. A study which monitored the temperature profile of Washington State W74MG girders during fabrication recently reported that a temperature gradient that exists when the concrete sets will induce mechanical strains that result in a loss of prestressing force after cooling occurs (Barr et al. 2004). Since a loss in prestressing force is opposite of what is observed, this may not explain the behavior of these girders. Also, it is

believed that the concrete set very early, before any significant thermal gradient due to the heat of hydration or steam curing could be established.

## **Discussion of Static Phase**

### **Early Age Restraint Moments**

Some interesting conclusions can be derived from an overall review of the development of the restraint moments in the two tests with the continuity diaphragms. First, it is apparent that some restraint moments develop early, within hours after casting the deck. Many current design procedures do not consider any development of restraint moments until the deck has cured and shrinkage is believed to begin, often at 7 days. The increase in reactions over the first day is consistent with expansion of the deck due to thermal effects. As the deck wants to expand, the composite section wants to rise in the center. However, since the section acts at least partly indeterminate, positive restraint moments are developed in the center and the outside reactions increase.

After approximately 1 day, the outside reactions begin to decrease rapidly. A decrease in reaction indicates that the top of the composite section wants to contract. As the composite section attempts to bend in a positive curvature, the partly indeterminate action causes the reactions at the outside to decrease. For both tests, the outside reactions actually decreased to values less than the reactions when the decks were first cast. This indicates that some negative restraint moment is present even at the early ages of approximately four days.

After four days until the end of monitoring, the reactions did not change as much as expected. This phenomenon has been noticed by other engineers who have stated that once the deck is cast, not much significant bending, or change in curvature, occurs in the section. Since bending is required to cause the development of restraint moments, restraint moments will not develop if bending is not present.

### **Conventional Prediction of Early Age Restraint Moments**

For precast, prestressed multi-girder construction made continuous with a continuity diaphragm, most designers typically only consider restraint moments due to creep and shrinkage of the concrete. Many of the design procedures also consider shrinkage to start at 7 days. Since this study as well as the recent NCHRP 519 study has noticed the development of restraint moments in the continuous system as early as one day after the casting of the deck, it is apparent that the typical design procedure which waits to consider shrinkage after an age of 7 days needs reconsidering (Miller et al. 2004).

Since positive restraint moments develop at an age of approximately one day, expansion of the deck due to thermal effects is most likely occurring. After that time, shrinkage of the deck dominates, causing the development of negative restraint moments. A conventional analysis of the actual system is performed to predict the restraint moments due to the superposition of the thermal effects and the shrinkage effects. It is assumed that the deck and the girder act compositely from the time the deck is cast. Since the observed reactions begin to change almost

immediately, some composite action is occurring early on. Actual values for the properties of the deck and girder concrete are used in the analysis. Both the thermal effects and the shrinkage effects cause changes in curvature in the system that are resisted by the restraint moments. The procedure outlined in the *AASHTO Guide Specifications – Thermal Effects in Concrete Bridge Superstructures* (AASHTO 1989) is used to determine the final distribution of stresses and strains in the composite section due to a nonlinear temperature gradient. The Composite Section Method is used to determine the final distribution of stresses and strains in the composite section due to the differential shrinkage. Therefore, two restraint moments are determined and added together for the final predicted restraint moment.

### *Comparison of Observed versus Predicted Restraint Moments*

Using conventional analyses, the restraint strains at the center of the two span section and the restraint moments are predicted for Test 1 and Test 2. Table 13 shows a summary of the predicted strains and moments and a ratio of the predicted divided by the observed values. The actual thermal gradients observed were used for all cases. The ACI Predicted shrinkage values of 15  $\mu\epsilon$ , 55  $\mu\epsilon$ , 190  $\mu\epsilon$ , and 232  $\mu\epsilon$  were used for 1, 4, 20, and 28 days respectively. For most cases, the predicted strains are less than the observed strains at the center of the two span system. However, the predicted restraint moments are much more than observed, especially at 20 and 28 days, where the predicted restraint moments are 21 to 39 times more than the observed restraint moments. Since the predicted values and observed values differ so much, a modified approach needs to be taken to predict behavior of the continuous system.

**Table 13. Conventional Analysis Summary**

Test No.	Age days	Gauge Location	Strain $\mu\epsilon$		A/B Ratio	Moment k-ft		C/D Ratio
			Predicted	Observed		Predicted	Observed	
1	0.9	Top	32	-55	-0.58	288	52.4	5.49
		Bottom	44	35	1.26			
	3.8	Top	-4	-160	0.03	-144	-25.7	5.60
		Bottom	-10	-109	0.09			
	28	Top	-76	-341	0.22	-1104.	-53.1	20.8
		Bottom	-121	-291	0.42			
2	0.7	Top	32	-45	-0.71	233	25.2	9.23
		Bottom	34	-4	-8.50			
	4.2	Top	-6	-121	0.05	-108	-23.4	4.62
		Bottom	-8	-42	0.19			
	20	Top	-68	-217	0.31	-884	-22.5	39.3
		Bottom	-120	-72	1.67			

### **Modified Approach for Prediction of Early Age Restraint Moments**

Newhouse presents a modified approach to predict the restraint moments observed in Tests 1 and 2 (Newhouse, 2005). The degree of continuity or composite action is modeled at all ages and the amount of differential shrinkage is estimated by considering the shrinkage in the

girder that occurs during the testing phase. The reinforcing in the deck is considered, but not within the model. An equivalent thermal strain is added to the predicted differential shrinkage and the quantity multiplied by a factor estimating the amount of composite action present. The final equivalent strain is then applied to the composite section using the Composite Section Method, and the restraining moment determined using the Conjugate Beam Method.

The modified analysis presented by Newhouse, which accounts for the fact that the section may not be fully composite, predicts more accurately the restraint moments at early ages when thermal effects dominate, which for these tests is less than 7 days. However, moments after 20 days are still greatly overpredicted. After the early period where thermal effects dominate, not much restraint moment develops in the two tests. This has been observed in the field where engineers have stated that once the deck is made composite, that the system does not bend or undergo as much curvature as conventional design procedures predict. Since the observed shrinkage in the electrical resistance gauges attached to the bars is higher than predicted, there is evidence that shrinkage of the system is occurring; however, it is not manifesting itself as differential shrinkage which causes bending or changes in curvature.

#### *Other Possible Explanations of Restraint Moments Observed*

The modified approach for predicting restraint moments at early ages, when thermal influences dominate, works reasonably well for the first few days. However, after an age of approximately 7 days, the method does not predict restraint moments adequately. In spite of the fact that shrinkage is measured in the shrinkage specimens and in the electrical resistance gauges in the deck, not much net differential shrinkage appears to occur after approximately 7 days. Other reasons for this phenomenon are proposed.

**Softening at Diaphragm and Girder Interface.** It is possible that a region of reduced stiffness forms at the interface of the end of the girder and the continuity diaphragm. The girder-to-diaphragm interface acts as a bond break since the concrete for the diaphragm is placed against the already cured ends of the girders. Cracking at the interface would cause the moment of inertia of the section to decrease at the interface. A decreased moment of inertia would then cause less restraint moment for a given end rotation.

**Girder and Slab Shrink at the Same Rate.** If the girder and slab were to undergo shrinkage at the same rate, then no differential shrinkage would occur. If the development of shrinkage strains is such that after the first seven to ten days of rapid shrinkage, the rate of continued shrinkage is similar to the rate of shrinkage of older concrete, then the additional differential shrinkage restraint moment would be very small.

**Extensibility of the Deck Concrete.** According to Mehta, extensibility can be defined as the ability of a concrete to deform in tension without cracking (Mehta 1986). A concrete with a low modulus of elasticity generally has better extensibility than a concrete with a high modulus of elasticity. At the early age when a majority of the shrinkage is occurring, the modulus of elasticity is also lower. From Hooke's Law, a lower modulus of elasticity also produces lower stress for a given strain. When shrinkage is occurring at early ages, the actual tensile stresses produced by the strains are likely to be less because of a combination of the lower modulus of

elasticity and the extensibility of the concrete. Smaller forces would then result in smaller restraint moments.

## Discussion of Service/Cyclic Phase

### Service Load Testing

#### *Initial Cracking Moment*

As shown in Table 11 the ratio of the designed initial cracking moment to the observed cracking moment is calculated for all three tests. Values closest to unity indicate the best prediction of the initial cracking moment. For all three tests, the currently used method of predicting initial cracking moment, Method 1, over predicts the actual cracking moment by a significant amount, with ratios ranging from 1.52 to 3.29. For Test 1 and 2, Method 5 is the best at predicting initial cracking moment with ratios of 0.90 to 1.19. For Test 3, the cracking moments presented are the cracking moments of the deck which is continuous over the supports. Since the deck is continuous, it is expected to initially crack at a higher tensile stress than the sections in Test 1 and Test 2 which are cast against the ends of the girders. This is shown in the table where Method 5 under predicts the capacity by a factor of 0.61. Method 4 provides the best predictor for the initial cracking with ratios of 0.90 and 0.93.

Figure 32 shows the initial cracking of 0.016 in along the interface of the girder and the diaphragm for Test 2B at the loading of  $1.0M_{cr}$ . The initial cracking of Test 1 and Test 2 at the interface was well defined for both tests. Since the interface at the ends of the girders acts as a cold joint (no bonding agent was used), the cracking can be considered as debonding of the diaphragm concrete from the end of the girder. Although the debonding does produce an opening that is large enough to allow the intrusion of water into the section, the crack caused by the debonding can be mitigated with a sealant since the debonding is well defined.

For prediction of the initial positive cracking moment at the interface of the girder and the diaphragm, it is recommended that the tensile capacity of the concrete at the bottom of the connection be estimated with Method 5 from Table 11. Gross section properties considering the full profile of the end of the girder, the bolster, and the full width of the deck should be used for determining the cracking moment capacity. For the initial cracking of the deck, the capacity of the deck to resist moments across the opening between the ends of the girders is generally not considered in the design.

#### *Prediction of Initial Crack Widths*

Figure 33 presents a simplified model to predict the initial crack widths at the interface of the end of the girder and the diaphragm for Test 1 and Test 2. The model assumes that once first cracking occurs, cracked section properties can be used to determine the strain in the steel,  $\epsilon_a$ , at the crack opening. The strain in the concrete at the crack opening is assumed to be zero. At the end of the embedded strand or bar in the continuity diaphragm, a distance  $f$  as shown, uncracked transformed section properties are used to determine the strain in the steel and the concrete which will be equal,  $\epsilon_b$ . Assuming that the load on the bar is symmetric about the crack, half of

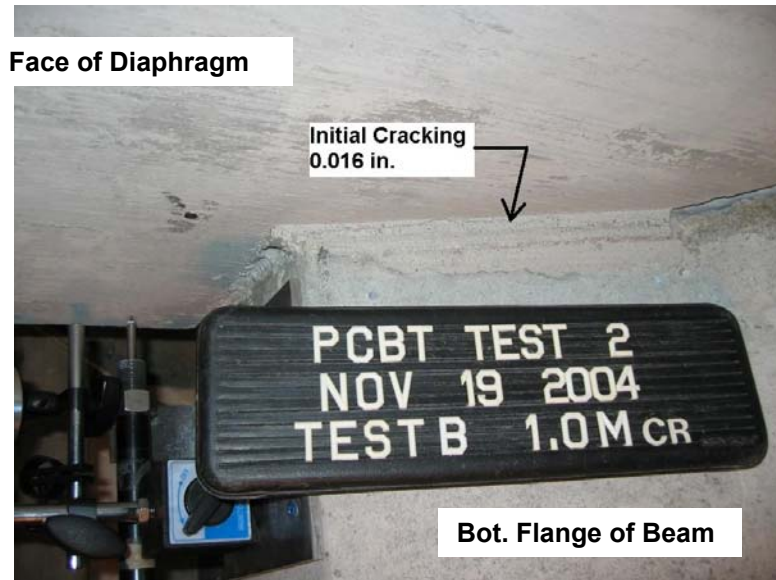


Figure 32. Initial Cracking at Interface

the predicted crack opening,  $w$ , can then be determined by integrating the difference in the strain in the steel and the strain in the concrete over the distance,  $f$  as:

$$\frac{w}{2} = \int_0^f \varepsilon_s - \varepsilon_c \, df \quad (4)$$

where  $\varepsilon_s$  is an expression for the strain in the steel and  $\varepsilon_c$  is an expression for the strain in the concrete. For the expressions shown, the crack width reduces to the simple formula of:

$$w = f\varepsilon_a \quad (5)$$

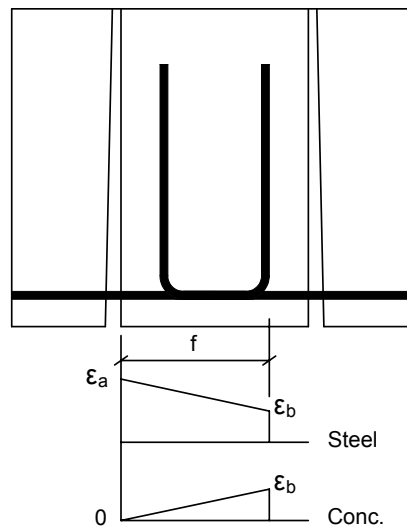


Figure 33. Model for Predicted Crack Widths

For the initial service load test, Test A, for Test 1 with the strands, the model predicts a crack opening of 0.016 in and the observed average LVDT reading was 0.012 in, similar in magnitude but over predicted by a ratio of 1.30. For Test 2, the model predicts a crack opening of 0.011 in and the observed average LVDT reading was 0.009 in, also similar in magnitude but over predicted by a ratio of 1.20. Although simplified, the model does reasonably well at predicting the average opening at the moment causing initial cracking. This model is also used to predict crack widths due to positive moments applied during the cyclic testing in the following section where the calculations are provided.

## **Cyclic Testing**

### *Behavior During Cyclic Loads*

The behavior of Test 1 changed throughout the duration of the cyclic loads. During cyclic loads, untensioned prestressing strands have been known to develop a tendency to slip (Salmons 1974). As the strands are pulled in tension, the wires have a tendency to twist and locally unwind through the surrounding concrete, causing some localized crushing. For a tensioned strand, Hoyer's effect acts to counteract the loss in development due to the twisting action. However, for untensioned strands, such as are in the Test 1 continuity diaphragm, Hoyer's effect does not help to increase the bond stresses. Throughout the cycles, the strands experience a reduction in bond from the location of the interface to the 90 degree bend.

The response of Test 2 to the cyclic loads remains virtually unchanged throughout the testing. Following the service load testing, the role of the aggregate to aggregate friction in increasing the tensile force capacity is diminished as the tensile steel becomes the dominate provider of tensile capacity.

### *Increase in Crack Openings due to Cyclic Loads*

It is typical to compare the stress to number of cycles, or S-N curve, for a test performed with cyclic loads. For Test 1 and 2, the applied moment at testing was kept the same, so a comparison of stress does not provide any useful information. Instead, a comparison is made showing the average LVDT reading, or average crack opening, at the bottom of the interface versus the number of cycles shown on a log scale. Figure 34 shows this comparison.

The graph shows that over the 10,000 cycles, the crack opening for Test 2 increases only slightly and remains fairly linear throughout the life of the testing. However, for Test 1, the crack opening starts off linear, at nearly the same slope as Test 2, but at approximately 5000 cycles, begins to increase rapidly. This type of behavior is undesirable, indicating that the system is softening during the cyclic loads. Although the connection is still able to transfer the moment across the connection, this behavior indicates that the system has a decrease in continuity during the loading. For a given moment, more rotation occurs at the connection.

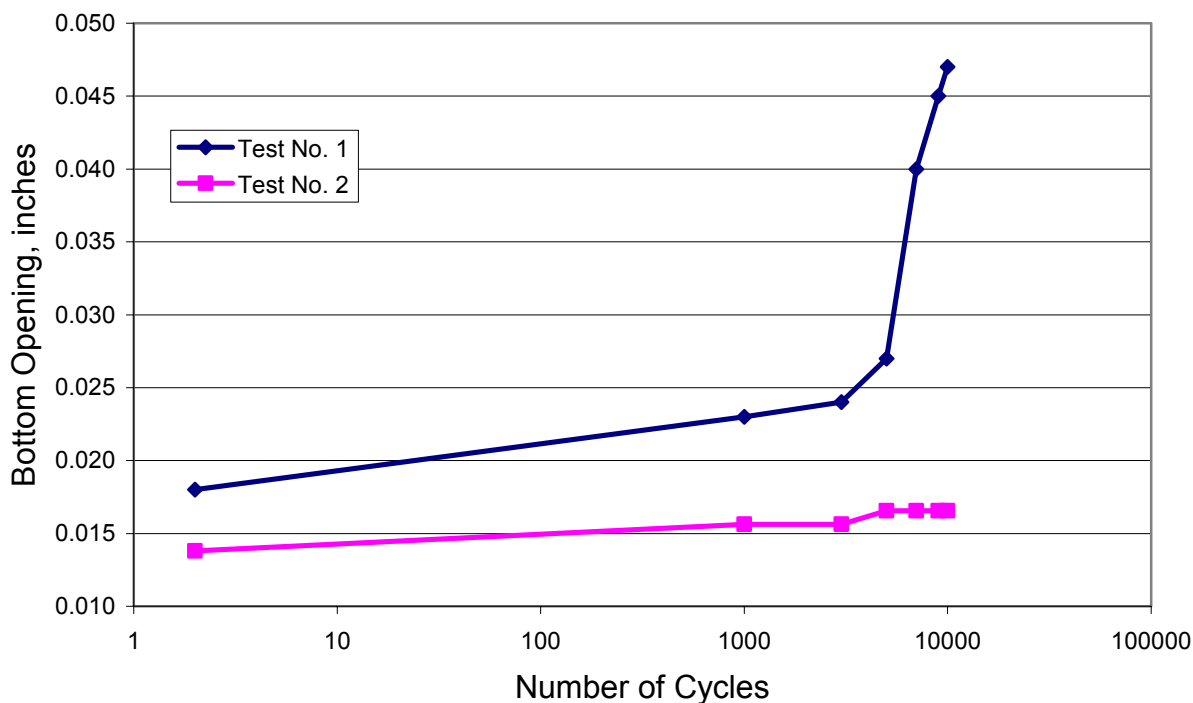


**Figure 34. Opening versus Life Comparison for Test 1 and Test 2**

Using the previously described model for the prediction of crack widths, Figure 35 shows a comparison of the ratio of the predicted crack opening to the average crack opening measured at the bottom of the interface with the LVDTs. The ratios are plotted versus the number of cycles. A perfect prediction is indicated with a ratio of 1.0.

The model for predicting the crack opening through the cyclic phase does reasonably well for Test 2, but under predicts the crack openings for Test 1 as the number of cycles is increased. The decreased bond of the prestressing strand causes the assumptions of strains along the length of the strand to become invalid. Table 14 shows the calculations for the predicted crack openings and the ratio of the predicted to observed crack openings.

### *Continuity*

Both continuity connections for Test 1 and Test 2 were able to resist the service loads applied during the service and cyclic phases. Also, both connections were able to transfer the service loads (up to  $1.2M_{cr}$ ) through the connection throughout the testing. Both connections showed some softening during the initial service load testing. Throughout the cyclic load testing, Test 1, with the strands, required more end rotation to resist the moments than did Test 2, with the bars. Opinions about the definition of continuity in a continuous system differ widely. From a load standpoint, neither connection exhibited a decrease in continuity during the testing. However, from a rotational standpoint, both sections did see a reduction in the continuity of the system during the testing because more rotation was required to transfer the same moment.

### Comparison of Crack Openings

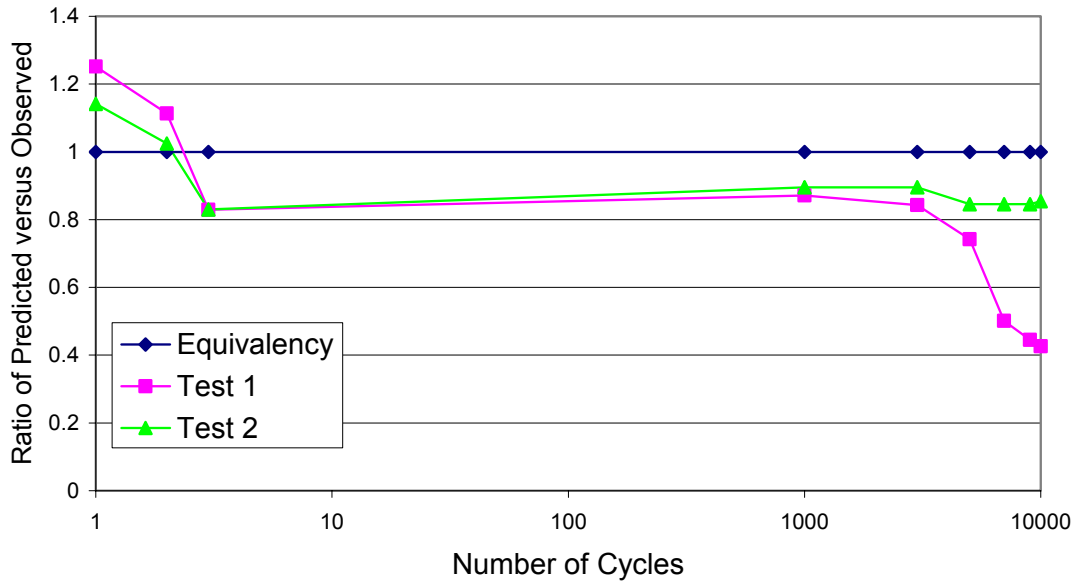


Figure 35. Predicted versus Observed Crack Openings

Table 14. Calculations for Crack Opening Widths

Test	M applied k-ft	No. Cycles	Strand		Observed Opening in	Predicted Opening in	Ratio Pred./Obs.
			Stress, $f_s$ ksi	Strain, $\epsilon_s$ $\mu\epsilon$			
1-A	392.9	1	50.6	1733	0.012	0.016	1.30
1-B	523.8	2	67.5	2310	0.018	0.021	1.16
1-C	628.6	3	81.0	2772	0.029	0.025	0.86
1-D	523.8	1000	67.5	2310	0.023	0.021	0.90
1-E	529.0	3000	68.1	2333	0.024	0.021	0.88
1-F	523.8	5000	67.5	2310	0.027	0.021	0.77
1-G	523.8	7000	67.5	2310	0.040	0.021	0.52
1-H	523.8	9000	67.5	2310	0.045	0.021	0.46
1-J	523.8	10000	67.5	2310	0.047	0.021	0.44
Test	M applied k-ft	No. Cycles	Bar		Observed Opening in	Predicted Opening in	Ratio Pred./Obs.
			Stress, $f_s$ ksi	Strain, $\epsilon_s$ $\mu\epsilon$			
2-A	392.9	1	28.2	1017	0.009	0.011	1.22
2-B	529.0	2	37.9	1369	0.014	0.015	1.09
2-C	628.6	3	45.1	1626	0.020	0.018	0.88
2-D	523.8	1000	37.5	1355	0.016	0.015	0.95
2-E	523.8	3000	37.5	1355	0.016	0.015	0.95
2-F	523.8	5000	37.5	1355	0.017	0.015	0.90
2-G	523.8	7000	37.5	1355	0.017	0.015	0.90
2-H	523.8	9000	37.5	1355	0.017	0.015	0.90
2-J	529.0	10000	37.9	1369	0.017	0.015	0.91

## **Resolution of Design Issues**

### *Preparing Bent Strands at the Fabricator*

In the design phase of the project, there was concern expressed about cutting and bending the prestressing strands. Fraying of the strands has been noticed at the fabricator when strands are cut under tension with a torch. The fabricator avoided this problem by first cutting the end strands longer than required for the end connection. For this test, the strands needed to extend 24 in, so the fabricator first cut at approximately 36 in and then made a final cut with the strands not under tension at the 24 in location. This eliminated the problem with fraying. The strands were bent at the fabricator prior to delivery. A discussion with the foreman indicated that there were no problems with bending the strands, and that the strands were cold bent (no torch was used for the bending process).

### *Placing Mild Steel at the Fabricators*

There was also concern expressed about placing the U shaped mild steel used in Test 2. The steel was designed to be placed within the end of the girder allowing for the typical 2 in on center grid of prestressing strands to remain at 2 in on center. The bars were placed directly against the strands, or bundled, and tied to the strands. The end form was modified by cutting slotted holes in a plywood section used on the bottom only. After casting the girders, the form was pulled straight back off of the end of the girder. The foreman indicated that the method worked well, and that a plywood section is generally used anyway if any type of steel is extended from the ends of the girder.

There was also concern that the end termination of the mild steel may cause cracking to occur at the termination location. The termination was designed to stagger from top to bottom, the top length being longer than the bottom length, as proposed in NCHRP 519. However, the bars were fabricated with same length legs, and were already installed. There was no cracking at the bar termination location in the test beams, however staggering the cutoff is recommended to avoid a sudden change in stiffness in the bottom flange.

### *Embedment of Girders into Diaphragm*

Many states use a detail in which the ends of the girders are embedded typically from 3 in to 6 in into the diaphragm. This detail was not tested for two reasons. First, some reports indicate that the embedment does not significantly increase the capacity of the section. Second, it is suspected that any cracking that occurs due to rotations at the interface will cause spalling of the section because the end of the girder exerts forces on the edge wedges of concrete. The results of this study indicate that sufficient strength can be achieved without embedding the ends of the girders. Also, the cracking which occurs when the girders are not embedded is well defined and can be mitigated whereas cracking and spalling of embedded girder ends may be much more difficult to mitigate.

## *Modification of Center Stirrups for Girders*

The VDOT recently modified the center stirrups that extend from the top of the girder from two separate stirrups with 90 degree legs to one single U shaped stirrup. The modification was made to help eliminate a tripping hazard on the top of the girders. Although not specifically tested, the testing performed did not provide any indication that the modification reduced the performance of the section.

## **CONCLUSIONS**

### **Design Phase**

- When compared to the theoretical cracking moment of a section at the continuity diaphragm, the predicted positive thermal restraint moments can be significant for commonly used girder spacings and span lengths. The thermal restraint moment ranges from about 0.7 to 1.3 times the theoretical cracking moment.
- When comparing the most commonly used current methods, the PCA Method generally predicts the most conservative positive restraint moments due to time dependent effects such as creep and shrinkage.
- For typically used span and strand arrangements, as the span length decreases, the predicted positive restraint moment due to creep and shrinkage generally also decreases.
- For very early ages of continuity, some predicted positive restraint moments due to creep and shrinkage are greater than 1.2 times the cracking moment,  $M_{cr}$ , but usually only for early ages of continuity.
- For ages of continuity greater than approximately 60 days, Comparison Method 1 and the RMCalc Method predict similar positive restraint moments due to creep and shrinkage.
- For ages of continuity greater than approximately 90 days, most current methods predict that no positive restraint moment will develop due to time dependent effects such as creep and shrinkage

### **Laboratory Phase**

- The ACI equation for predicting the modulus of rupture,  $f_r = 7.5(f'c)^{0.5}$ , under predicts the modulus of rupture for the high strength girder concrete by an average of 180 psi but predicts the modulus of rupture for the lower strength deck concrete well.
- The ACI equation for predicting the modulus of elasticity,  $E = 57,000(f'c)^{0.5}$ , predicts the modulus of elasticity reasonable well for the high strength girder concrete and predicts the modulus of elasticity very well for the lower strength deck concrete.
- For shrinkage specimens monitored from day 1, one of the two tests indicates that significant expansion occurs during the first week prior to the onset of shrinkage.

- For shrinkage specimens monitored from day 7, one of the three tests shows shrinkage similar to the ACI-209 predicted shrinkage while the other two tests show significantly more shrinkage than predicted by ACI. The MC-90 under predicts the early age shrinkage for all three tests.
- The coefficients of thermal expansion for both the girder and the deck concrete are lower than the recommended value of  $5.8 \mu\epsilon/^\circ\text{F}$  for typical concrete proposed by the vibrating wire gauge manufacturer. For the girder, a value of  $4.7 \mu\epsilon/^\circ\text{F}$  was determined; for the deck, a value of  $5.1 \mu\epsilon/^\circ\text{F}$  was determined.
- Vibrating wire gauge readings corrected for temperature changes are sensitive to the differences in the actual values of the coefficients of thermal expansion for the concrete and the gauge. The correction for temperature can introduce significant errors if the actual coefficients of thermal expansion for the concrete and the gauge are not known.

### **Fabrication Phase**

- Prior to casting the girders, bed temperatures potentially change significantly due to the heating or cooling of the steel forms, causing the strands to either elongate or contract and change the prestressing force prior to casting. In this study, the heating of the forms may have caused a prestress loss of 3.6 ksi prior to casting the concrete.
- Actual bed temperatures during steam curing may be much higher than believed by the fabricator. Recorded bed temperatures for this study are nearly  $40^\circ\text{F}$  higher than recorded by the fabricator.
- Considerable variation in the bed temperatures during steam curing may exist because of the locations of the steam line outputs and the fact that the steam rises to the top of the girders under the tarps. Recorded differences in the concrete temperatures for this study vary by as much as  $48^\circ\text{F}$ .
- The control cylinder displays early age shrinkage, possibly due to the autogenous shrinkage, while the girders display early age expansion, possibly due to thermal effects.
- The strain profile of the girders during steam curing when high temperature changes occur is significantly influenced by the assumptions used in the temperature correction for the vibrating wire gauges. The presence of water in the concrete at early ages may contribute to the inability to determine the coefficient of thermal expansion of the concrete at early ages with good certainty.
- Measured changes in strain (and curvature) at detensioning indicate that the loss of prestress force during casting may be less than predicted by others. Measuring the change of stress in the strands outside of the girder may not be a good indicator of actual stress loss in the strand at detensioning. However, without monitoring the changes in strain at detensioning both within the girders and in the strands outside the girders, it is impossible to know the exact prestress loss at detensioning.

### **Static Phase**

- Immediately after casting the deck on a girder in a continuous system, some positive restraint moments begin to develop due to thermal expansion of the deck. The positive restraint moments continue to develop for approximately one day.
- After an age of one day, negative restraint moments begin to develop, and continue to develop rapidly until the deck is approximately four days old. After a deck age of approximately four days, some negative restraint moments continue to develop, but at slower rate.
- The magnitudes of the restraint moments observed are less than predicted by conventional analysis. At early deck ages (less than seven days) conventional analysis can not be used to predict the restraint moments. At the later deck ages observed, one or more mechanisms prevent conventional analysis from predicting the correct magnitudes of the restraint moments.
- Significant compressive strains are measured in the reinforcing in the deck throughout the static phase, indicating that shrinkage of the deck is occurring. However, the shrinkage which occurs does not completely manifest itself as a differential shrinkage causing changes in restraint moments as measured by the changes in reactions.
- Possible reasons for the difference in the restraint moments observed and the restraint moments predicted include: restraint due to the reinforcing in the deck, softening in the continuity diaphragm connection, shrinkage of deck and girder occur at approximately the same rate, and the extensibility of the deck concrete reduces the forces to the top of the girder.

### **Service and Cyclic Phase**

- The predicted initial positive cracking moment capacity at the interface of the end of the girder and the diaphragm is lower than current recommendations predict. The fact that the end of the girder acts as a cold joint causes debonding at the section, reducing the cracking moment capacity.
- Both continuity tests, Test 1 with the extended strands and Test 2 with the extended 180 degree U bars, display acceptable behavior during the initial service tests. Test 2 is slightly stiffer, with average crack openings at the bottom of the interface of 0.022 in versus 0.029 in for Test 1 at a loading of 1.2Mcr. Therefore, the crack openings of Test 1 are 1.3 times larger than the crack openings of Test 2 following the service tests.
- Following the cyclic phase testing, both test sections are capable of withstanding anticipated service load moments (up to 1.2Mcr). But, during the cyclic phase of testing, Test 1 begins to display some undesirable behavior. The crack openings begin to increase at approximately 5,000 thermal cycles and continue to increase during cycling. At the end of testing, crack openings for Test 1 are 2.6 times larger than crack openings for Test 2, 0.047 in versus 0.018 in respectively at a loading of 1.0Mcr.

- Both Test 1 and Test 2 display good repeatability during the negative moment testing phase.
- Both Test 1 and Test 2 exceed the predicted ultimate positive moment capacities by ratios of 1.32 and 1.35 respectively. The predicted ultimate positive moment strength for Test 1 is based on the method proposed in *End Connections of Pretensioned I-Beam Bridges* (Salmons 1975). The predicted ultimate positive moment strength for Test 2 is based on current design procedures using Whitney's Equivalent Stress Block (ACI Building 2002).
- For Test 2, minor cracking in the ends of the girder was noticed at the web-bottom flange re-entrant corner.
- For Test 3, which did not have a continuity connection, two distinct cracks instead of one developed during the service load testing in the deck.
- For Test 3, after the initial deck damage which occurs during the initial service load testing, not much additional damage occurs during the cyclic testing.

## RECOMMENDATIONS

### General

1. For design, thermal restraint moments determined from the *AASHTO Guide Specifications – Thermal Effects in Concrete Bridge Superstructures, 1989*, should be considered. For ages of continuity over approximately 60 days, the thermal restraint moments generally control over restraint moments due to creep and shrinkage. The results of this study indicate that it is possible that final restraint moments due to both thermal effects and creep and shrinkage effects may be less than predicted. However, the restraint moments due to thermal influences measured during the study appear equally significant, or even more significant, than the restraint moments due to creep and shrinkage.
2. Since the temperature correction for vibrating wire gauges is sensitive to the actual coefficient of thermal expansion of the concrete, any experimental testing using vibrating wire gauges should attempt to monitor the actual coefficient of thermal expansion of the concrete during the testing. This is especially important at early ages, when the influence of water in the system may significantly alter the coefficient of thermal expansion of the concrete.
3. During fabrication of girders, the fabricator should consider the potential prestress losses in the strands due to heating or cooling of the strands in the forms prior to casting the concrete by either slightly altering the jacking force or controlling the strand and concrete temperatures. To avoid temperature related prestress losses, the strand temperature should be approximately the temperature of the concrete at its initial set. The fabricator should also monitor bed temperatures near the top of the forms, where the steam tends to collect and the highest temperatures are present. Any attempt to measure the actual force in the prestressing strands should include both the monitoring of the strains and temperature in the girder and the strains and temperatures in the strands outside the girder at detensioning. Once the

concrete gains sufficient strength, both changes in strand stress and temperature at detensioning are needed to estimate the prestress force released at transfer.

4. Conventional analysis should not be used to estimate restraint moments at early ages of the deck. Additional research is needed to identify the exact mechanisms that take place during differential shrinkage of composite systems.
5. To determine the moment that will cause initial cracking, the initial positive cracking moment of the girder at the diaphragm should be determined with an allowable tensile capacity of the concrete,  $f_t$ , equal to  $(1/4)(w f_c')^{0.5}$  where  $w$  is the unit weight of the concrete (in pcf) and  $f_c'$  is the compressive strength of the concrete (in psi).
6. Although the continuity connections for both Test 1 and Test 2 perform adequately under service and ultimate loads, the connection for Test 2, with the 180 degree U bars, is recommended for use. Details are provided in Figures 36 through 38. The connection remains stiffer during the testing and is expected to provide for a better long term connection. The cyclic testing performed on Test 2 induced stresses of 31.6 ksi tension in the bars. The maximum service stresses induced at  $1.0M_{cr}$  and  $1.2M_{cr}$  were 37.5 ksi and 45.0 ksi in tension, respectively. Two transverse joints above the ends of the girders instead of one should be used if the continuous deck detail tested in Test 3 is implemented.

### **Design Procedure**

1. It is recommended that PCBT girders that are to have a continuous deck be detailed to have a continuity diaphragm. For negative moment continuity, the reinforcing steel in the deck should be designed to resist the tensile loads using factored loading.
2. The ends of the girders should be detailed to remain flush with the continuity diaphragm. Embedment of the girders into the diaphragm is not recommended.
3. For positive moment, the continuity diaphragm should be designed to resist the maximum factored anticipated service load. This load should be determined as the maximum of the restraint moment due to thermal gradient or the restraint moment due to creep and shrinkage effects. For ages of continuity over 60 days, the thermal restraint moments will usually govern. Ultimate strength analysis (for the extended bars) or the method proposed by Salmons (for the extended strands) should be used to determine the capacity of the section. A load factor of 1.0 is recommended for factoring the service load. It is believed that the prediction of the restraint moments using a conventional analysis sufficiently over-predicts the magnitude of the moment at the continuity connection, allowing for the load factor of 1.0.
4. In lieu of an advanced analysis considering both early and late ages of continuity, thermal effects and shrinkage and creep effects should not be considered for the design of the girders or the negative moment connection of the diaphragm. For flexural design under service conditions, the girders should be designed as simple spans for dead and live loads. For

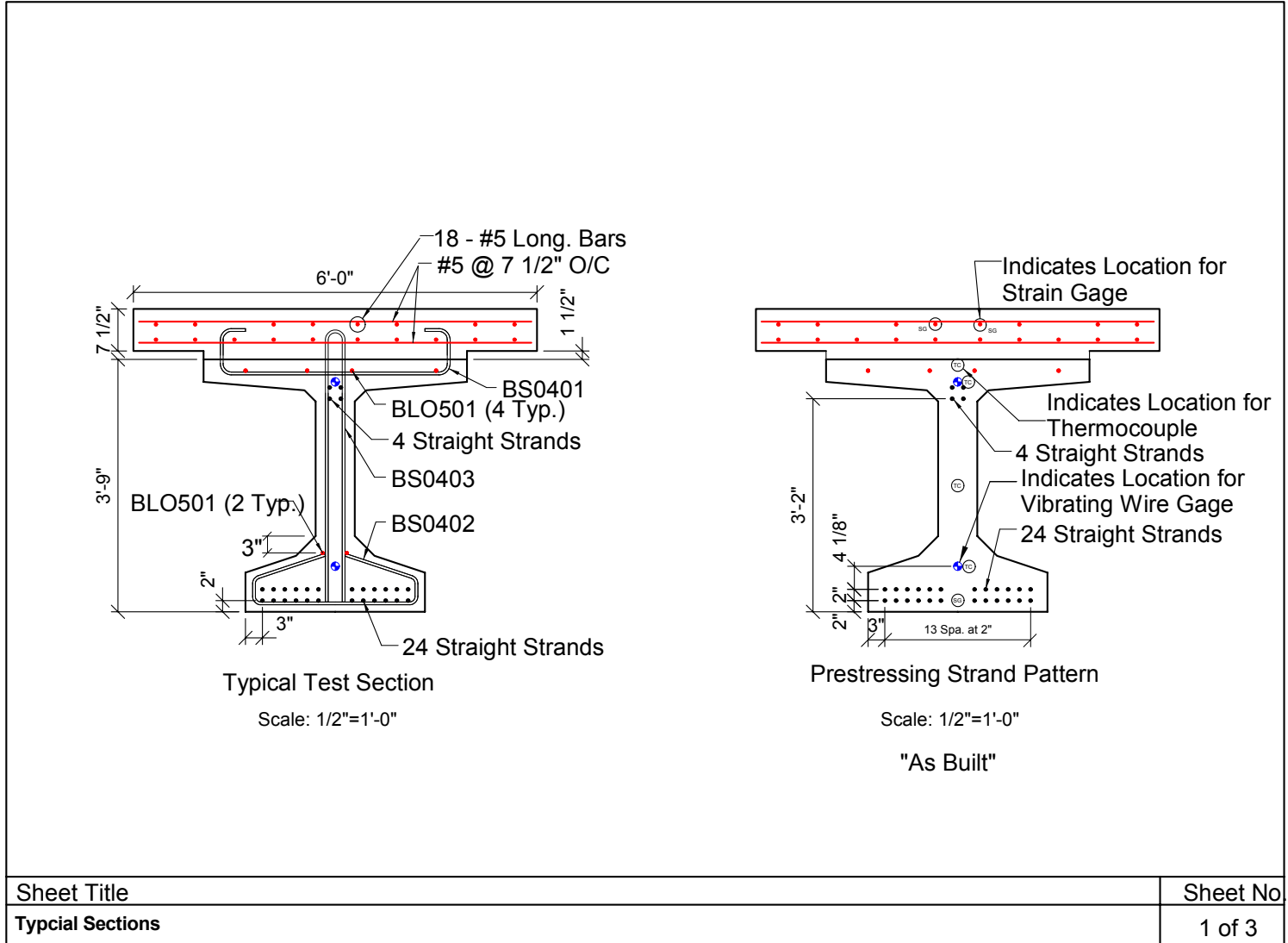


Figure 36. Details of PCBT 45 Girder with Recommended Diaphragm Detail.

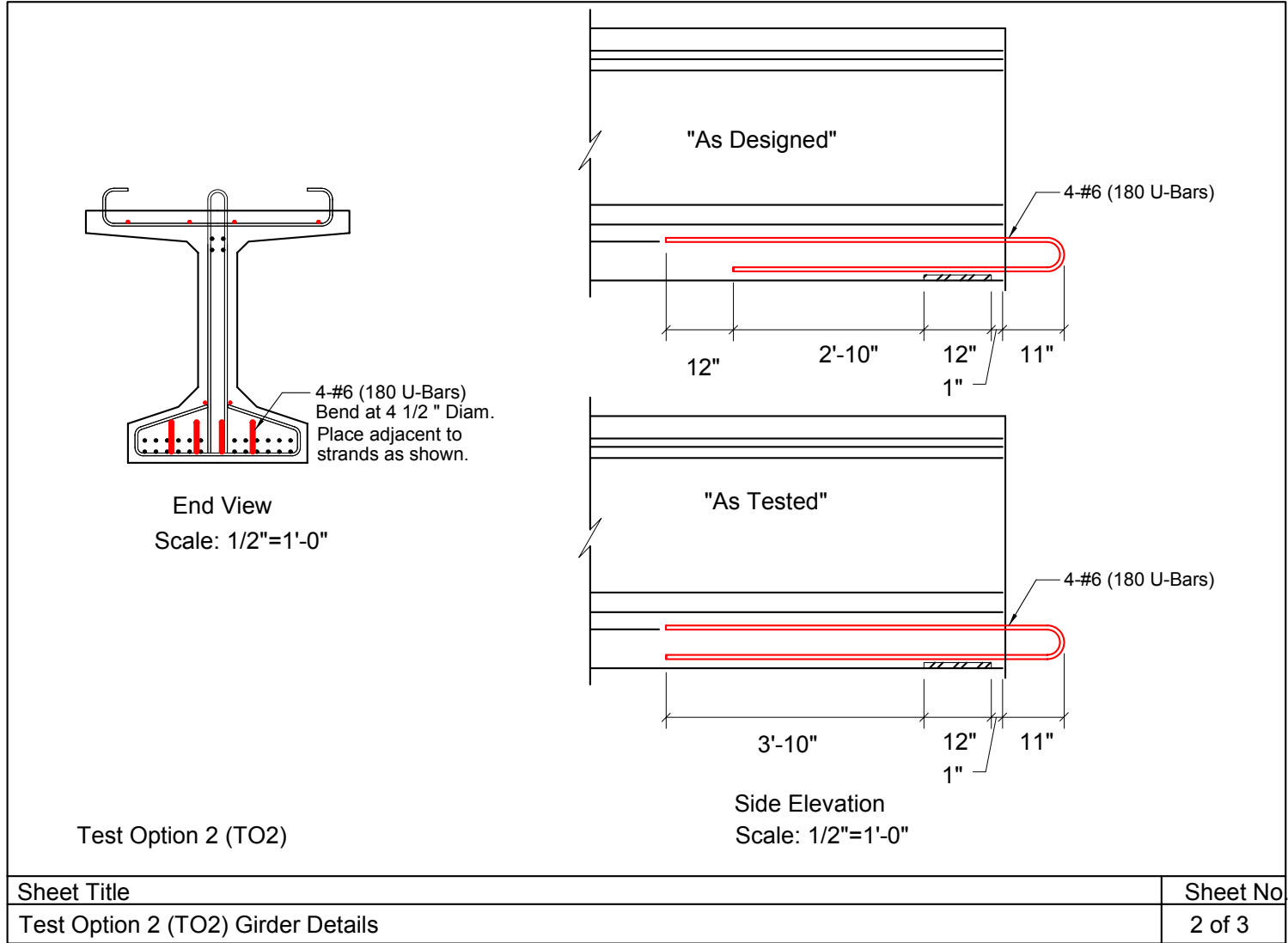


Figure 37. Details of Hairpin Bars for Recommended Diaphragm Detail.

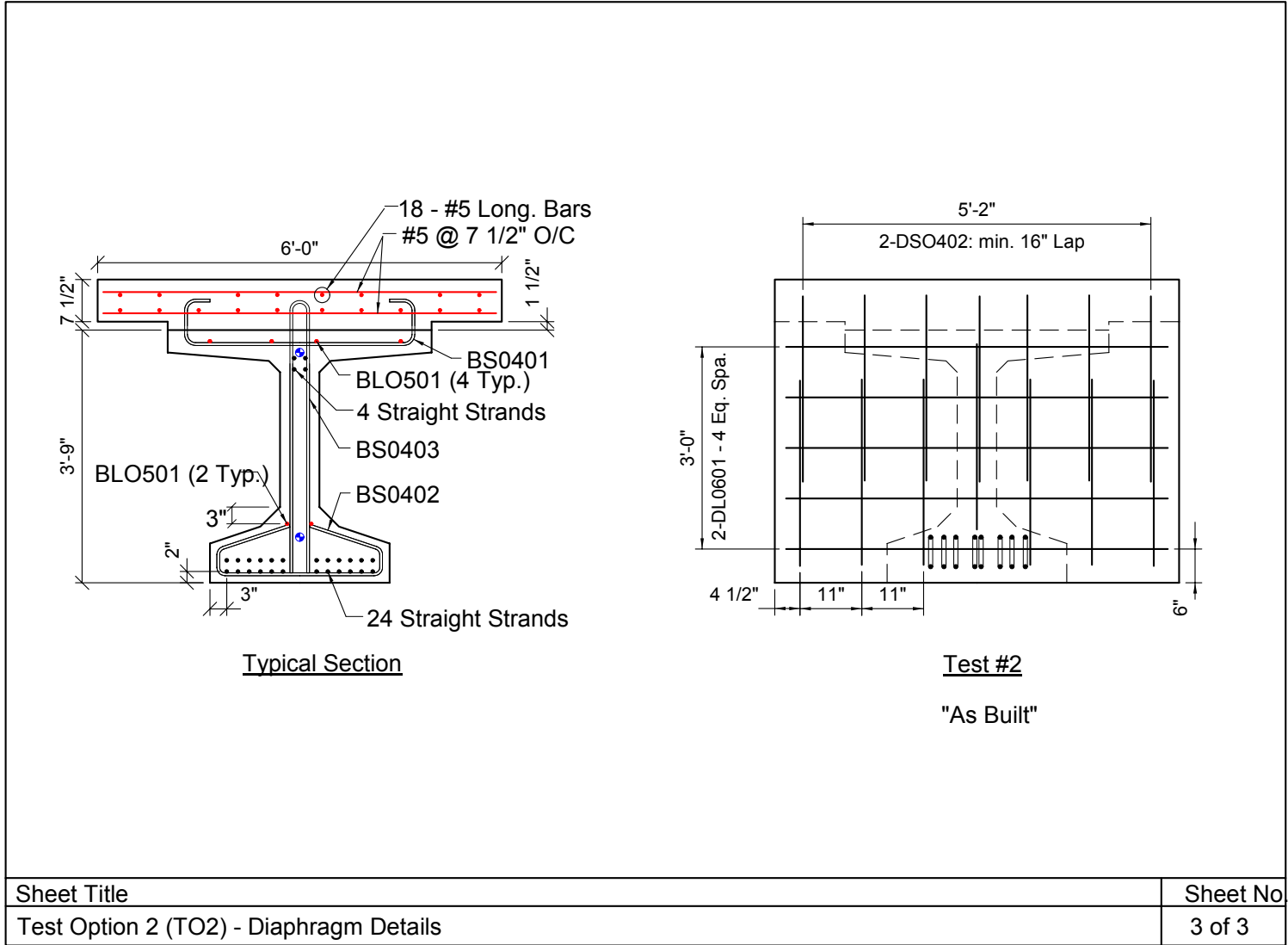


Figure 38. Recommended Diaphragm Reinforcing Details.

ultimate strength conditions, the girders should be designed using Load Factor Design assuming a fully continuous system for both flexure and shear. The negative moment above the continuity connection should also be designed based on a fully continuous structure using Load Factor Design, recognizing that the additional capacity in negative moment will help to redistribute any restraint moments due to creep, shrinkage, or thermal effects that would otherwise increase moments at midspan. Analytical work in the NCHRP 322 Report (with confirmation by NCHRP 519 Report and this project) indicates that a structure with a continuity diaphragm is able to transfer moments through the joint during the service load range. A loss in continuity is not anticipated until loading approaches failure. Even though during the service load range the connection is able to transfer moments, additional rotations are required to transfer the moments because of cracking in the diaphragm. The benefits of reduced moments in mid-span due to the continuous design may not be realized fully due to the fact that the structure may have to rotate an additional amount to allow the reduced loading to occur. The uncertainty caused by this fact, coupled with the fact that the restraint moments induced because of the continuity can increase the moments at mid-span, leads to this recommendation.

5. Whether or not cracking due to positive restraint moments will occur at a continuity connection can be checked by calculating the cracking moment based on an upper bound for the tensile capacity at the bottom of the interface of  $(1/4)(w_f'c)0.5$ . Gross section properties at the interface using the material properties of the continuity diaphragm should be used in determining the actual cracking moment. The full slab width and profile of the girder should be used in determine the gross properties.
6. It should be recognized that the interface of the girder and the continuity diaphragm will most likely crack or debond at a fairly low load level (lower than the conventional calculated cracking moment,  $M_{cr}$ ). The edges at the end of the girder diaphragm interface should be sealed with a material able to withstand movements (up to 0.050 in) at the time of initial construction. This type of material may require a backer rod.
7. For constructability, the design service moments (due to either thermal effects or creep and shrinkage effects) at the diaphragm should be kept at or below the conventional  $1.2M_{cr}$ . This limit is based on the amount of steel that can easily extend from the bottom of a girder for the positive moment connection and the fact that no tests have been performed on girders with larger amounts of steel.

### **COST AND BENEFITS ASSESSMENT**

There will be no specific increase or decrease in costs associated with the performance of the recommended design procedures. There may be a few additional hours of design effort required to determine the restraint moments due to thermal gradients, which is not currently required in the design of prestressed I-girder bridges made continuous. It should be simple to program a spreadsheet to perform this calculation, thereby minimizing the required time to determine the thermal restraint moment for design. There also will not be a noticeable increase or decrease in the initial cost of constructing a bridge in which the recommended detail is implemented. It should be similar to the cost of currently utilized details. The primary benefit from implementing the new detail is expected to be in reduced maintenance costs. Any cracking

that may occur in the diaphragm will be at the interface between the end of the girder and the diaphragm. This type of cracking will be well controlled by the reinforcing across the interface, and the cracks are expected to remain small. The only expected maintenance would be the application of a sealer at the interface to prevent the intrusion of water and salts into the crack. The sealing can be performed at construction, in which case the diaphragm should be maintenance free for the remainder of its service life.

Another benefit to the proposed detail is in the aesthetics of the bridge. With the recommended detail the location of the expected cracking is known and cracks can be easily sealed if desired. With current diaphragm details, particularly those in which the ends of the girders are embedded in the diaphragm, unsightly cracking can occur through the diaphragm. The unattractive appearance of these cracks can be aggravated by corrosion by-products or efflorescence leaking from the cracks. Diaphragms constructed with the recommended detail should remain uncracked and therefore more attractive.

Ultimately, the continuity diaphragm benefits the structure by adding redundancy and reducing the magnitudes of crack widths in the deck above the diaphragm (when compared to a structure made continuous without a continuity diaphragm). The service life of structures, relative to water infiltration and corrosion, will be extended by limiting the presence and size of cracks in the deck, particularly over superstructure connections. This will result in reduced maintenance costs over the life of the bridge structure.

## REFERENCES

- American Association of State Highway and Transportation Officials (1989). *AASHTO Guide Specifications: Thermal Effects in Concrete Bridge Superstructures*, Washington, DC.
- American Association of State Highway and Transportation Officials (2001). *AASHTO LRFD Design Specifications-U.S. Units: 2001 Interim Revisions*, Washington, DC.
- American Association of State Highway and Transportation Officials (2002). *Standard Specifications for Highway Bridges, 17<sup>th</sup> Edition*, Washington, DC.
- American Concrete Institute Manual of Concrete Practice (2002). Prediction of Creep, Shrinkage, and Temperature Effects in Concrete Structures, *ACI 209R-92 (Reapproved 1997)*, Farmington Hills, MI.
- American Concrete Institute (2002). *Building Code Requirements for Structural Concrete (ACI 318-02) and Commentary (ACI 318R-02)*, Reported by ACI Committee 318, Farmington Hills, MI.
- American Society for Testing and Materials (1984). C 78–84: Standard Test Method for Flexural Strength of Concrete Using Simple Beam with Third-Point Loading, *Compilation of ASTM Standards Relating to Aggregates and Concrete*, National Ready Mixed Concrete Association, Silver Spring, MD, 1990.

- American Society for Testing and Materials (1986). C 39–86: Standard Test Method for Compressive Strength of Cylindrical Concrete Specimens, *Compilation of ASTM Standards Relating to Aggregates and Concrete*, National Ready Mixed Concrete Association, Silver Spring, MD, 1990.
- American Society for Testing and Materials (1997). A 370–97a: Standard Test Methods and Definitions for Mechanical Testing of Steel Products, *Annual Book of ASTM Standards*, Vol. 01.03.
- American Society for Testing and Materials (1999). A 416–99: Standard Specifications for Steel Strand, Uncoated Seven-Wire for Prestressed Concrete, *Annual Book of ASTM Standards*, Vol. 01.04.
- American Society for Testing and Materials (2003). A 615–01b: Standard Specification for Deformed and Plain Billet-Steel Bars for Concrete Reinforcement, *Annual Book of ASTM Standards*, 01.04.
- American Society for Testing and Materials (2003). C 31–03A: Standard Practice for Making and Curing Concrete Test Specimens in the Field, *Annual Book of ASTM Standards*, Vol. 04.02.
- American Society for Testing and Materials (2003). C 469-02: Standard Test Method for Modulus of Elasticity and Poisson’s Ratio of Concrete in Compression, *Annual Book of ASTM Standards*, Vol. 04.02.
- American Society for Testing and Materials (2003). C 496-96: Standard Test Method for Splitting Tensile Strength of Cylindrical Concrete Specimens, *Annual Book of ASTM Standards*, Vol. 04.02.
- American Society for Testing and Materials (2003). C 617-98: Standard Practice for Capping Cylindrical Concrete Specimens, *Annual Book of ASTM Standards*, Vol. 04.02.
- Barr, P.J., Stanton, J.F., and Eberhard, M.O. (2005). Effects of Temperature Variations on Precast, Prestressed Concrete Bridge Girders, *ASCE Journal of Bridge Engineering*, Vol. 10, No. 2, 186-194..
- Bentz, D.P., and Jensen, O.M. (2004). Mitigation Strategies for Autogenous Shrinkage Cracking, Reprint from *Cement and Concrete Composites*, Vol. 26, No. 6, 677-685.
- Branson, D.E. (1977). *Deformation of Concrete Structures*, McGraw-Hill Inc.
- Comite Euro-Internationale du Beton (1990). CEB-FIP model code 1990. *Buletin D’Information No. 213/214*, Lausanne, Switzerland.
- Contemporary College Physics* (1990). Addison-Wesley Publishing Company, Inc.

- Freyermuth, C.L. (1969). Design of Continuous Highway Bridges with Precast, Prestressed Concrete Girders. *Journal of the Prestressed Concrete Institute*, Vol. 14, No. 2.
- Hastak, M., Mirmiran, A., Miller, R., Shah, R., and Casterdale, R. (2003). State of Practice for Positive Moment Connections in Prestressed Concrete Girders Made Continuous, *Journal of Bridge Engineering*, September/October 2003.
- Huo, X.S., Nabil, A., and Tadros, M.K. (2001). Creep, Shrinkage, and Modulus of Elasticity of High Performance Concrete, *ACI Materials Journal*, Vol. 98, No. 6.
- Kaar, P.H., Ladislav, B.K., and Hognestad, E. (1960). Precast-Prestressed Concrete Bridges. 1. Pilot Tests of Continuous Bridges. Development Department Bulletin D34, *Portland Cement Association, Research and Development Laboratories*, Skokie, IL.
- Kada, H., Lachemi, M., Petrov, N., Bonneau, O., Aitcin, P-C. (2002). Determination of the Coefficient of Thermal Expansion of High Performance Concrete from Initial Setting, *Materials and Structures*, Vol. 35, Jan-Feb 2002, 35-41.
- MacGregor, J.G. (1988). *Reinforced Concrete: Mechanics and Design, 3<sup>rd</sup> Edition*, Prentice Hall, Upper Saddle River, NJ.
- Mehta, P. Kumar (1986). *Concrete – Structure, Properties, and Materials*. Prentice-Hall, Inc., Englewood Cliffs, NJ.
- Miller, R.A., Castrodale, R., Mirmiran, A., Hastak, M. (2004). Connection of Simple-Span Precast Concrete Girders for Continuity, *Transportation Research Board's National Cooperative Highway Research Program, NCHRP Report 519*.
- Newhouse, C.D. (2005). *Design and Behavior of Precast, Prestressed Girders Made Continuous: An Analytical and Experimental Study*, Ph.D. Dissertation, Virginia Polytechnic Institute and State University, Blacksburg.
- Nilson, A.H. (1987). *Design of Prestressed Concrete, 2<sup>nd</sup> Edition*, John Wiley and Sons.
- Oesterle, R.G., Glikin, J.D., and Larson, S.C. (1989). Design of Precast Prestressed Girders Made Continuous, *National Cooperative Highway Research Program Report 322*, National Research Council, Washington, DC.
- Precast/Prestressed Concrete Institute (1997). MNL-133-97, *Precast Prestressed Concrete Bridge Design Manual*, Chicago.
- Roller, J.J., Russell, H.G., Bruce, R.N., and Hasset, B. (2003). Effect of Curing Temperatures on High Strength Concrete Bridge Girders, *PCI Journal*, March-April 2003.
- Salmons, J.R. (1974). End Connections of Pretensioned I-Beam Bridges, Missouri Cooperative Highway Report 73-5C, Missouri State Highway Department, Jefferson City.

Townsend, B.D. (2003). *Creep and Shrinkage of a High Strength Concrete Mixture*, Masters of Science Thesis, Virginia Tech, Blacksburg.

Zia, P., Preston, H.K., Scott, N.L., and Workman, E.B. (1979). Estimating Prestress Losses, *Concrete International*, Vol. 1, No. 6.